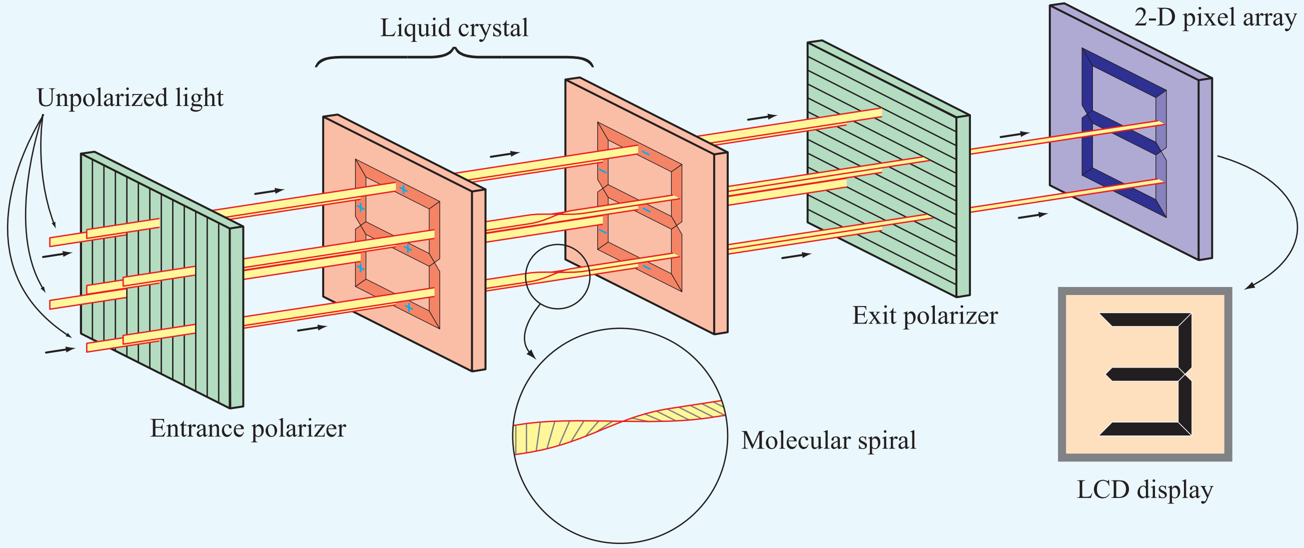

Figure 1-1 2-D LCD array.

Figure 1-2 Electromagnetics is at the heart of numerous systems and applications.

Table 1-1 Fundamental SI units.

Dimension	Unit	Symbol
Length	meter	m
Mass	kilogram	kg
Time	second	s
Electric current	ampere	A
Temperature	kelvin	K
Amount of substance	mole	mol

Table 1-2 **Multiple and submultiple prefixes.**

Prefix	Symbol	Magnitude
exa	E	10^{18}
peta	P	10^{15}
tera	T	10^{12}
giga	G	10^{9}
mega	M	10^{6}
kilo	k	10^{3}
milli	m	10^{-3}
micro	μ	10^{-6}
nano	n	10^{-9}
pico	p	10^{-12}
femto	f	10^{-15}
atto	a	10^{-18}

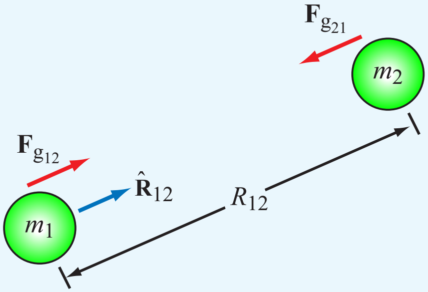

Figure 1-3 Gravitational forces between two masses.

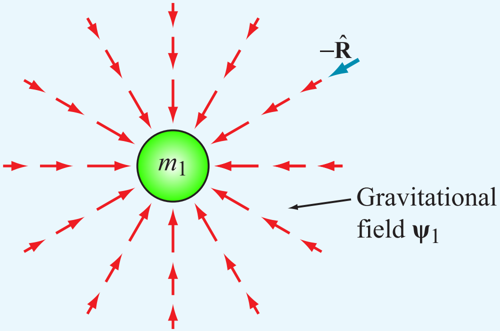

Figure 1-4 Gravitational field $\boldsymbol{\psi}_1$ induced by a mass m_1.

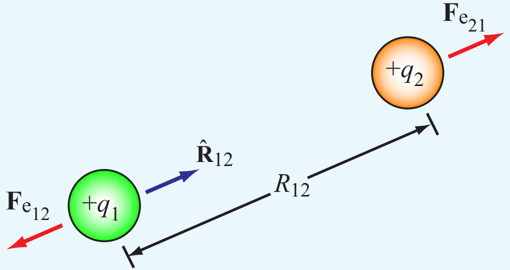

Figure 1-5 Electric forces on two positive point charges in free space.

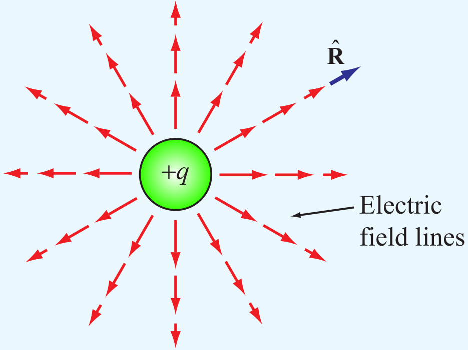

Figure 1-6 Electric field $\mathbf{E}$ due to charge q.

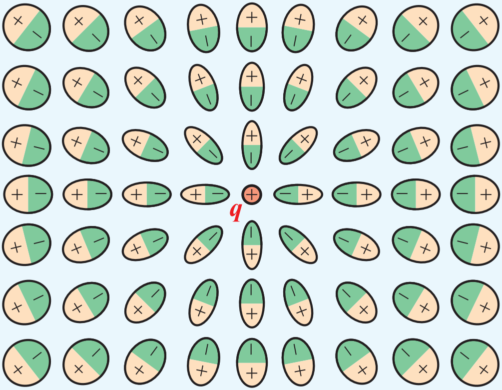

Figure 1-7 Polarization of the atoms of a dielectric material by a positive charge q.

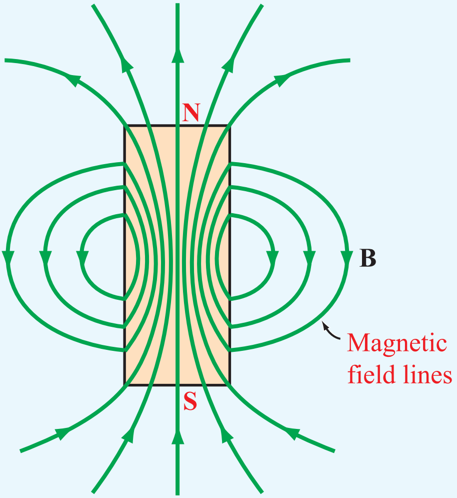

Figure 1-8 Pattern of magnetic field lines around a bar magnet.

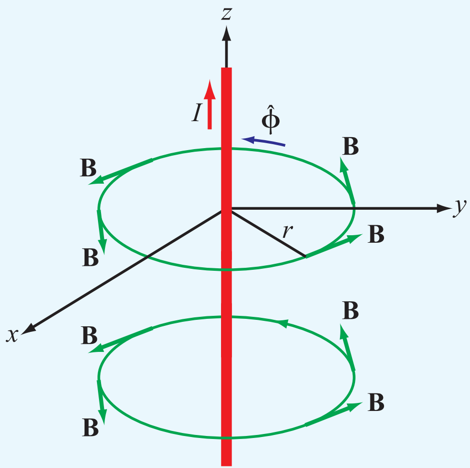

Figure 1-9 The magnetic field induced by a steady current flowing in the z direction.

Table 1-3 The three branches of electromagnetics.

Branch	Condition	Field Quantities (Units)
Electrostatics	Stationary charges ($\partial q/\partial t = 0$)	Electric field intensity $\mathbf{E}$ (V/m) Electric flux density $\mathbf{D}$ (C/m^2) $\mathbf{D} = \varepsilon \mathbf{E}$
Magnetostatics	Steady currents ($\partial I/\partial t = 0$)	Magnetic flux density $\mathbf{B}$ (T) Magnetic field intensity $\mathbf{H}$ (A/m) $\mathbf{B} = \mu \mathbf{H}$
Dynamics (time-varying fields)	Time-varying currents ($\partial I/\partial t \neq 0$)	$\mathbf{E}$, $\mathbf{D}$, $\mathbf{B}$, and $\mathbf{H}$ $(\mathbf{E}, \mathbf{D})$ coupled to $(\mathbf{B}, \mathbf{H})$

Table 1-4 Constitutive parameters of materials.

Parameter	Units	Free-Space Value
Electrical permittivity ε	F/m	$\varepsilon_0 = 8.854 \times 10^{-12}$ $\approx \frac{1}{36\pi} \times 10^{-9}$
Magnetic permeability μ	H/m	$\mu_0 = 4\pi \times 10^{-7}$
Conductivity σ	S/m	0

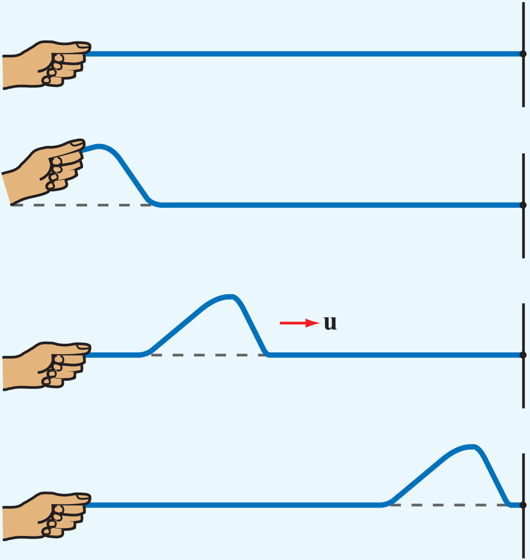

Figure 1-10 A one-dimensional wave traveling on a string.

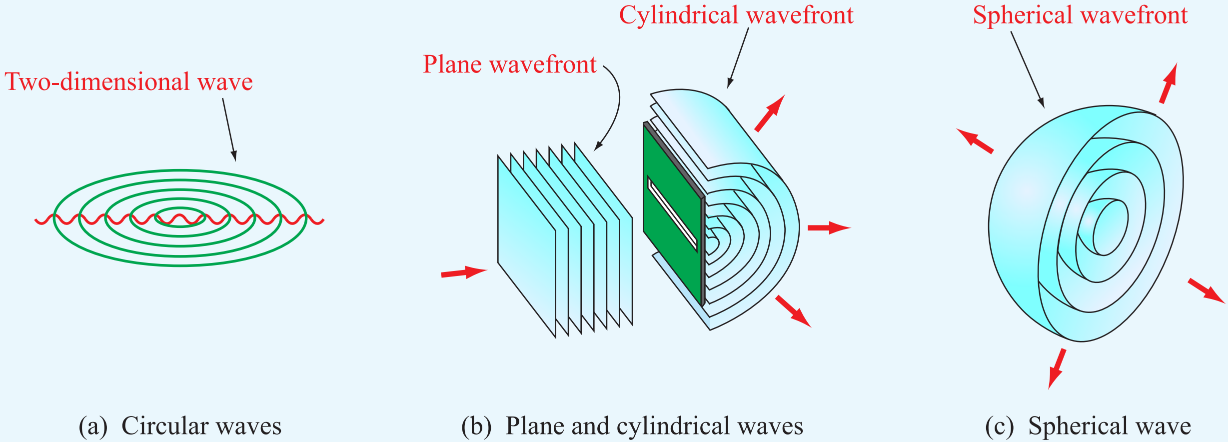

Figure 1-11 Examples of two-dimensional and three-dimensional waves: (a) circular waves on a pond, (b) a plane light wave exciting a cylindrical light wave through the use of a long narrow slit in an opaque screen, and (c) a sliced section of a spherical wave.

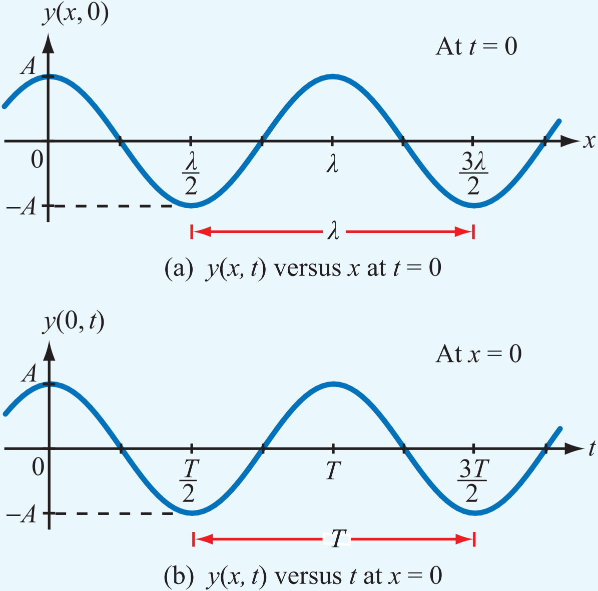

Figure 1-12 Plots of $y(x,t) = A\cos\left(\frac{2\pi t}{T} - \frac{2\pi x}{\lambda}\right)$ as a function of (a) x at $t = 0$ and (b) t at $x = 0$.

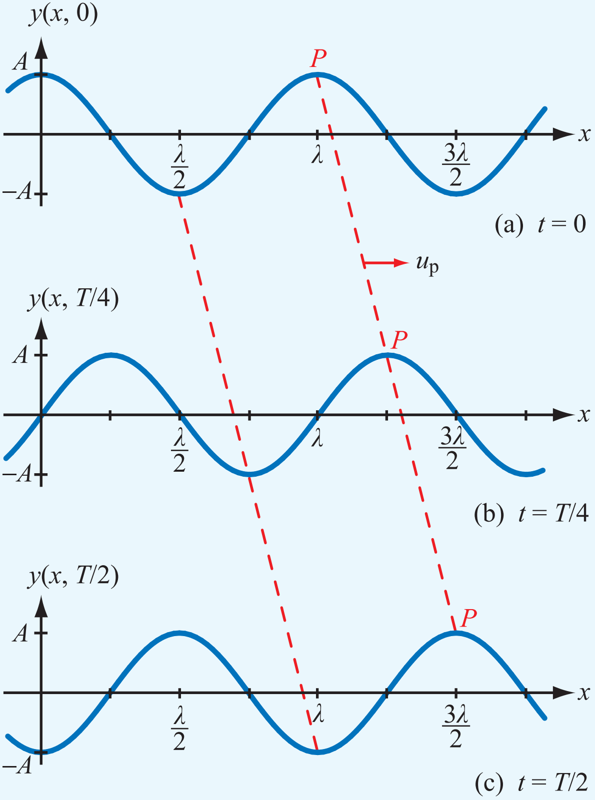

Figure 1-13 Plots of $y(x,t) = A\cos\left(\frac{2\pi t}{T} - \frac{2\pi x}{\lambda}\right)$ as a function of x at (a) $t = 0$, (b) $t = T/4$, and (c) $t = T/2$. Note that the wave moves in the $+x$ direction with a velocity $u_p = \lambda/T$.

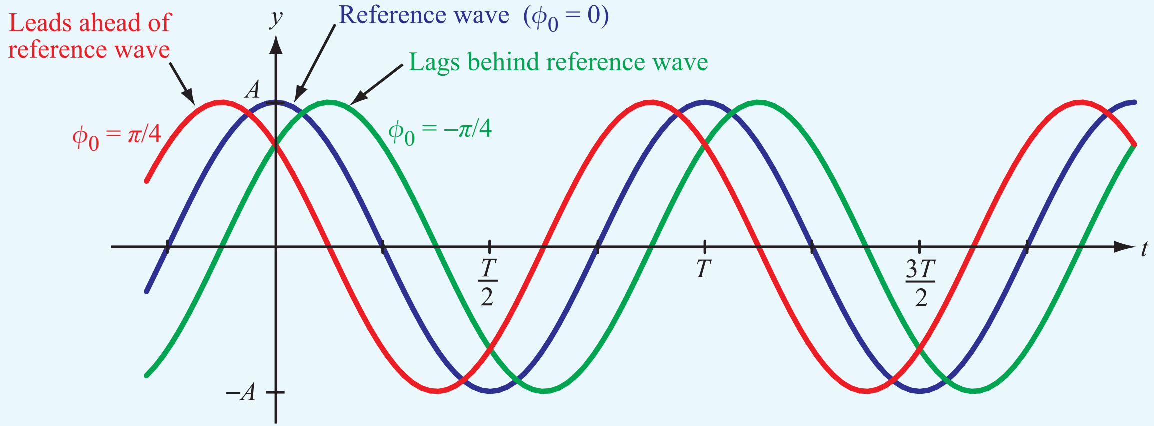

Figure 1-14 Plots of $y(0,t) = A\cos[(2\pi t/T) + \phi_0]$ for three different values of the reference phase ϕ_0.

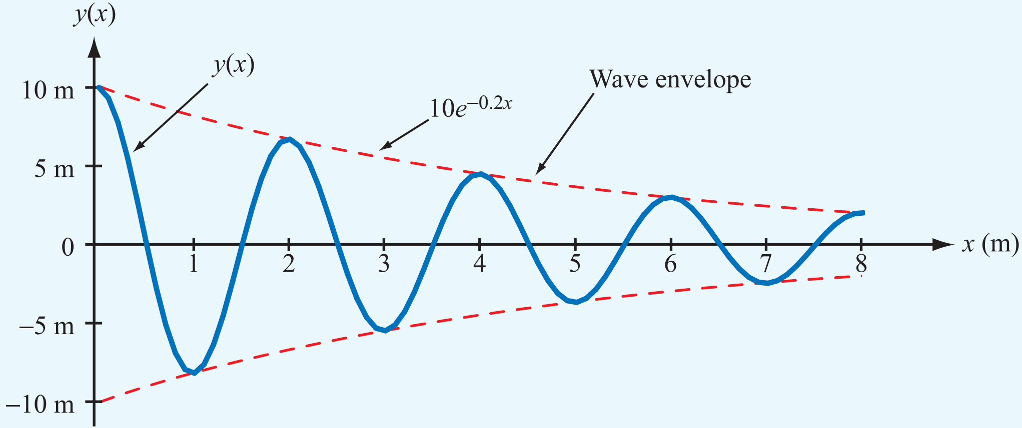

Figure 1-15 Plot of $y(x) = (10e^{-0.2x} \cos \pi x)$ meters. Note that the envelope is bounded between the curve given by $10e^{-0.2x}$ and its mirror image.

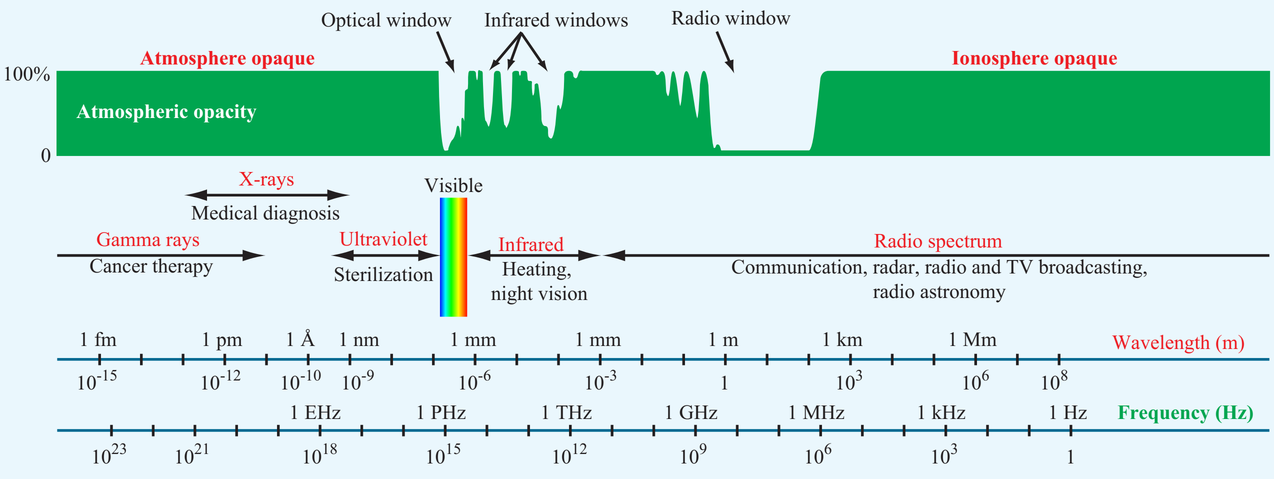

Figure 1-16 The electromagnetic spectrum.

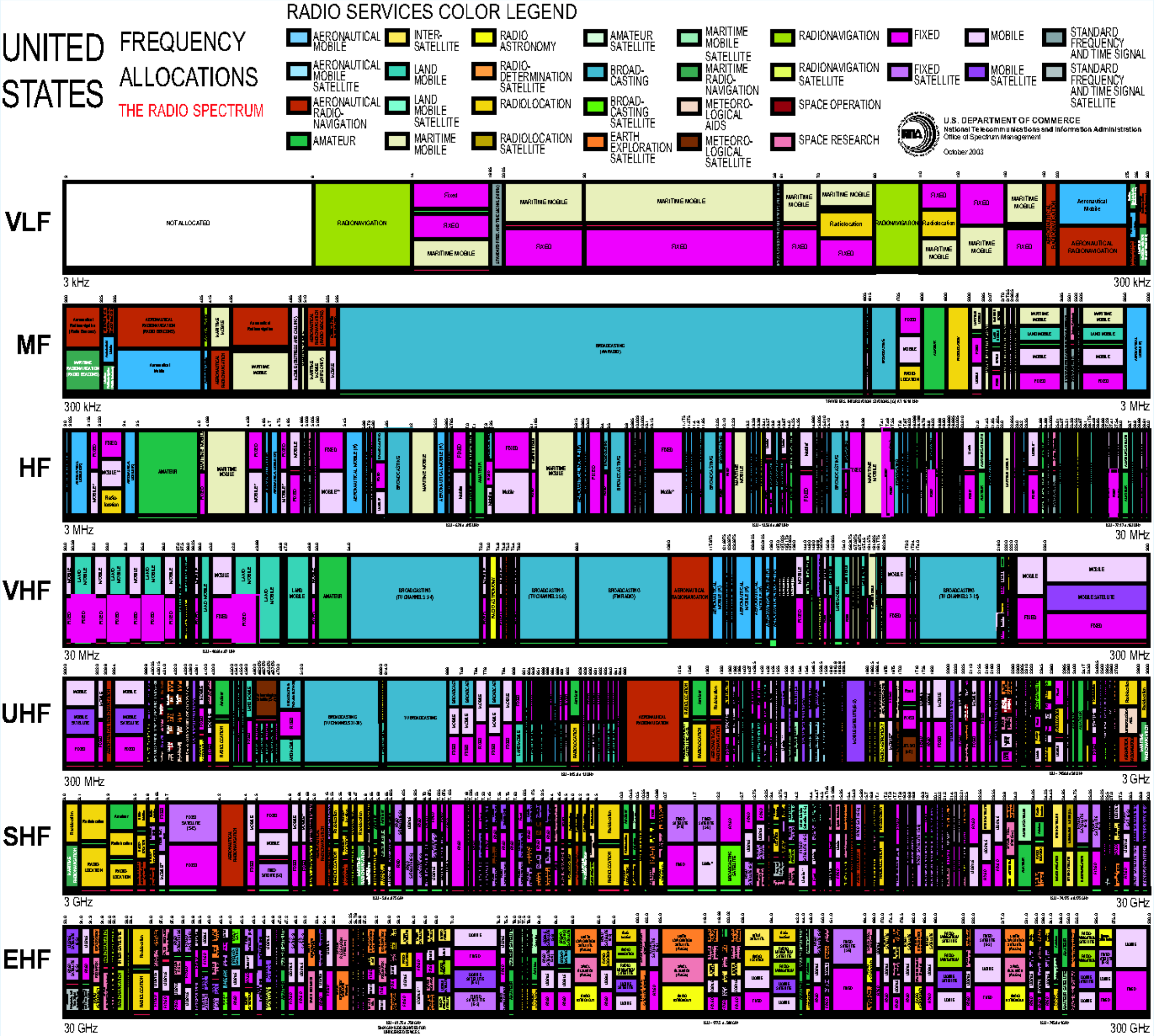

Figure 1-17 Individual bands of the radio spectrum and their primary allocations in the US. [See expandable version on book website: em.eecs.umich.edu.]

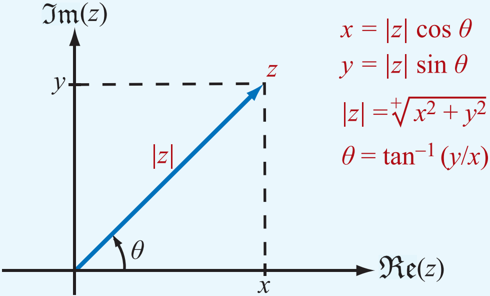

Figure 1-18 Relation between rectangular and polar representations of a complex number $z = x + jy = |z|e^{j\theta}$.

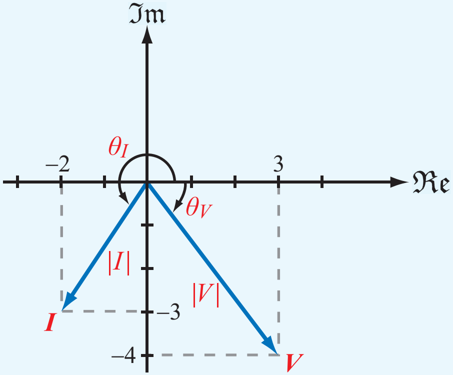

Figure 1-19 Complex numbers V and I in the complex plane (Example 1-3).

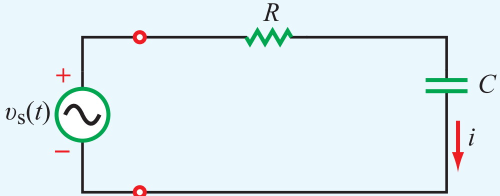

Figure 1-20 RC circuit connected to a voltage source $\upsilon_s(t)$.

Table 1-5 Time-domain sinusoidal functions $z(t)$ and their cosine-reference phasor-domain counterparts $\widetilde{Z}$, where $z(t) = \mathfrak{Re}[\widetilde{Z}e^{j\omega t}]$.

$z(t)$		$\widetilde{Z}$
$A\cos\omega t$	$\leftrightarrow$	A
$A\cos(\omega t + \phi_0)$	$\leftrightarrow$	$Ae^{j\phi_0}$
$A\cos(\omega t + \beta x + \phi_0)$	$\leftrightarrow$	$Ae^{j(\beta x + \phi_0)}$
$Ae^{-\alpha x}\cos(\omega t + \beta x + \phi_0)$	$\leftrightarrow$	$Ae^{-\alpha x}e^{j(\beta x + \phi_0)}$
$A\sin\omega t$	$\leftrightarrow$	$Ae^{-j\pi/2}$
$A\sin(\omega t + \phi_0)$	$\leftrightarrow$	$Ae^{j(\phi_0 - \pi/2)}$
$\dfrac{d}{dt}(z(t))$	$\leftrightarrow$	$j\omega\widetilde{Z}$
$\dfrac{d}{dt}[A\cos(\omega t + \phi_0)]$	$\leftrightarrow$	$j\omega Ae^{j\phi_0}$
$\int z(t)\, dt$	$\leftrightarrow$	$\dfrac{1}{j\omega}\widetilde{Z}$
$\int A\sin(\omega t + \phi_0)\, dt$	$\leftrightarrow$	$\dfrac{1}{j\omega}Ae^{j(\phi_0 - \pi/2)}$

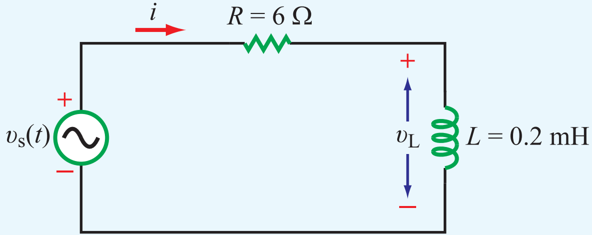

Figure 1-21 RL circuit (Example 1.4).

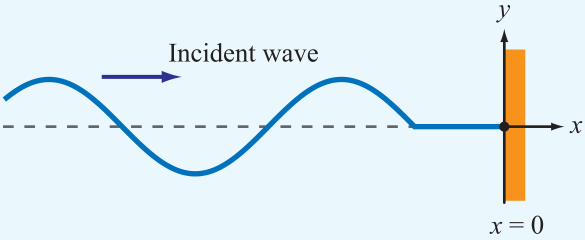

Figure P1.7 Wave on a string tied to a wall at $x = 0$ (Problem 1.7).

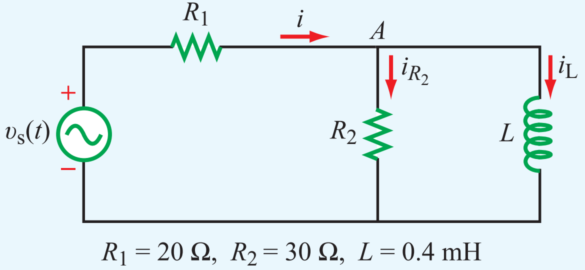

Figure P1.29 Circuit for Problem 1.29.

Figure 2-1 A transmission line is a two-port network connecting a generator circuit at the sending end to a load at the receiving end.

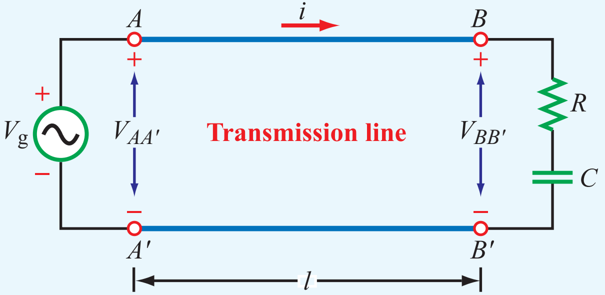

Figure 2-2 Generator connected to an RC circuit through a transmission line of length l.

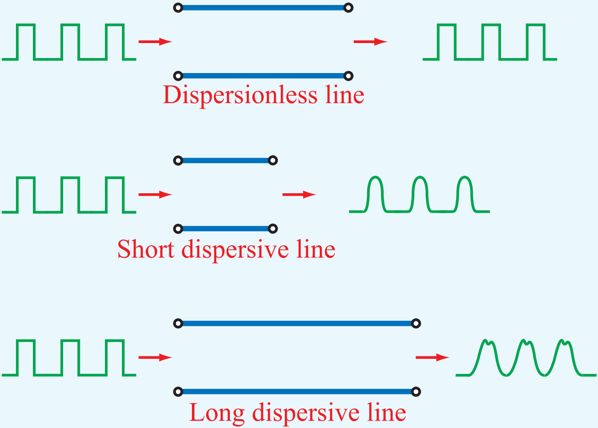

Figure 2-3 A dispersionless line does not distort signals passing through it regardless of its length, whereas a dispersive line distorts the shape of the input pulses because the different frequency components propagate at different velocities. The degree of distortion is proportional to the length of the dispersive line.

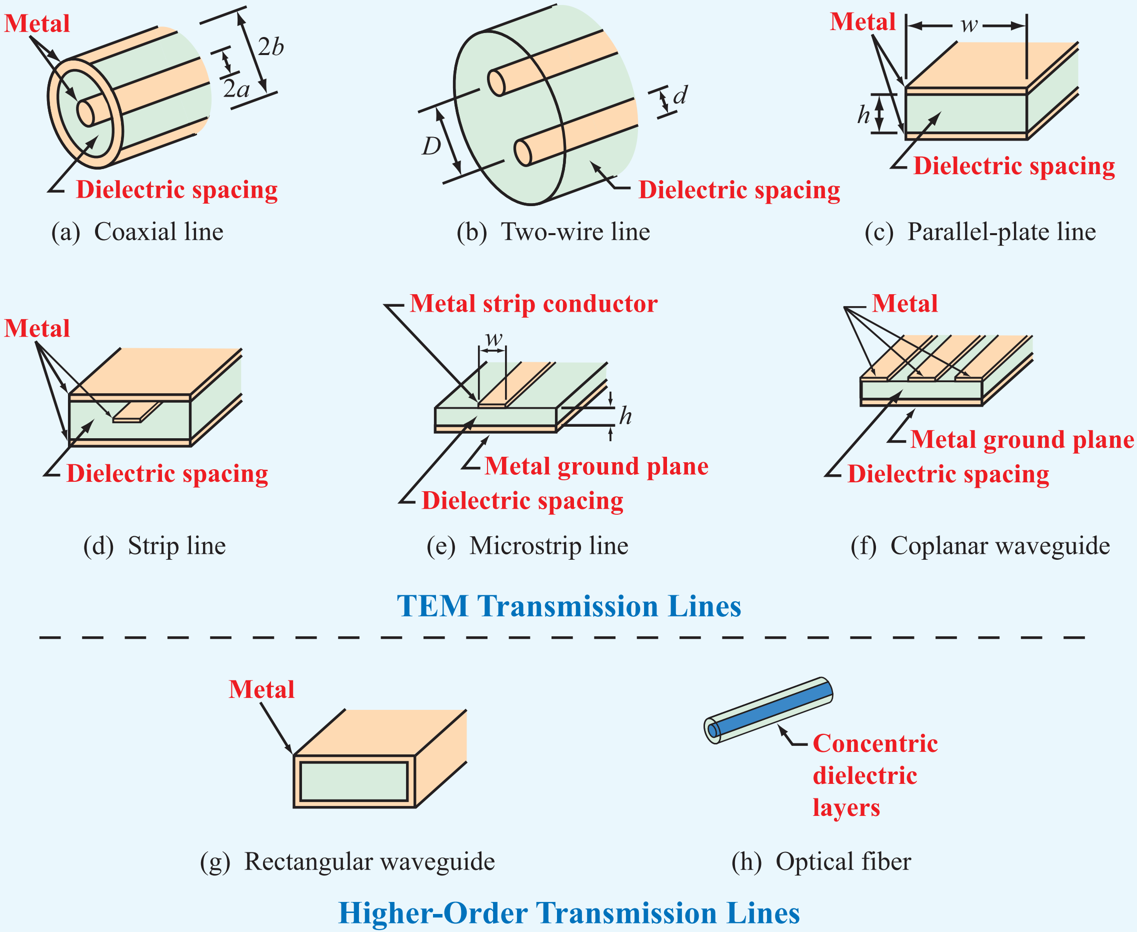

Figure 2-4 A few examples of transverse electromagnetic (TEM) and higher-order transmission lines.

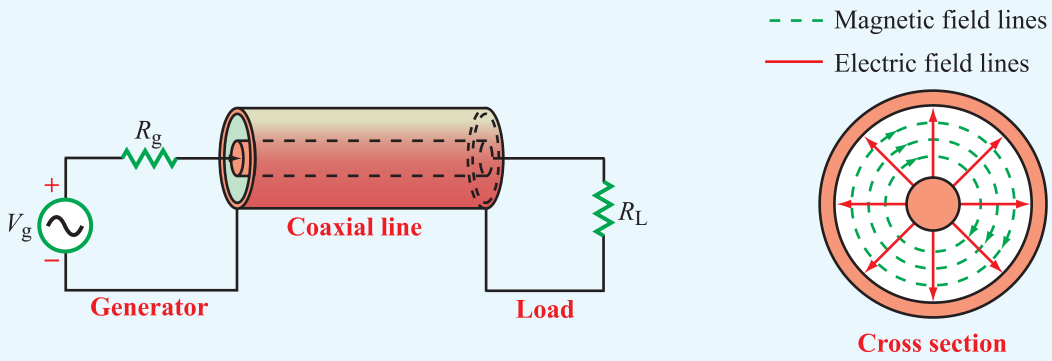

Figure 2-5 In a coaxial line, the electric field is in the radial direction between the inner and outer conductors, and the magnetic field forms circles around the inner conductor. The coaxial line is a transverse electromagnetic (TEM) transmission line because both the electric and magnetic fields are orthogonal to the direction of propagation between the generator and the load.

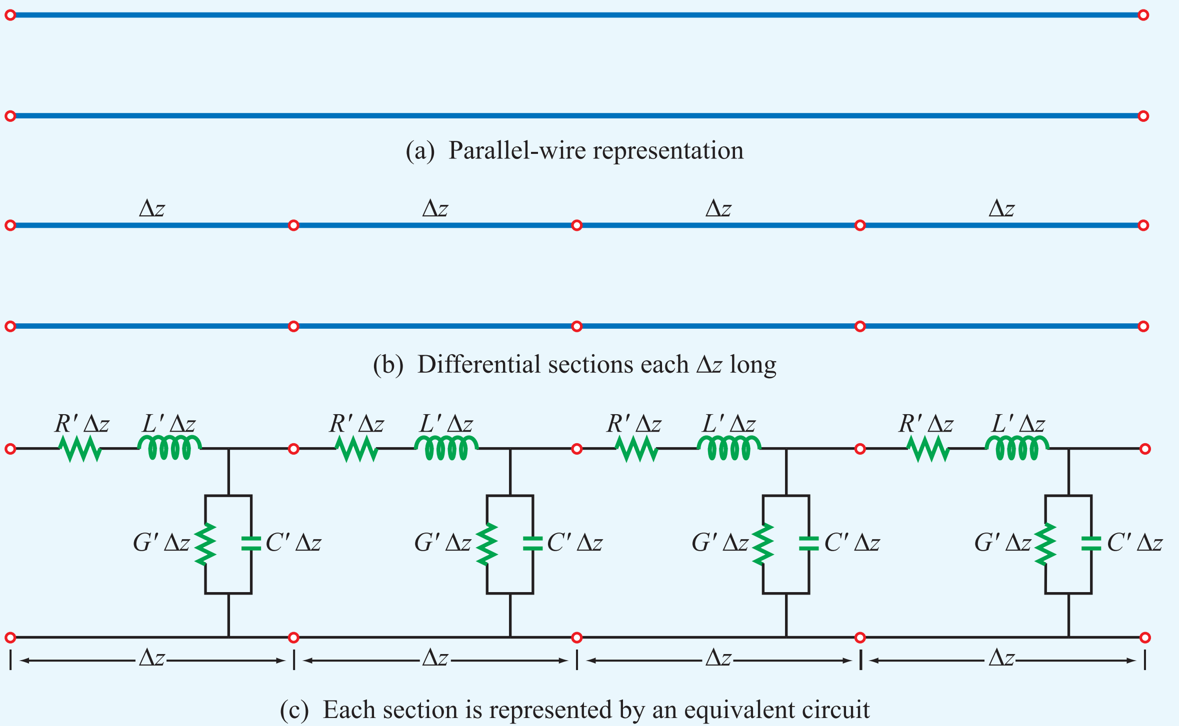

Figure 2-6 Regardless of its cross-sectional shape, a TEM transmission line is represented by the parallel-wire configuration shown in (a). To obtain equations relating voltages and currents, the line is subdivided into small differential sections (b), each of which is then represented by an equivalent circuit (c).

Table 2-1 **Transmission-line parameters R', L', G', and C' for three types of lines.**

Parameter	Coaxial	Two-Wire	Parallel-Plate	Unit
R'	$\dfrac{R_s}{2\pi}\left(\dfrac{1}{a}+\dfrac{1}{b}\right)$	$\dfrac{2R_s}{\pi d}$	$\dfrac{2R_s}{w}$	Ω/m
L'	$\dfrac{\mu}{2\pi}\ln(b/a)$	$\dfrac{\mu}{\pi}\ln\left[(D/d)+\sqrt{(D/d)^2-1}\right]$	$\dfrac{\mu h}{w}$	H/m
G'	$\dfrac{2\pi\sigma}{\ln(b/a)}$	$\dfrac{\pi\sigma}{\ln\left[(D/d)+\sqrt{(D/d)^2-1}\right]}$	$\dfrac{\sigma w}{h}$	S/m
C'	$\dfrac{2\pi\varepsilon}{\ln(b/a)}$	$\dfrac{\pi\varepsilon}{\ln\left[(D/d)+\sqrt{(D/d)^2-1}\right]}$	$\dfrac{\varepsilon w}{h}$	F/m

Notes: (1) Refer to **Fig. 2-4** for definitions of dimensions. (2) μ, ε, and σ pertain to the insulating material between the conductors. (3) $R_s = \sqrt{\pi f \mu_c/\sigma_c}$. (4) μ_c and σ_c pertain to the conductors. (5) If $(D/d)^2 \gg 1$, then $\ln\left[(D/d)+\sqrt{(D/d)^2-1}\right] \approx \ln(2D/d)$.

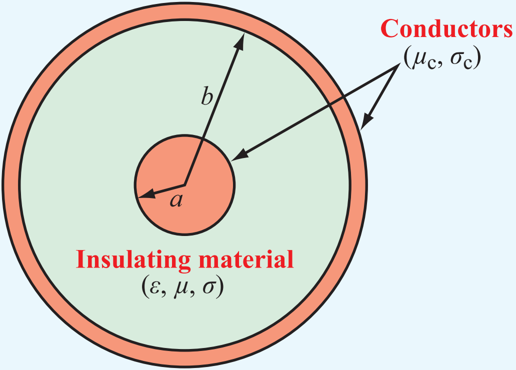

Figure 2-7 Cross section of a coaxial line with inner conductor of radius a and outer conductor of radius b. The conductors have magnetic permeability μ_c, and conductivity σ_c, and the spacing material between the conductors has permittivity ε, permeability μ, and conductivity σ.

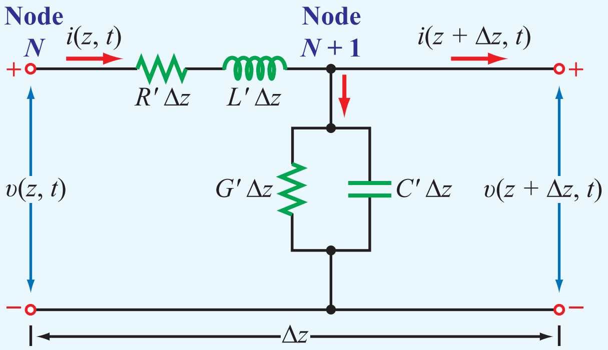

Figure 2-8 Equivalent circuit of a two-conductor transmission line of differential length Δz.

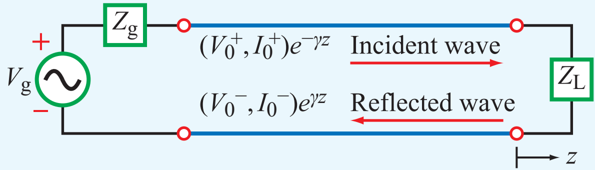

Figure 2-9 In general, a transmission line can support two traveling waves, an incident wave (with voltage and current amplitudes (V_0^+, I_0^+)) traveling along the $+z$ direction (towards the load) and a reflected wave (with (V_0^-, I_0^-)) traveling along the $-z$ direction (towards the source).

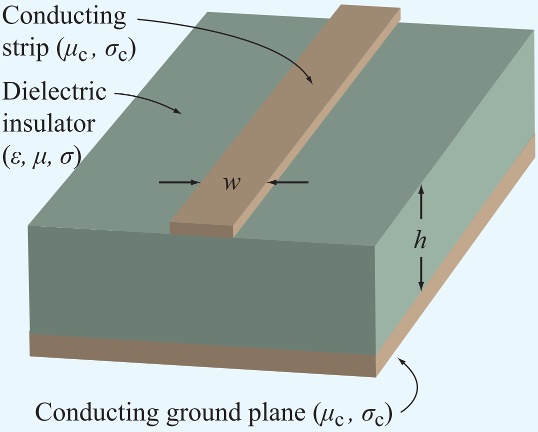

(a) Longitudinal view

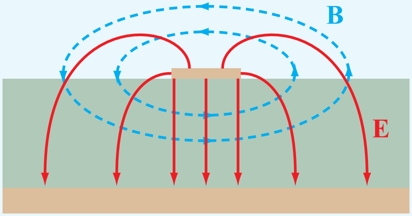

(b) Cross-sectional view with **E** and **B** field lines

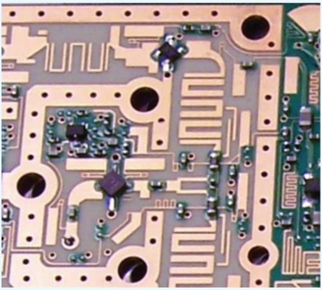

(c) Microwave circuit

Figure 2-10 Microstrip line: (a) longitudinal view, (b) cross-sectional view, and (c) circuit example. (Courtesy of Prof. Gabriel Rebeiz, U. California at San Diego.)

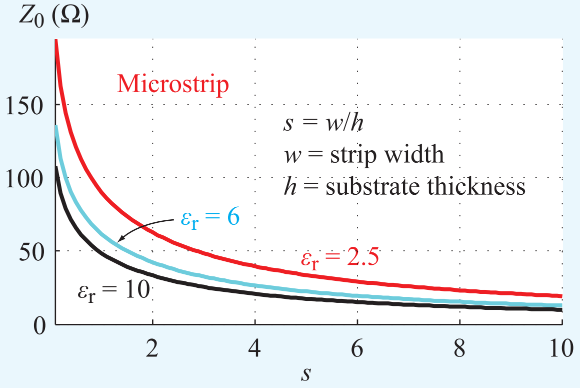

Figure 2-11 Plots of Z_0 as a function of s for various types of dielectric materials.

Table 2-2 Characteristic parameters of transmission lines.

	Propagation Constant $\gamma = \alpha + j\beta$	Phase Velocity u_p	Characteristic Impedance Z_0
General case	$\gamma = \sqrt{(R' + j\omega L')(G' + j\omega C')}$	$u_p = \omega/\beta$	$Z_0 = \sqrt{\dfrac{(R' + j\omega L')}{(G' + j\omega C')}}$
Lossless $(R' = G' = 0)$	$\alpha = 0,\ \beta = \omega\sqrt{\varepsilon_r}/c$	$u_p = c/\sqrt{\varepsilon_r}$	$Z_0 = \sqrt{L'/C'}$
Lossless coaxial	$\alpha = 0,\ \beta = \omega\sqrt{\varepsilon_r}/c$	$u_p = c/\sqrt{\varepsilon_r}$	$Z_0 = (60/\sqrt{\varepsilon_r})\ln(b/a)$
Lossless two-wire	$\alpha = 0,\ \beta = \omega\sqrt{\varepsilon_r}/c$	$u_p = c/\sqrt{\varepsilon_r}$	$Z_0 = (120/\sqrt{\varepsilon_r}) \cdot \ln\left[(D/d) + \sqrt{(D/d)^2 - 1}\right]$ $Z_0 \approx (120/\sqrt{\varepsilon_r})\ln(2D/d)$, if $D \gg d$
Lossless parallel-plate	$\alpha = 0,\ \beta = \omega\sqrt{\varepsilon_r}/c$	$u_p = c/\sqrt{\varepsilon_r}$	$Z_0 = (120\pi/\sqrt{\varepsilon_r})(h/w)$

Notes: (1) $\mu = \mu_0,\ \varepsilon = \varepsilon_r\varepsilon_0,\ c = 1/\sqrt{\mu_0\varepsilon_0}$, and $\sqrt{\mu_0/\varepsilon_0} \approx (120\pi)\ \Omega$, where ε_r is the relative permittivity of insulating material. (2) For coaxial line, a and b are radii of inner and outer conductors. (3) For two-wire line, $d =$ wire diameter and $D =$ separation between wire centers. (4) For parallel-plate line, $w =$ width of plate and $h =$ separation between the plates.

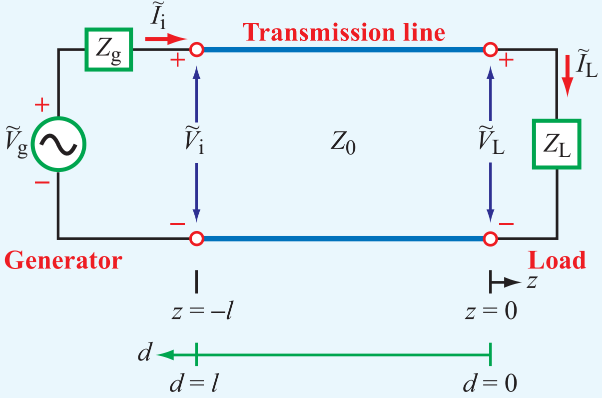

Figure 2-12 Transmission line of length l connected on one end to a generator circuit and on the other end to a load Z_L. The load is located at $z = 0$ and the generator terminals are at $z = -l$. Coordinate d is defined as $d = -z$.

Table 2-3 **Magnitude and phase of the reflection coefficient for various types of loads. The normalized load impedance $z_L = Z_L/Z_0 = (R + jX)/Z_0 = r + jx$, where $r = R/Z_0$ and $x = X/Z_0$ are the real and imaginary parts of z_L, respectively.**

Reflection Coefficient $\Gamma = |\Gamma| e^{j\theta_r}$

Load		$\lvert\Gamma\rvert$	θ_r
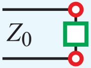	$Z_L = (r + jx)Z_0$	$\left[\dfrac{(r-1)^2 + x^2}{(r+1)^2 + x^2}\right]^{1/2}$	$\tan^{-1}\left(\dfrac{x}{r-1}\right) - \tan^{-1}\left(\dfrac{x}{r+1}\right)$
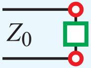	Z_0	0 (no reflection)	irrelevant
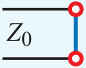	(short)	1	$\pm 180°$ (phase opposition)
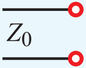	(open)	1	0 (in-phase)
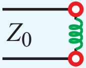	$jX = j\omega L$	1	$\pm 180° - 2\tan^{-1} x$
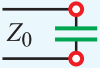	$jX = \dfrac{-j}{\omega C}$	1	$\pm 180° + 2\tan^{-1} x$

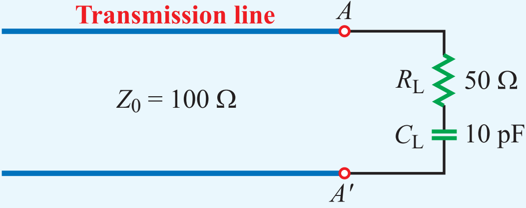

Figure 2-13 RC load (Example 2-3).

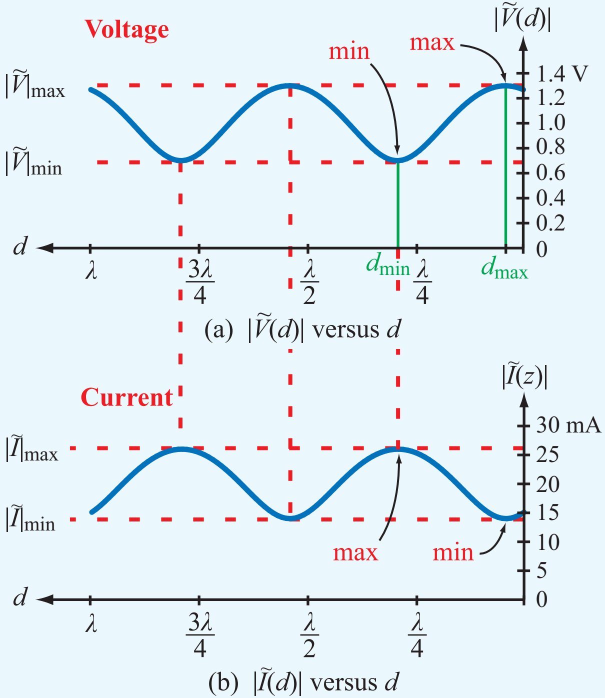

Figure 2-14 Standing-wave pattern for (a) $|\widetilde{V}(d)|$ and (b) $|\widetilde{I}(d)|$ for a lossless transmission line of characteristic impedance $Z_0 = 50\ \Omega$, terminated in a load with a reflection coefficient $\Gamma = 0.3e^{j30^\circ}$. The magnitude of the incident wave $|V_0^+| = 1$ V. The standing-wave ratio is $S = |\widetilde{V}|_{max}/|\widetilde{V}|_{min} = 1.3/0.7 = 1.86$.

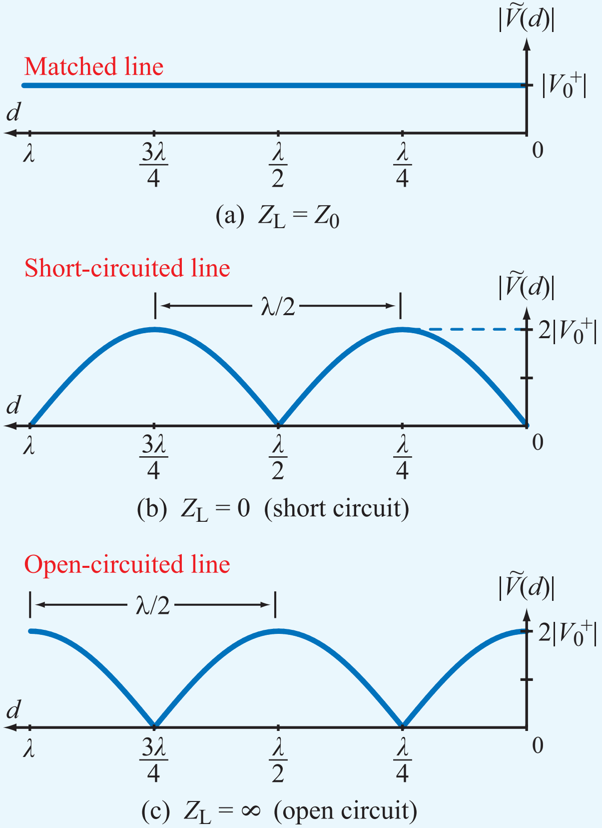

Figure 2-15 Voltage standing-wave patterns for (a) a matched load, (b) a short-circuited line, and (c) an open-circuited line.

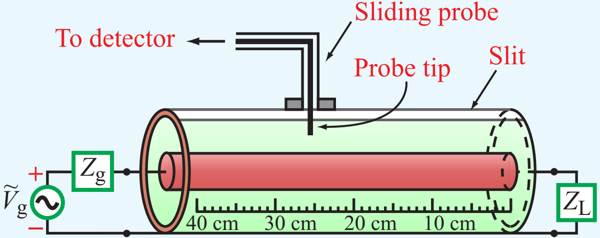

Figure 2-16 Slotted coaxial line (Example 2-6).

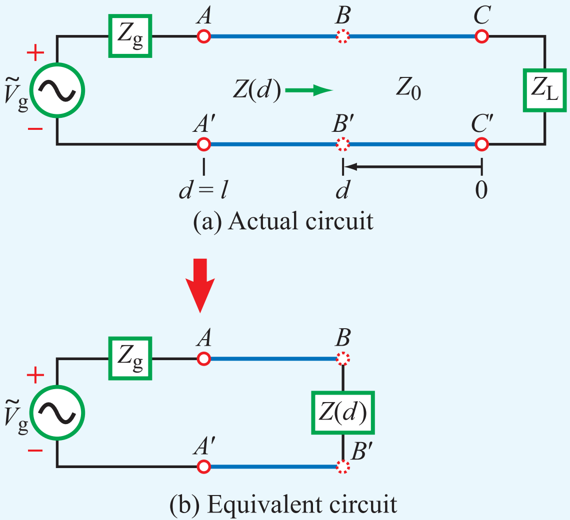

Figure 2-17 The segment to the right of terminals BB' can be replaced with a discrete impedance equal to the wave impedance $Z(d)$.

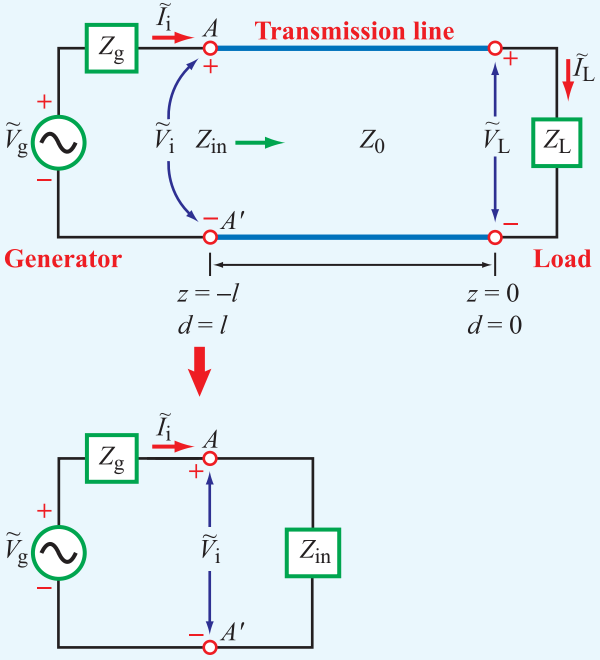

Figure 2-18 At the generator end, the terminated transmission line can be replaced with the input impedance of the line Z_{in}.

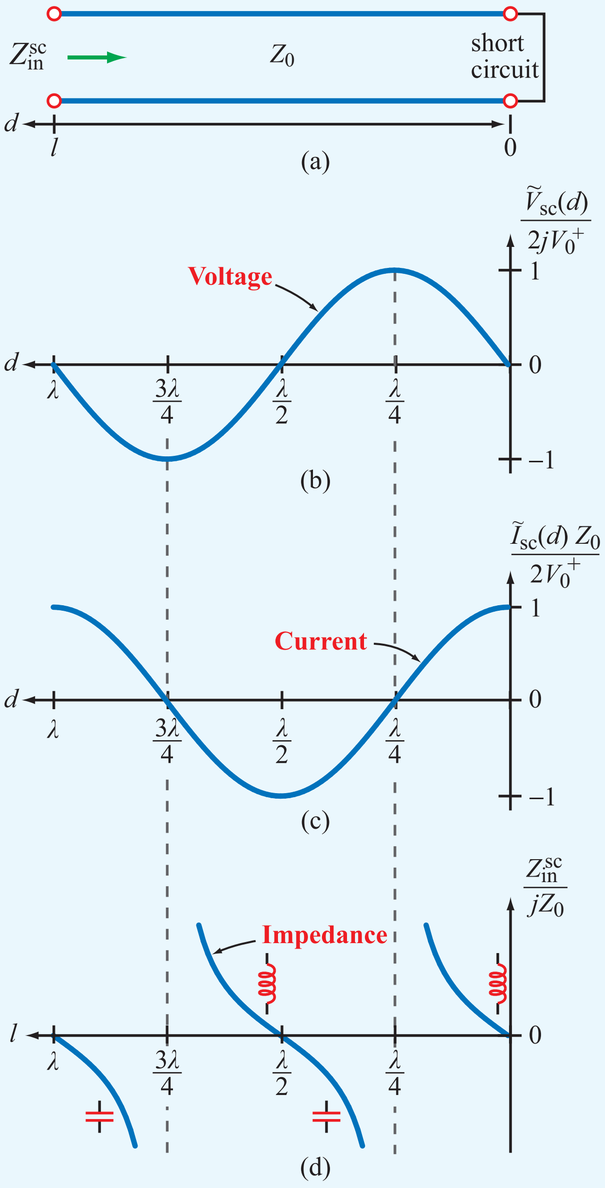

Figure 2-19 Transmission line terminated in a short circuit: (a) schematic representation, (b) normalized voltage on the line, (c) normalized current, and (d) normalized input impedance.

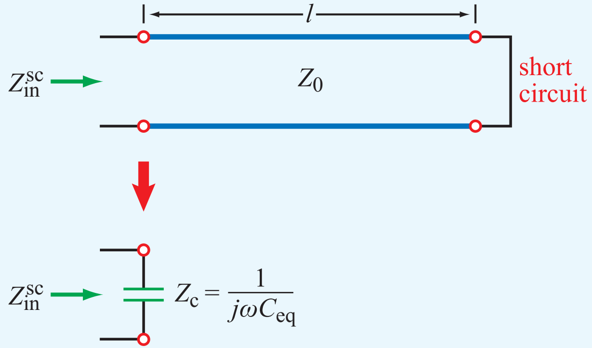

Figure 2-20 Shorted line as equivalent capacitor (Example 2-8).

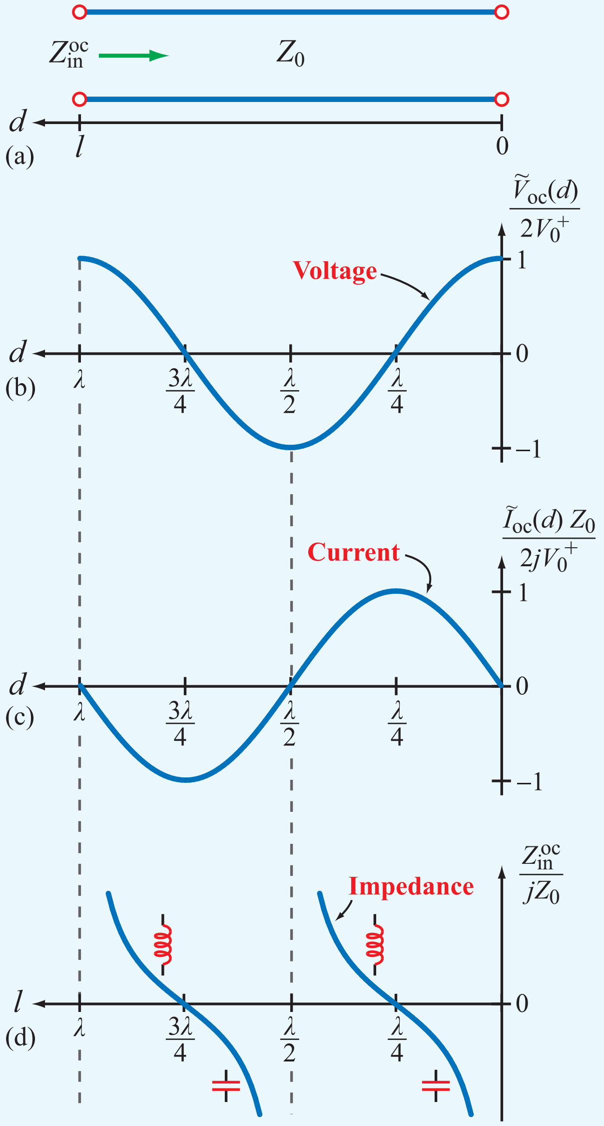

Figure 2-21 Transmission line terminated in an open circuit: (a) schematic representation, (b) normalized voltage on the line, (c) normalized current, and (d) normalized input impedance.

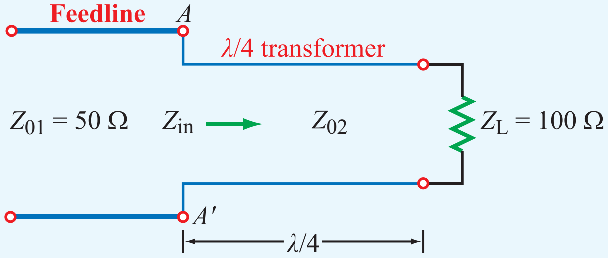

Figure 2-22 Configuration for Example 2-10.

Table 2-4 Properties of standing waves on a lossless transmission line.

Voltage maximum **Voltage minimum**	$\lvert\widetilde{V}\rvert_{\max} = \lvert V_0^+\rvert[1+\lvert\Gamma\rvert]$ $\lvert\widetilde{V}\rvert_{\min} = \lvert V_0^+\rvert[1-\lvert\Gamma\rvert]$
Positions of voltage maxima (also positions of current minima) Position of first maximum (also position of first current minimum)	$d_{\max} = \dfrac{\theta_r\lambda}{4\pi} + \dfrac{n\lambda}{2}, \quad n = 0,1,2,\ldots$ $d_{\max} = \begin{cases} \dfrac{\theta_r\lambda}{4\pi}, & \text{if } 0 \le \theta_r \le \pi \\ \dfrac{\theta_r\lambda}{4\pi} + \dfrac{\lambda}{2}, & \text{if } -\pi \le \theta_r \le 0 \end{cases}$
Positions of voltage minima (also positions of current maxima) Position of first minimum (also position of first current maximum)	$d_{\min} = \dfrac{\theta_r\lambda}{4\pi} + \dfrac{(2n+1)\lambda}{4}, \quad n = 0,1,2,\ldots$ $d_{\min} = \dfrac{\lambda}{4}\left(1+\dfrac{\theta_r}{\pi}\right)$
Input impedance	$Z_{\text{in}} = Z_0\left(\dfrac{z_L + j\tan\beta l}{1 + jz_L\tan\beta l}\right) = Z_0\left(\dfrac{1+\Gamma_l}{1-\Gamma_l}\right)$
Positions at which Z_{in} is real	at voltage maxima and minima
Z_{in} at voltage maxima	$Z_{\text{in}} = Z_0\left(\dfrac{1+\lvert\Gamma\rvert}{1-\lvert\Gamma\rvert}\right)$
Z_{in} at voltage minima	$Z_{\text{in}} = Z_0\left(\dfrac{1-\lvert\Gamma\rvert}{1+\lvert\Gamma\rvert}\right)$
Z_{in} of short-circuited line	$Z_{\text{in}}^{\text{sc}} = jZ_0\tan\beta l$
Z_{in} of open-circuited line	$Z_{\text{in}}^{\text{oc}} = -jZ_0\cot\beta l$
Z_{in} of line of length $l = n\lambda/2$	$Z_{\text{in}} = Z_L, \quad n = 0,1,2,\ldots$
Z_{in} of line of length $l = \lambda/4 + n\lambda/2$ Z_{in} of matched line	$Z_{\text{in}} = Z_0^2/Z_L, \quad n = 0,1,2,\ldots$ $Z_{\text{in}} = Z_0$

$\lvert V_0^+\rvert$ = amplitude of incident wave; $\Gamma = \lvert\Gamma\rvert e^{j\theta_r}$ with $-\pi < \theta_r < \pi$; θ_r in radians; $\Gamma_l = \Gamma e^{-j2\beta l}$.

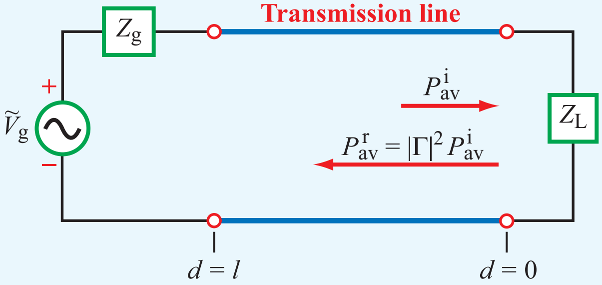

Figure 2-23 The time-average power reflected by a load connected to a lossless transmission line is equal to the incident power multiplied by $|\Gamma|^2$.

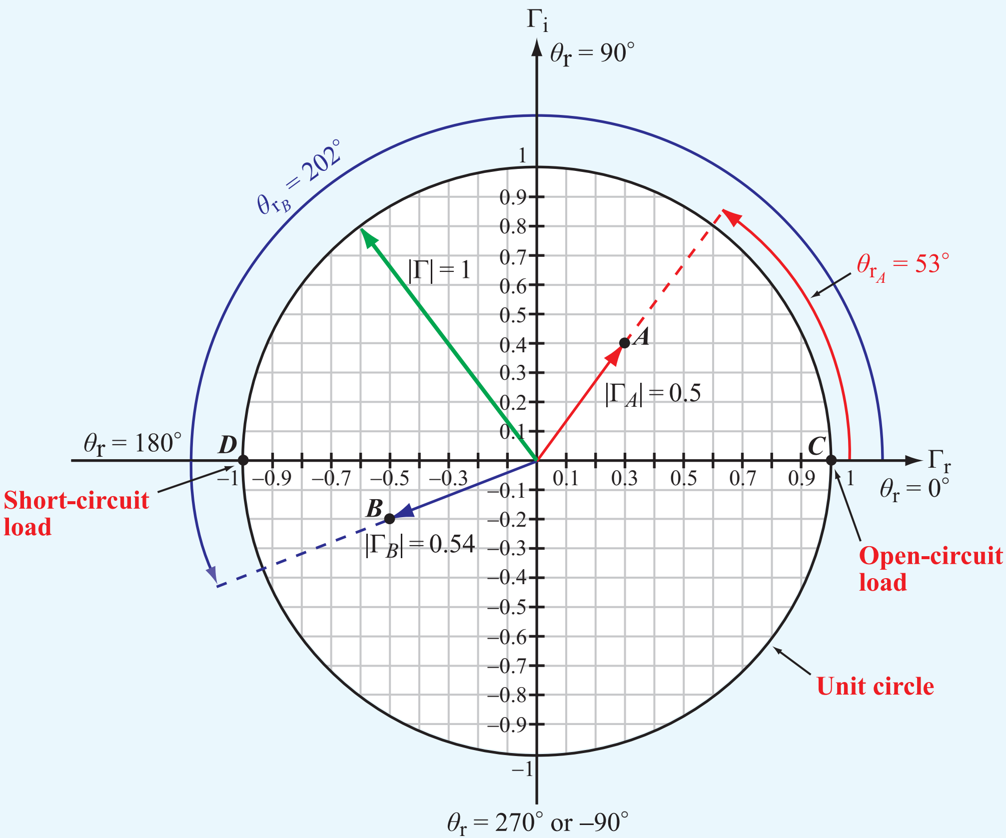

Figure 2-24 The complex Γ plane. Point A is at $\Gamma_A = 0.3 + j0.4 = 0.5e^{j53°}$, and point B is at $\Gamma_B = -0.5 - j0.2 = 0.54e^{j202°}$. The unit circle corresponds to $|\Gamma| = 1$. At point C, $\Gamma = 1$, corresponding to an open-circuit load, and at point D, $\Gamma = -1$, corresponding to a short circuit.

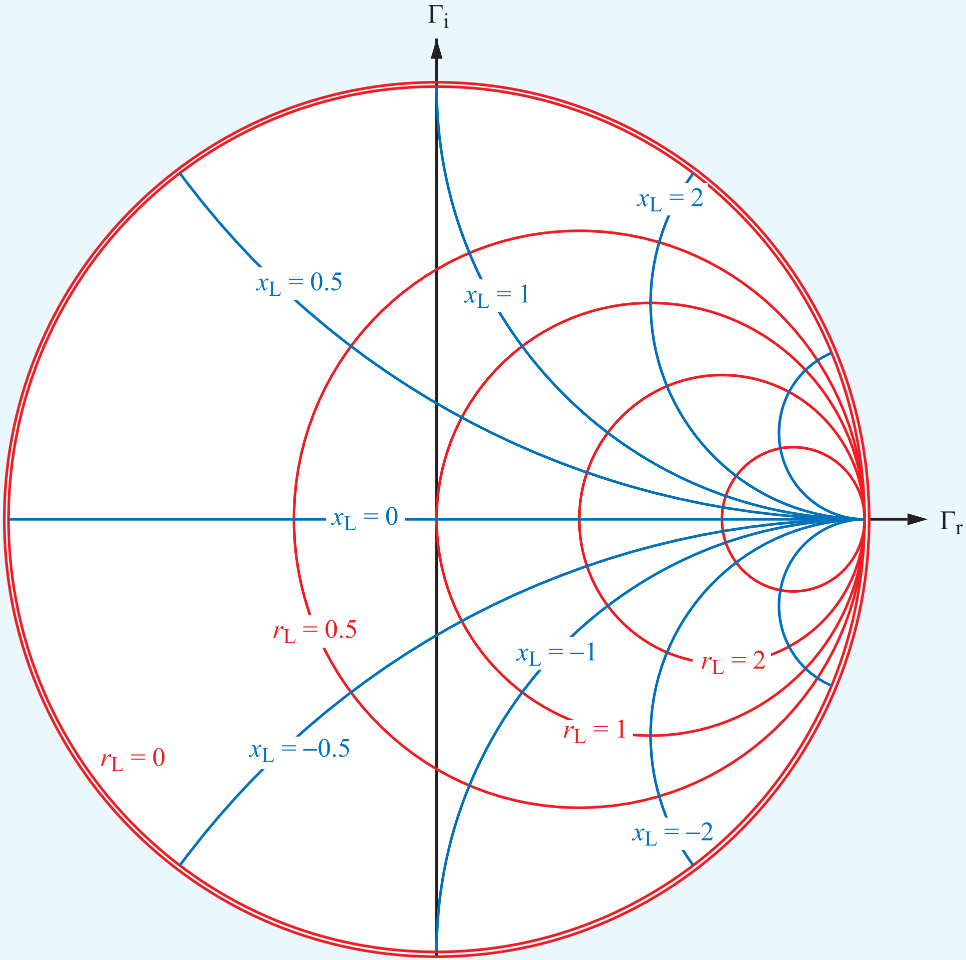

Figure 2-25 Families of r_L and x_L circles within the domain $|\Gamma| \leq 1$.

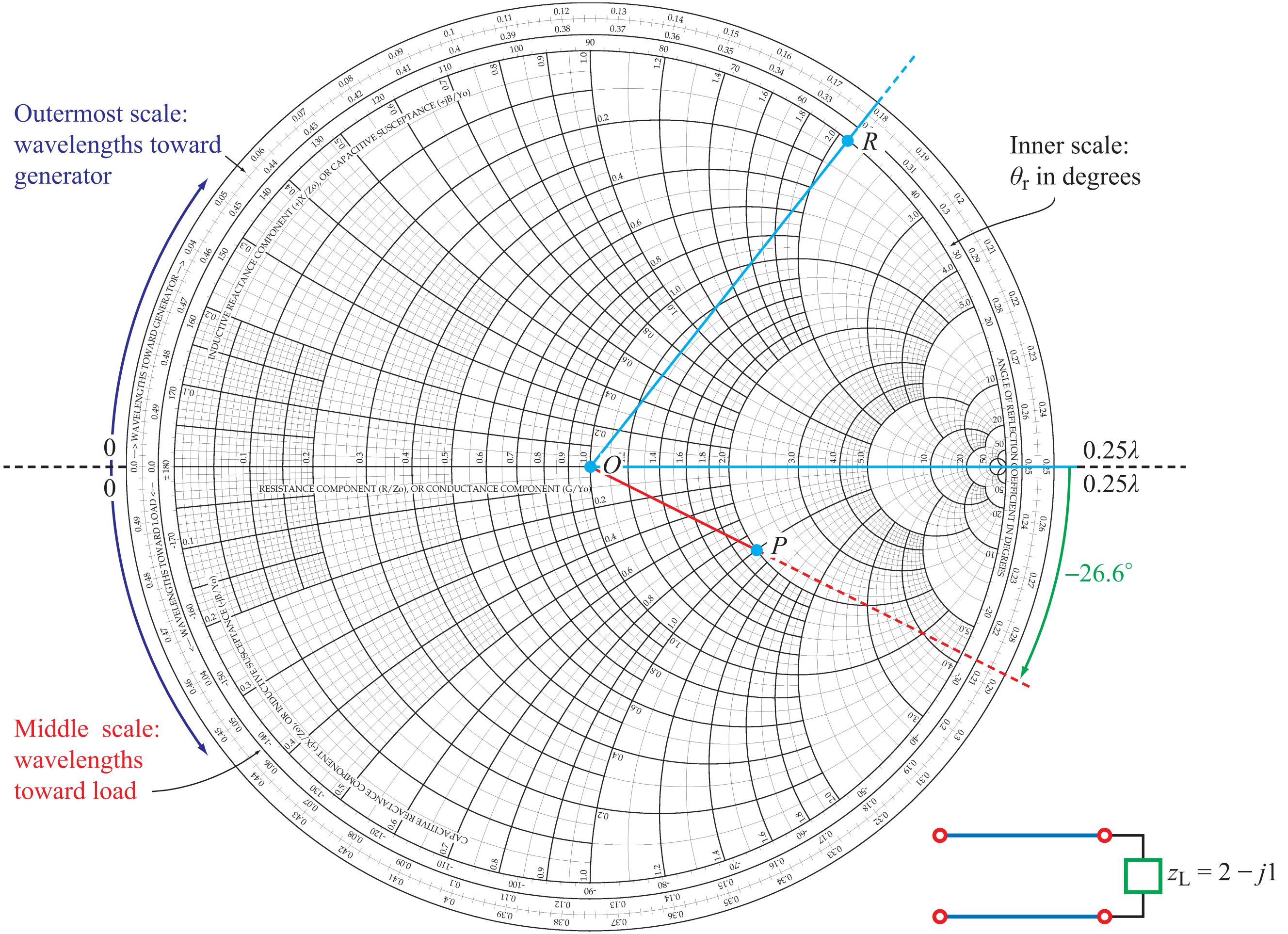

Figure 2-26 Point P represents a normalized load impedance $z_L = 2 - j1$. The reflection coefficient has a magnitude $|\Gamma| = \overline{OP}/\overline{OR} = 0.45$ and an angle $\theta_r = -26.6°$. Point R is an arbitrary point on the $r_L = 0$ circle (which also is the $|\Gamma| = 1$ circle).

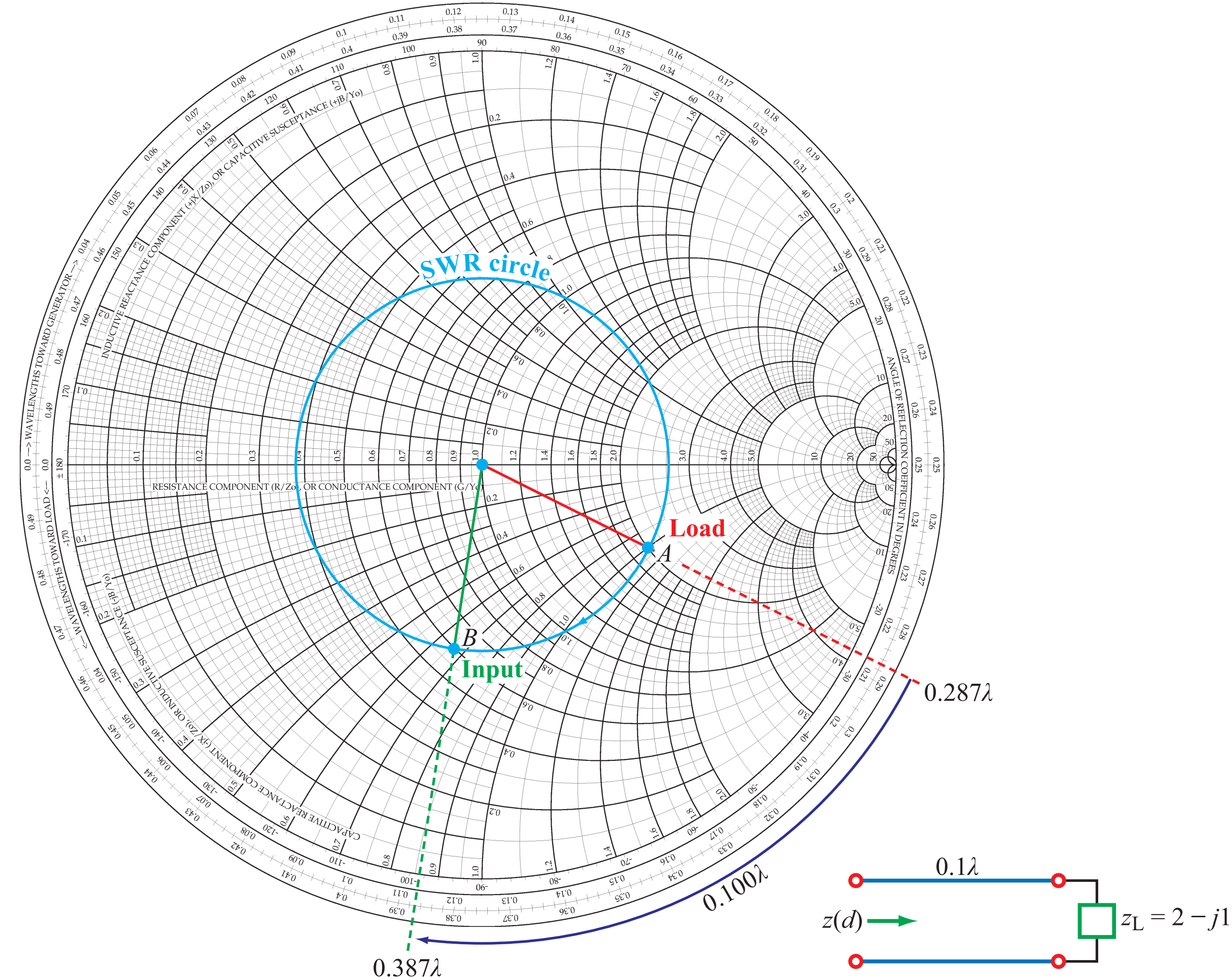

Figure 2-27 Point A represents a normalized load $z_L = 2 - j1$ at 0.287λ on the WTG scale. Point B represents the line input at $d = 0.1\lambda$ from the load. At B, $z(d) = 0.6 - j0.66$.

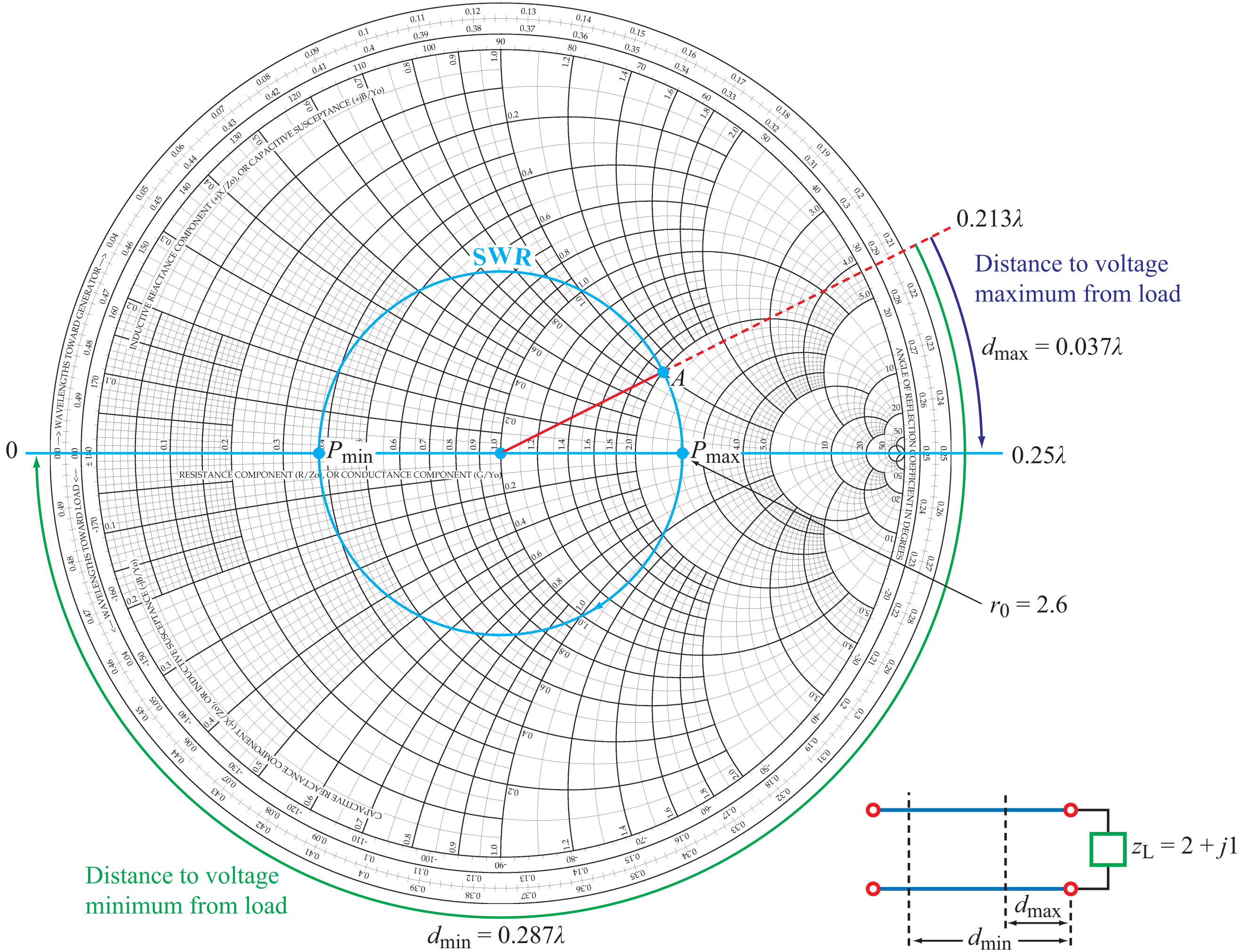

Figure 2-28 Point A represents a normalized load with $z_L = 2 + j1$. The standing wave ratio is $S = 2.6$ (at $P_{\max}$), the distance between the load and the first voltage maximum is $d_{\max} = (0.25 - 0.213)\lambda = 0.037\lambda$, and the distance between the load and the first voltage minimum is $d_{\min} = (0.037 + 0.25)\lambda = 0.287\lambda$.

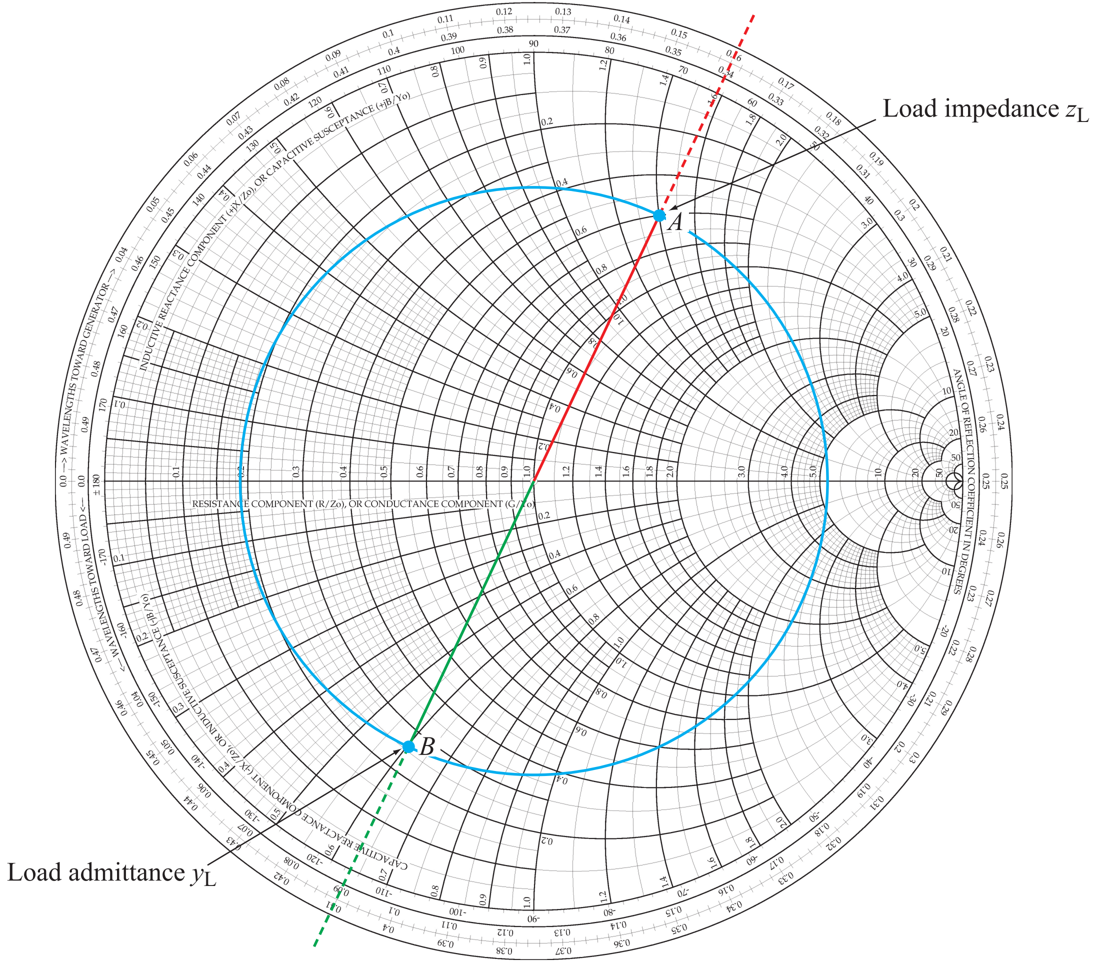

Figure 2-29 Point A represents a normalized load $z_L = 0.6 + j1.4$. Its corresponding normalized admittance is $y_L = 0.25 - j0.6$, and it is at point B.

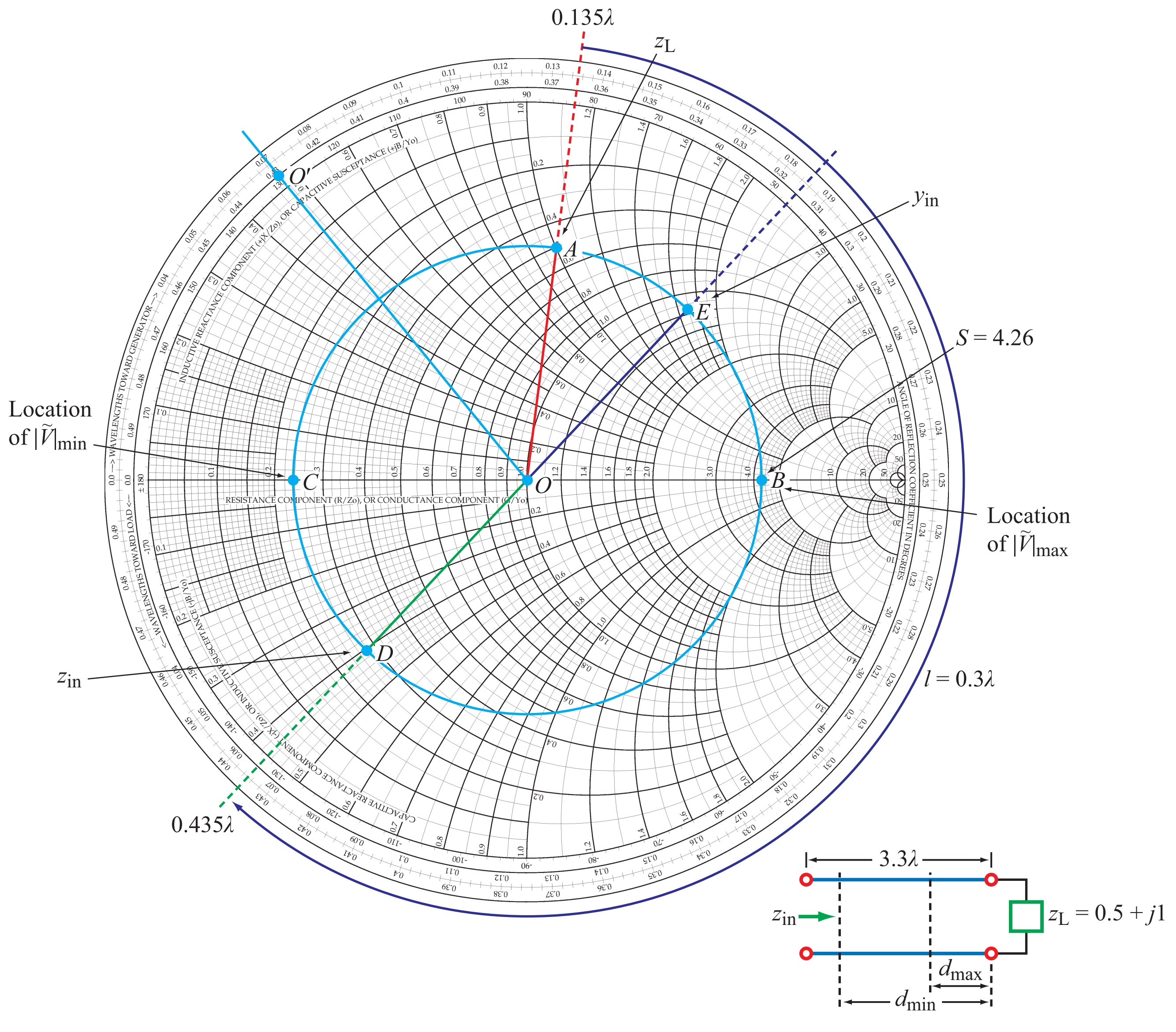

Figure 2-30 Solution for Example 2-11. Point A represents a normalized load $z_L = 0.5 + j1$ at 0.135λ on the WTG scale. At A, $\theta_r = 83^\circ$ and $|\Gamma| = \overline{OA}/\overline{OO'} = 0.62$. At B, the standing-wave ratio is $S = 4.26$. The distance from A to B gives $d_{max} = 0.115\lambda$ and from A to C gives $d_{min} = 0.365\lambda$. Point D represents the normalized input impedance $z_{in} = 0.28 - j0.40$, and point E represents the normalized input admittance $y_{in} = 1.15 + j1.7$.

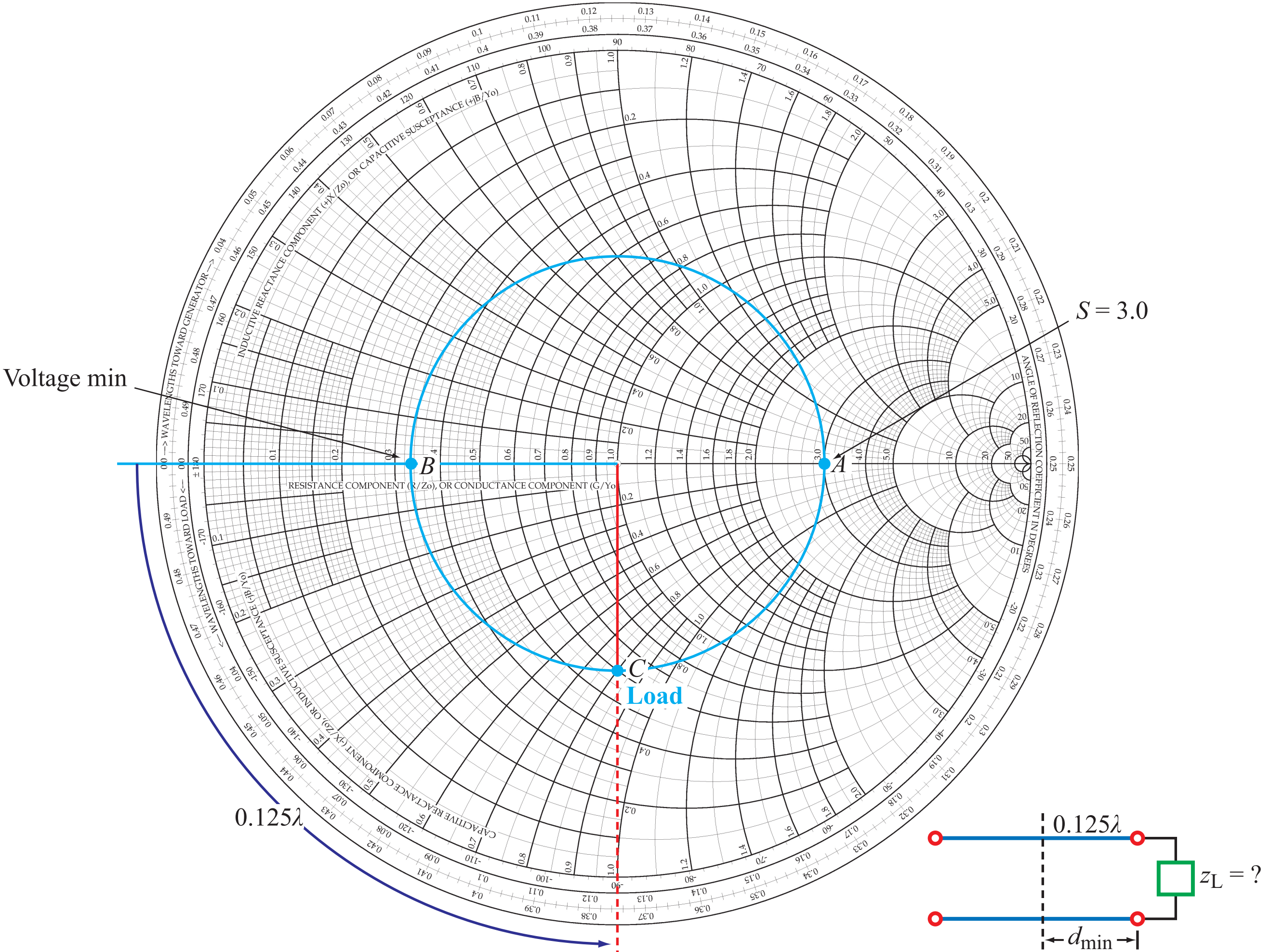

Figure 2-31 Solution for Example 2-12. Point A denotes that $S = 3$, point B represents the location of the voltage minimum, and point C represents the load at 0.125λ on the WTL scale from point B. At C, $z_L = 0.6 - j0.8$.

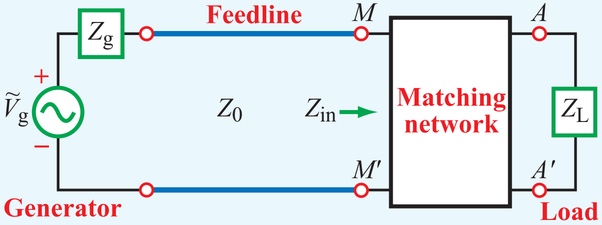

Figure 2-32 The function of a matching network is to transform the load impedance Z_L such that the input impedance Z_{in} looking into the network is equal to Z_0 of the feedline.

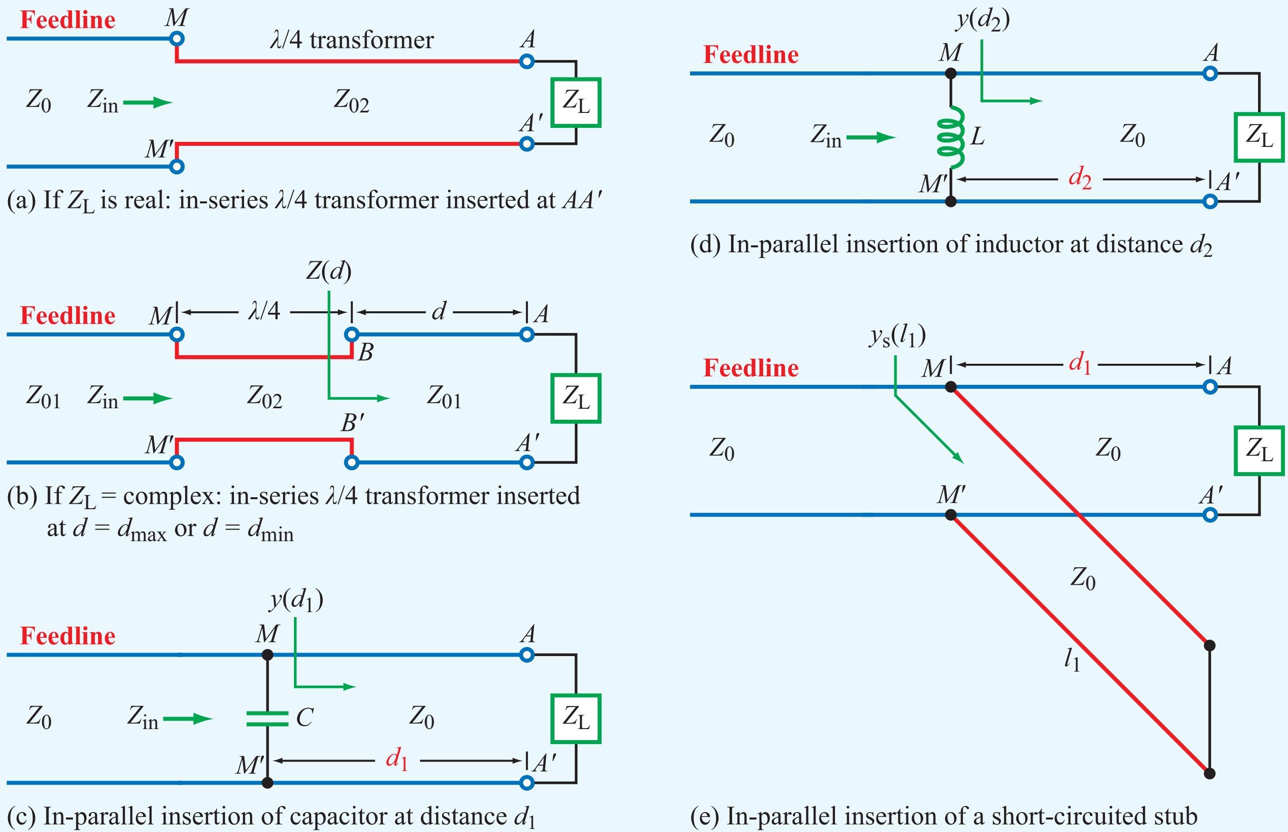

Figure 2-33 Five examples of in-series and in-parallel matching networks.

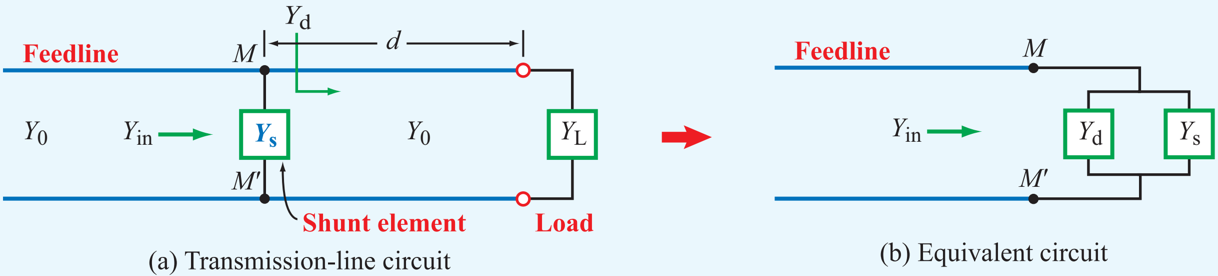

Figure 2-34 Inserting a reactive element with admittance Y_s at MM' modifies Y_d to Y_{in}.

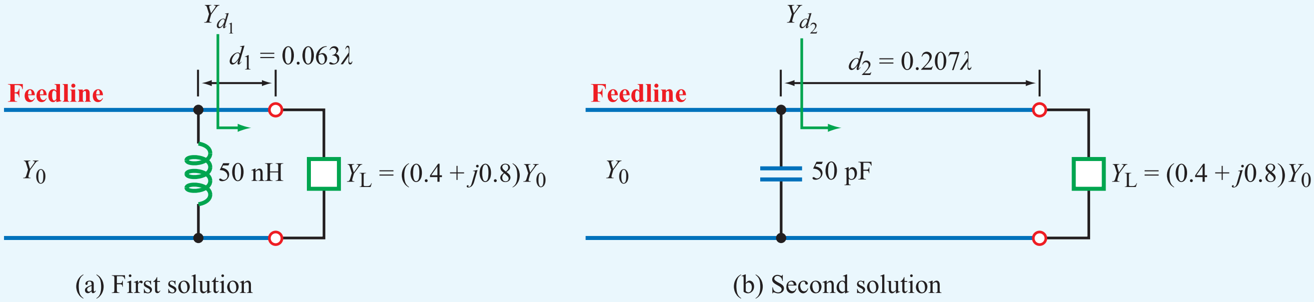

Figure 2-35 Solutions for Example 2-13.

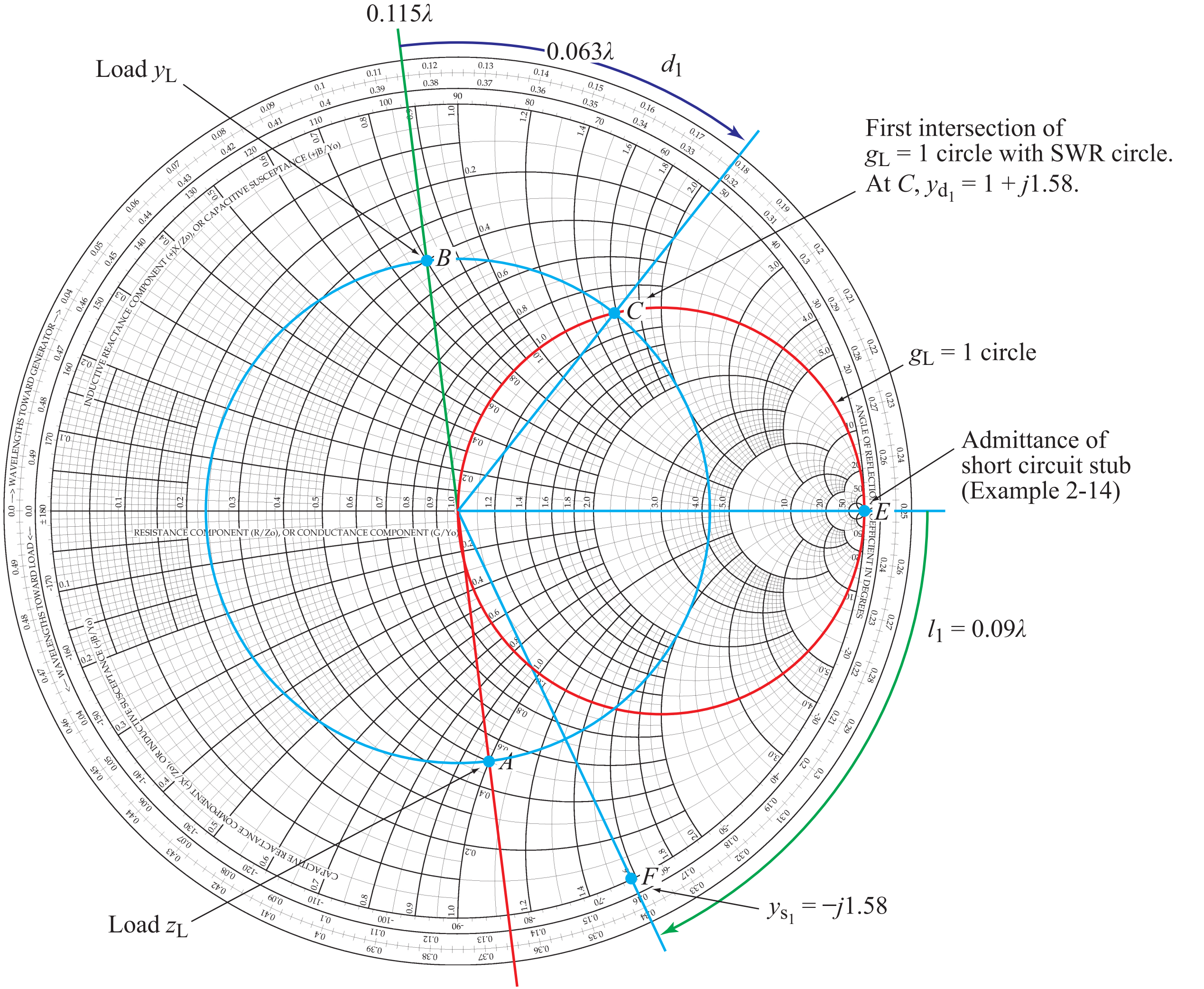

Figure 2-36 Solution for point C of Examples 2-13 and 2-14. Point A is the normalized load with $z_L = 0.5 - j1$; point B is $y_L = 0.4 + j0.8$. Point C is the intersection of the SWR circle with the $g_L = 1$ circle. The distance from B to C is $d_1 = 0.063\lambda$. The length of the shorted stub (E to F) is $l_1 = 0.09\lambda$ (Example 2-14).

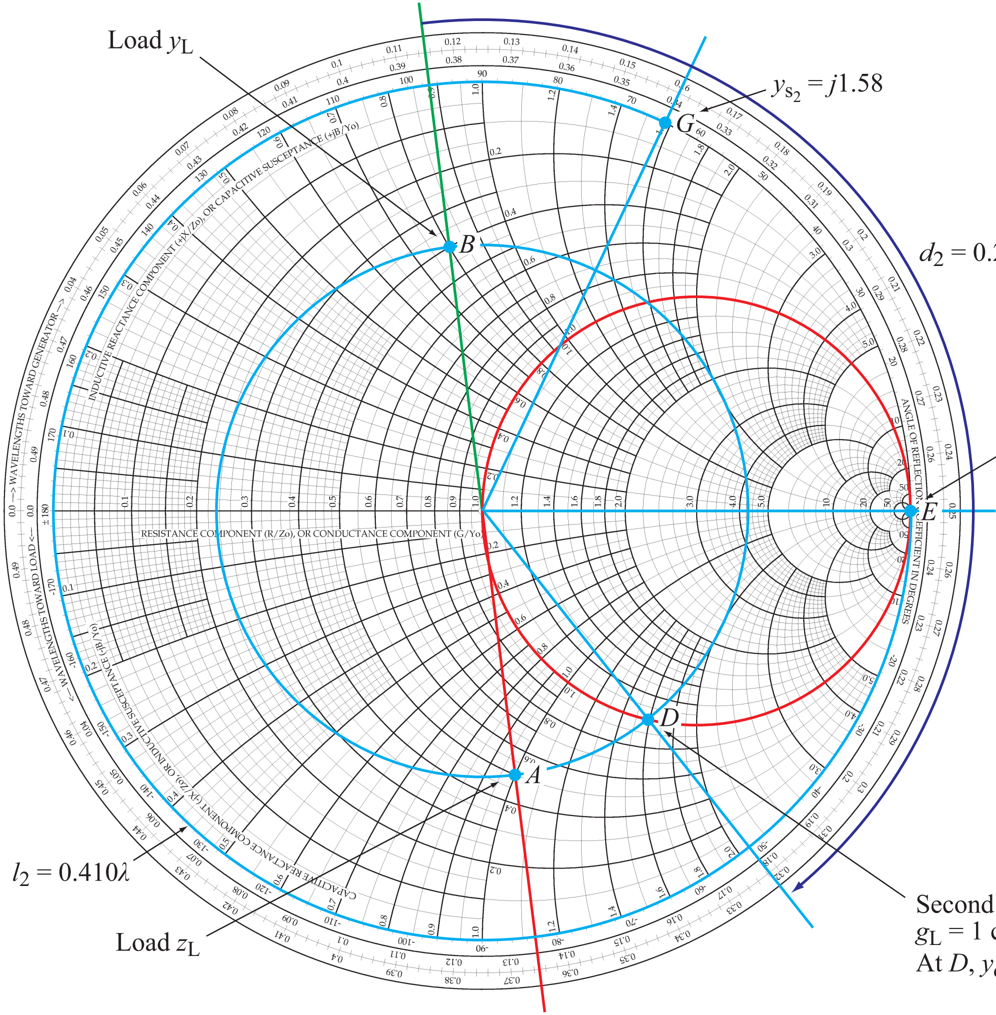

Figure 2-37 Solution for point D of Examples 2-13 and 2-14. Point D is the second point of intersection of the SWR circle and the $g_L = 1$ circle. The distance B to D gives $d_2 = 0.207\lambda$, and the distance E to G gives $l_2 = 0.410\lambda$ (Example 2-14).

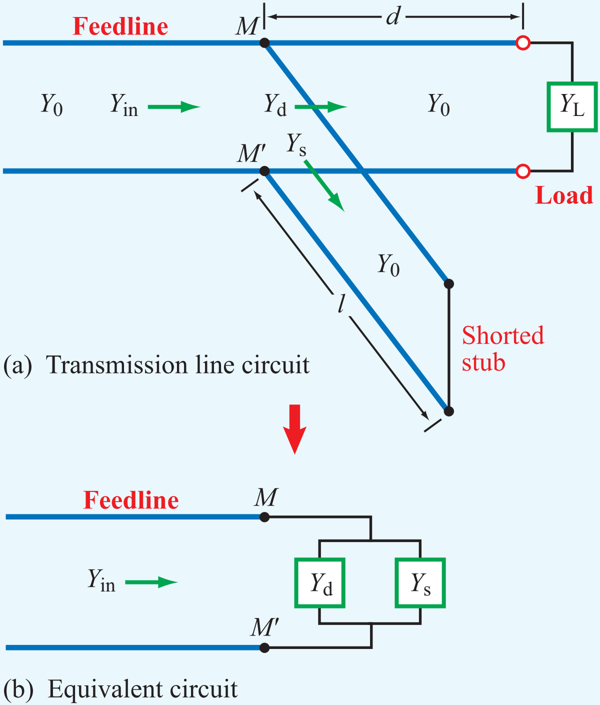

Figure 2-38 Shorted-stub matching network.

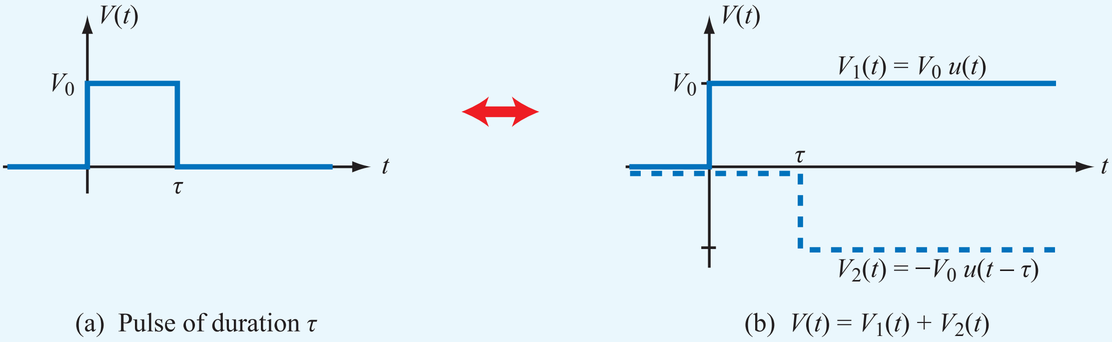

Figure 2-39 A rectangular pulse $V(t)$ of duration τ can be represented as the sum of two step functions of opposite polarities displaced by τ relative to each other.

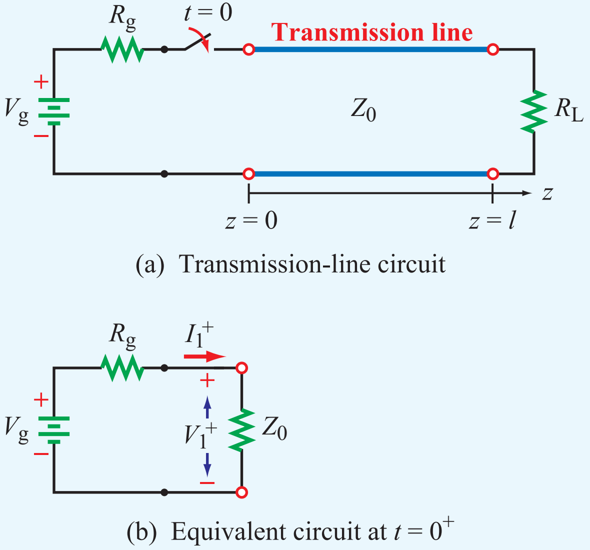

Figure 2-40 At $t = 0^+$, immediately after closing the switch in the circuit in (a), the circuit can be represented by the equivalent circuit in (b).

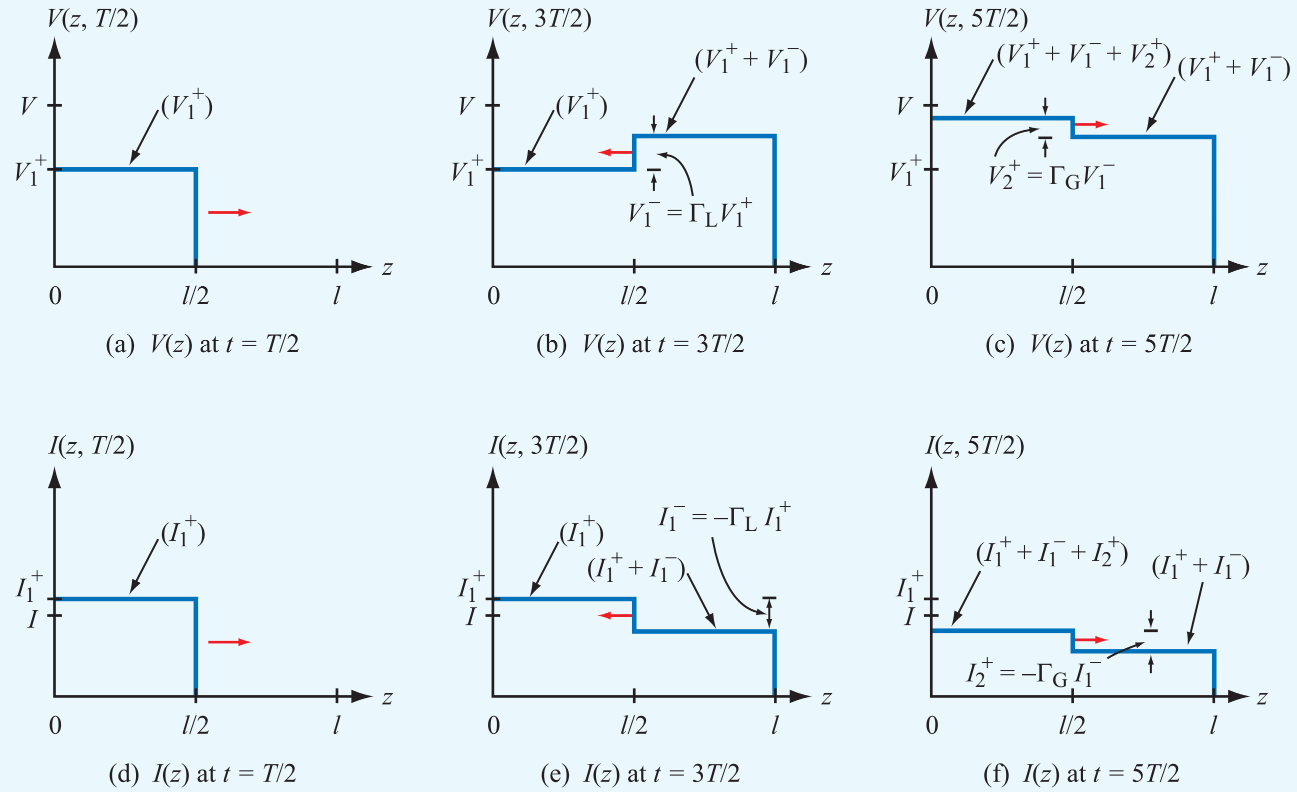

Figure 2-41 Voltage and current distributions on a lossless transmission line at $t = T/2$, $t = 3T/2$, and $t = 5T/2$, due to a unit step voltage applied to a circuit with $R_g = 4Z_0$ and $R_L = 2Z_0$. The corresponding reflection coefficients are $\Gamma_L = 1/3$ and $\Gamma_g = 3/5$.

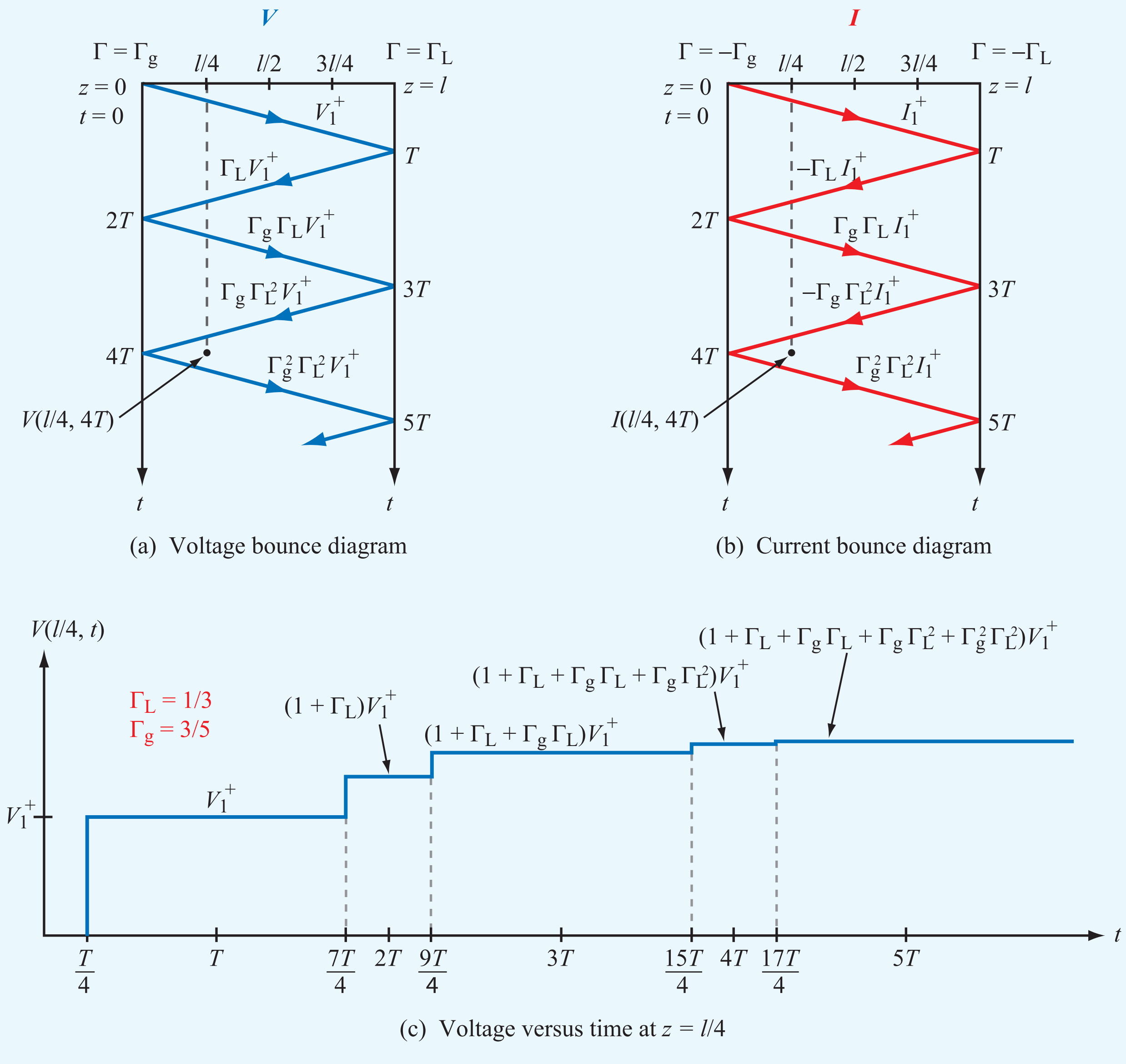

Figure 2-42 Bounce diagrams for (a) voltage and (b) current. In (c), the voltage variation with time at $z = l/4$ for a circuit with $\Gamma_g = 3/5$ and $\Gamma_L = 1/3$ is deduced from the vertical dashed line at $l/4$ in (a).

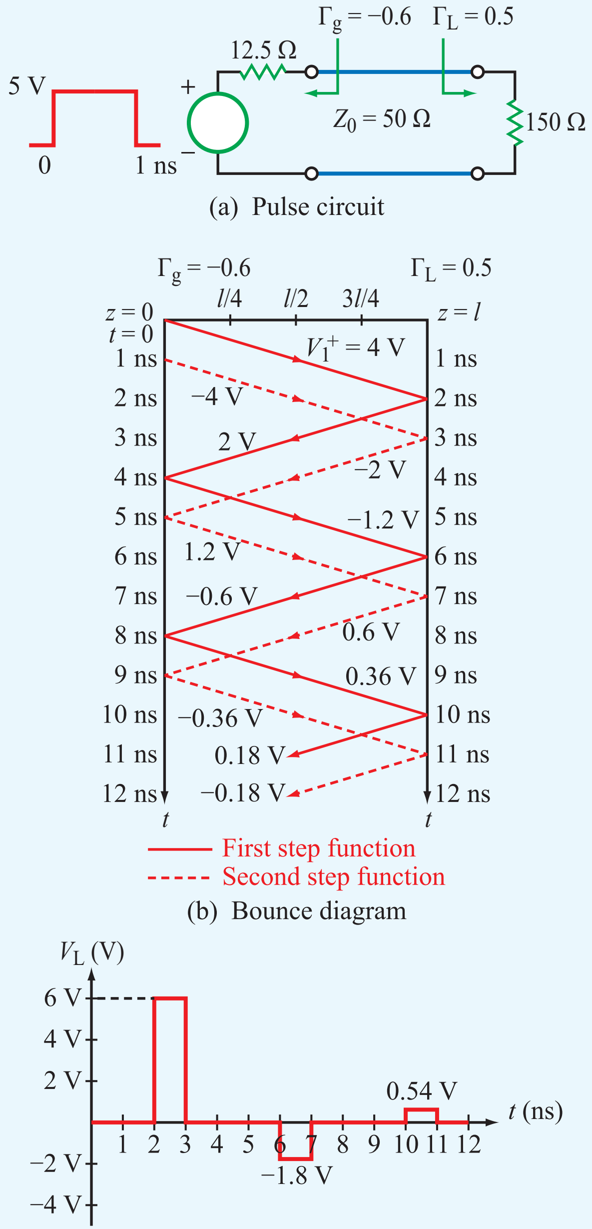

(a) Pulse circuit

(b) Bounce diagram

(c) Voltage waveform at the load

Figure 2-43 Example 2-15.

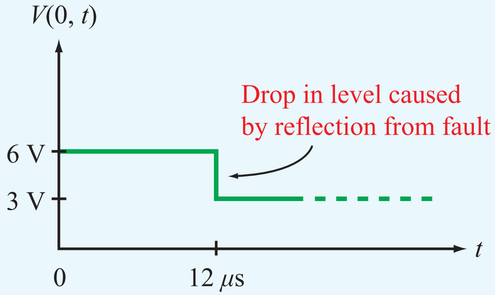

(a) Observed voltage at the sending end

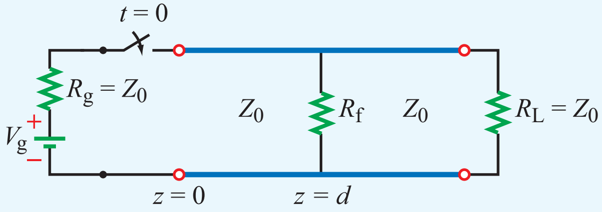

(b) The fault at $z = d$ is represented by a fault resistance R_f

Figure 2-44 Time-domain reflectometer of Example 2-16.

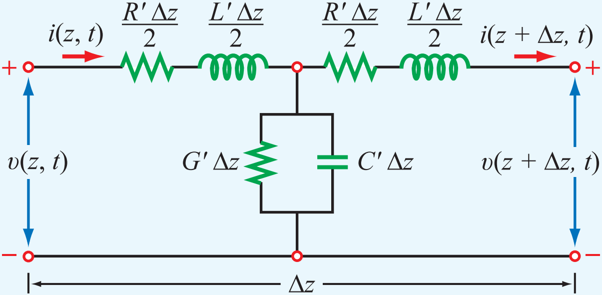

Figure P2.3 Transmission-line model for Problem 2.3.

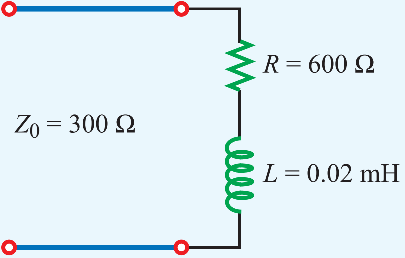

Figure P2.20 Circuit for Problem 2.20.

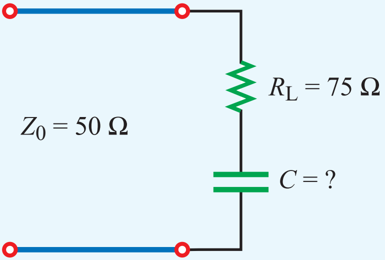

Figure P2.26 Circuit for Problem 2.26.

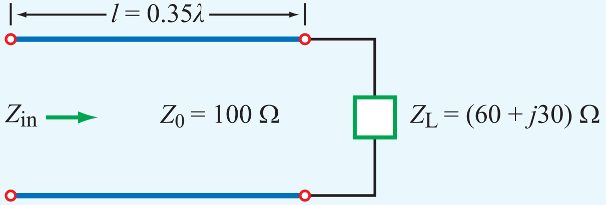

Figure P2.28 Circuit for Problem 2.28.

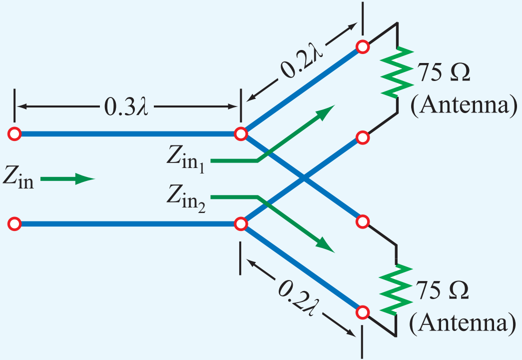

Figure P2.33 Circuit for Problem 2.33.

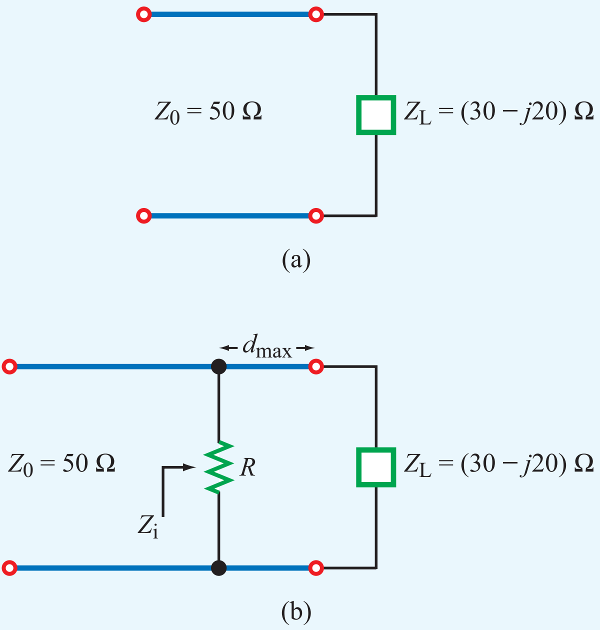

Figure P2.34 Circuit for Problem 2.34.

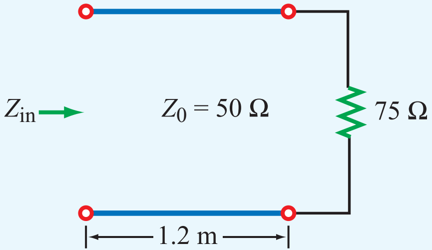

Figure P2.35 Circuit for Problem 2.35.

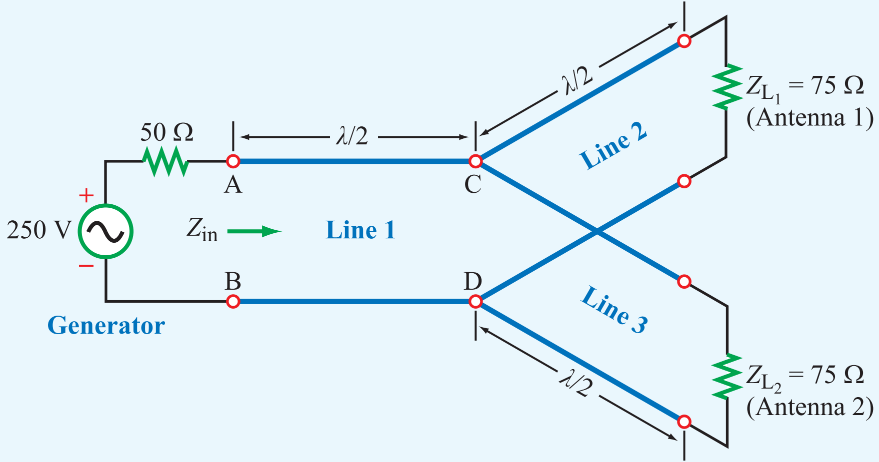

Figure P2.43 Antenna configuration for Problem 2.43.

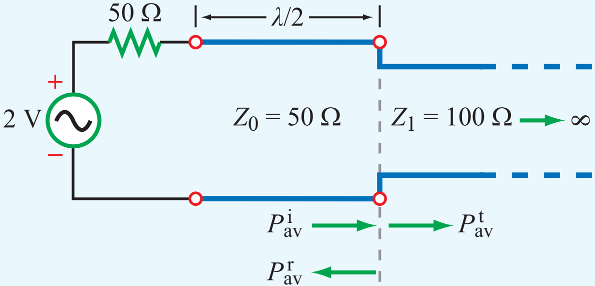

Figure P2.44 Circuit for Problem 2.44.

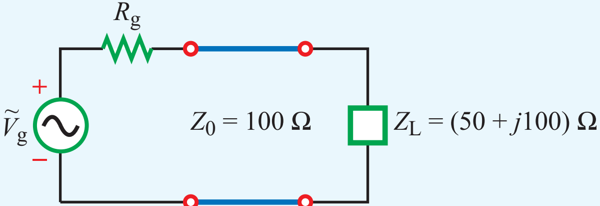

Figure P2.45 Circuit for Problem 2.45.

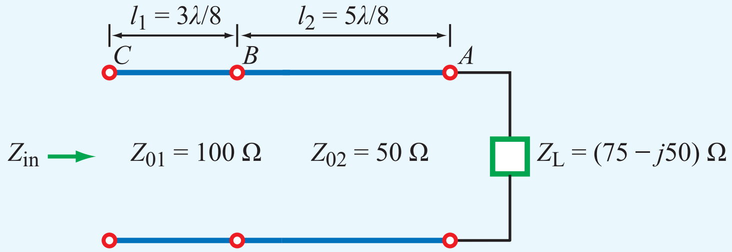

Figure P2.50 Circuit for Problem 2.50.

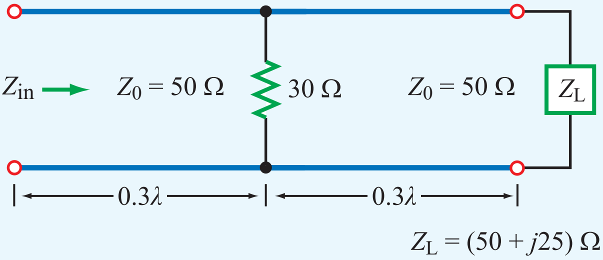

Figure P2.63 Circuit for Problem 2.63.

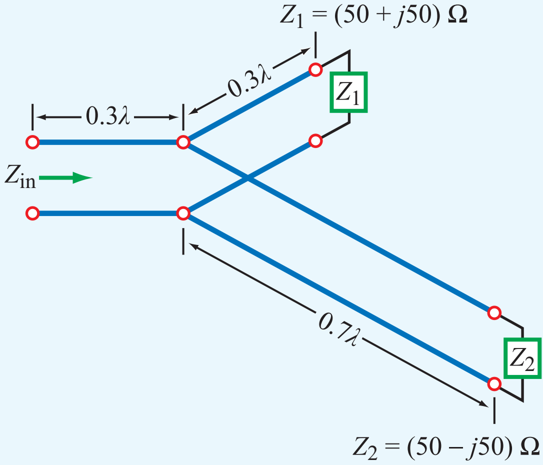

Figure P2.72 Network for Problem 2.72.

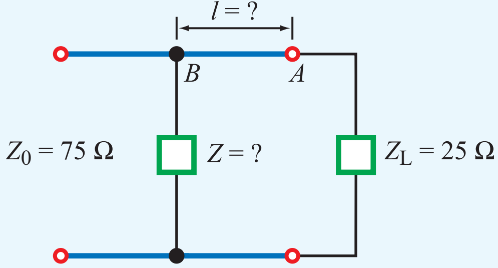

Figure P2.74 Circuit for Problem 2.74.

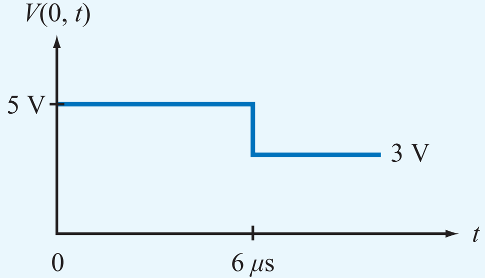

Figure P2.77 Voltage waveform for Problems 2.77 and 2.79.

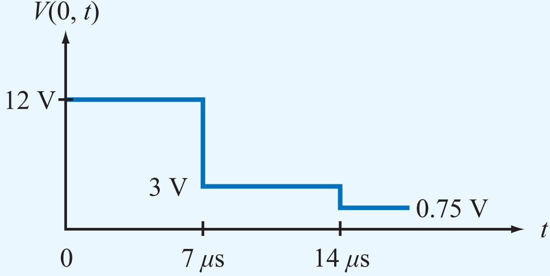

Figure P2.78 Voltage waveform of Problem 2.78.

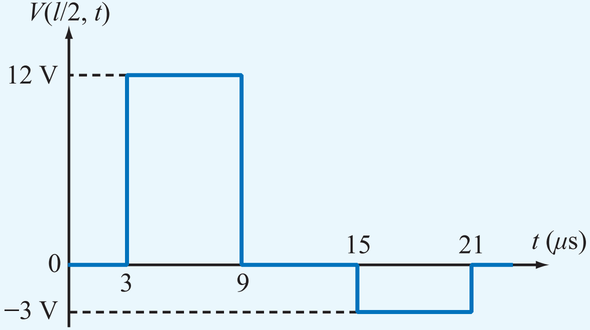

Figure P2.82 Circuit for Problem 2.82.

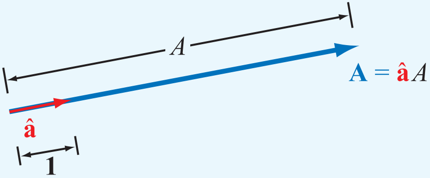

Figure 3-1 Vector $\mathbf{A} = \hat{\mathbf{a}}A$ has magnitude $A = |\mathbf{A}|$ and points in the direction of unit vector $\hat{\mathbf{a}} = \mathbf{A}/A$.

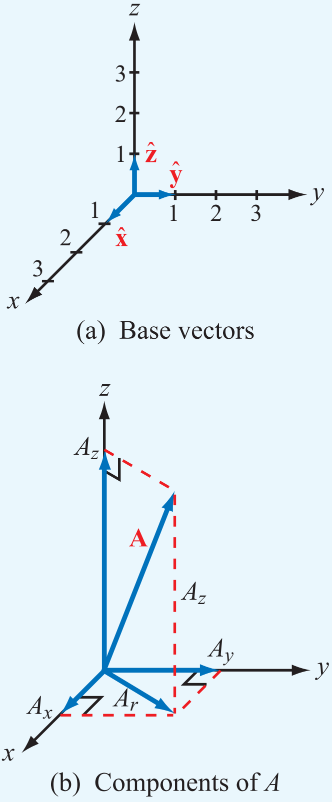

Figure 3-2 Cartesian coordinate system: (a) base vectors $\hat{\mathbf{x}}$, $\hat{\mathbf{y}}$, and $\hat{\mathbf{z}}$, and (b) components of vector $\mathbf{A}$.

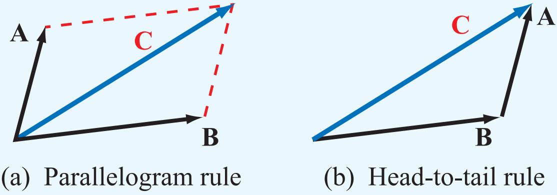

Figure 3-3 Vector addition by (a) the parallelogram rule and (b) the head-to-tail rule.

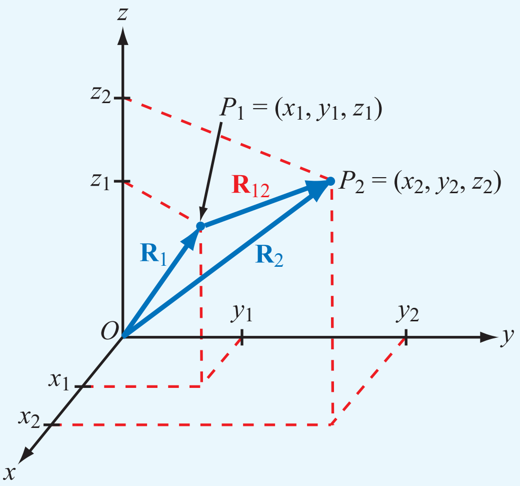

Figure 3-4 Distance vector $\mathbf{R}_{12} = \overrightarrow{P_1P_2} = \mathbf{R}_2 - \mathbf{R}_1$, where $\mathbf{R}_1$ and $\mathbf{R}_2$ are the position vectors of points P_1 and P_2, respectively.

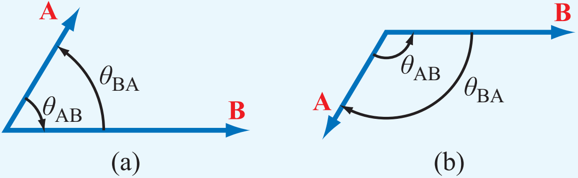

Figure 3-5 The angle θ_{AB} is the angle between **A** and **B**, measured from **A** to **B** between vector tails. The dot product is positive if $0 \leq \theta_{AB} < 90^\circ$, as in (a), and it is negative if $90^\circ < \theta_{AB} \leq 180^\circ$, as in (b).

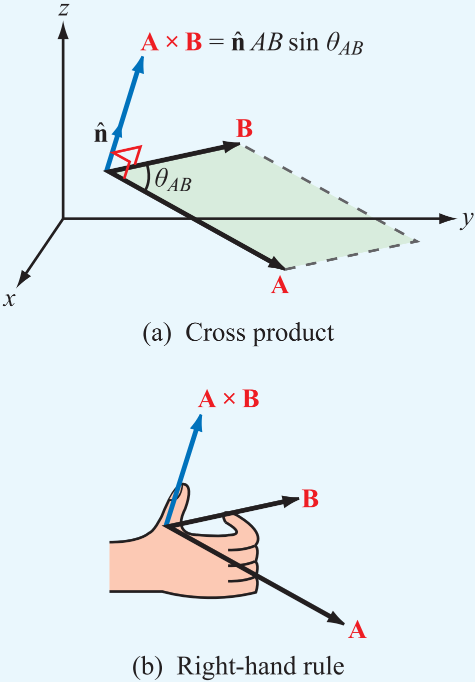

Figure 3-6 Cross product $\mathbf{A} \times \mathbf{B}$ points in the direction $\hat{\mathbf{n}}$, which is perpendicular to the plane containing **A** and **B** and defined by the right-hand rule.

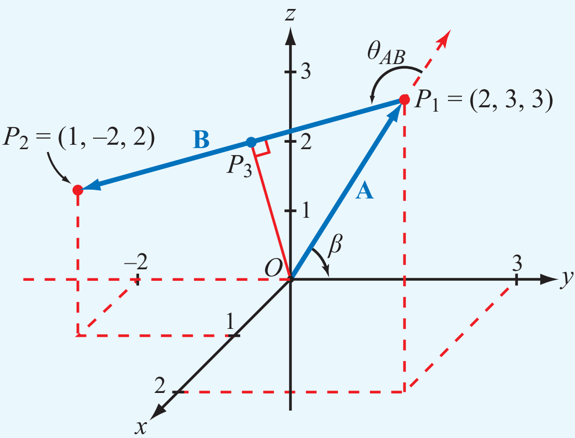

Figure 3-7 Geometry of Example 3-1.

Table 3-1 **Summary of vector relations.**

	Cartesian Coordinates	Cylindrical Coordinates	Spherical Coordinates
Coordinate variables	x, y, z	r, ϕ, z	R, θ, ϕ
Vector representation $\mathbf{A} =$	$\hat{\mathbf{x}}A_x + \hat{\mathbf{y}}A_y + \hat{\mathbf{z}}A_z$	$\hat{\mathbf{r}}A_r + \hat{\boldsymbol{\phi}}A_\phi + \hat{\mathbf{z}}A_z$	$\hat{\mathbf{R}}A_R + \hat{\boldsymbol{\theta}}A_\theta + \hat{\boldsymbol{\phi}}A_\phi$
Magnitude of A $\lvert\mathbf{A}\rvert =$	$\sqrt[+]{A_x^2 + A_y^2 + A_z^2}$	$\sqrt[+]{A_r^2 + A_\phi^2 + A_z^2}$	$\sqrt[+]{A_R^2 + A_\theta^2 + A_\phi^2}$
Position vector $\overrightarrow{OP_1} =$	$\hat{\mathbf{x}}x_1 + \hat{\mathbf{y}}y_1 + \hat{\mathbf{z}}z_1$, for $P(x_1, y_1, z_1)$	$\hat{\mathbf{r}}r_1 + \hat{\mathbf{z}}z_1$, for $P(r_1, \phi_1, z_1)$	$\hat{\mathbf{R}}R_1$, for $P(R_1, \theta_1, \phi_1)$
Base vectors properties	$\hat{\mathbf{x}}\cdot\hat{\mathbf{x}} = \hat{\mathbf{y}}\cdot\hat{\mathbf{y}} = \hat{\mathbf{z}}\cdot\hat{\mathbf{z}} = 1$ $\hat{\mathbf{x}}\cdot\hat{\mathbf{y}} = \hat{\mathbf{y}}\cdot\hat{\mathbf{z}} = \hat{\mathbf{z}}\cdot\hat{\mathbf{x}} = 0$ $\hat{\mathbf{x}}\times\hat{\mathbf{y}} = \hat{\mathbf{z}}$ $\hat{\mathbf{y}}\times\hat{\mathbf{z}} = \hat{\mathbf{x}}$ $\hat{\mathbf{z}}\times\hat{\mathbf{x}} = \hat{\mathbf{y}}$	$\hat{\mathbf{r}}\cdot\hat{\mathbf{r}} = \hat{\boldsymbol{\phi}}\cdot\hat{\boldsymbol{\phi}} = \hat{\mathbf{z}}\cdot\hat{\mathbf{z}} = 1$ $\hat{\mathbf{r}}\cdot\hat{\boldsymbol{\phi}} = \hat{\boldsymbol{\phi}}\cdot\hat{\mathbf{z}} = \hat{\mathbf{z}}\cdot\hat{\mathbf{r}} = 0$ $\hat{\mathbf{r}}\times\hat{\boldsymbol{\phi}} = \hat{\mathbf{z}}$ $\hat{\boldsymbol{\phi}}\times\hat{\mathbf{z}} = \hat{\mathbf{r}}$ $\hat{\mathbf{z}}\times\hat{\mathbf{r}} = \hat{\boldsymbol{\phi}}$	$\hat{\mathbf{R}}\cdot\hat{\mathbf{R}} = \hat{\boldsymbol{\theta}}\cdot\hat{\boldsymbol{\theta}} = \hat{\boldsymbol{\phi}}\cdot\hat{\boldsymbol{\phi}} = 1$ $\hat{\mathbf{R}}\cdot\hat{\boldsymbol{\theta}} = \hat{\boldsymbol{\theta}}\cdot\hat{\boldsymbol{\phi}} = \hat{\boldsymbol{\phi}}\cdot\hat{\mathbf{R}} = 0$ $\hat{\mathbf{R}}\times\hat{\boldsymbol{\theta}} = \hat{\boldsymbol{\phi}}$ $\hat{\boldsymbol{\theta}}\times\hat{\boldsymbol{\phi}} = \hat{\mathbf{R}}$ $\hat{\boldsymbol{\phi}}\times\hat{\mathbf{R}} = \hat{\boldsymbol{\theta}}$
Dot product $\mathbf{A}\cdot\mathbf{B} =$	$A_xB_x + A_yB_y + A_zB_z$	$A_rB_r + A_\phi B_\phi + A_zB_z$	$A_RB_R + A_\theta B_\theta + A_\phi B_\phi$
Cross product $\mathbf{A}\times\mathbf{B} =$	$\begin{vmatrix} \hat{\mathbf{x}} & \hat{\mathbf{y}} & \hat{\mathbf{z}} \\ A_x & A_y & A_z \\ B_x & B_y & B_z \end{vmatrix}$	$\begin{vmatrix} \hat{\mathbf{r}} & \hat{\boldsymbol{\phi}} & \hat{\mathbf{z}} \\ A_r & A_\phi & A_z \\ B_r & B_\phi & B_z \end{vmatrix}$	$\begin{vmatrix} \hat{\mathbf{R}} & \hat{\boldsymbol{\theta}} & \hat{\boldsymbol{\phi}} \\ A_R & A_\theta & A_\phi \\ B_R & B_\theta & B_\phi \end{vmatrix}$
Differential length $d\mathbf{l} =$	$\hat{\mathbf{x}}\,dx + \hat{\mathbf{y}}\,dy + \hat{\mathbf{z}}\,dz$	$\hat{\mathbf{r}}\,dr + \hat{\boldsymbol{\phi}}r\,d\phi + \hat{\mathbf{z}}\,dz$	$\hat{\mathbf{R}}\,dR + \hat{\boldsymbol{\theta}}R\,d\theta + \hat{\boldsymbol{\phi}}R\sin\theta\,d\phi$
Differential surface areas	$d\mathbf{s}_x = \hat{\mathbf{x}}\,dy\,dz$ $d\mathbf{s}_y = \hat{\mathbf{y}}\,dx\,dz$ $d\mathbf{s}_z = \hat{\mathbf{z}}\,dx\,dy$	$d\mathbf{s}_r = \hat{\mathbf{r}}r\,d\phi\,dz$ $d\mathbf{s}_\phi = \hat{\boldsymbol{\phi}}\,dr\,dz$ $d\mathbf{s}_z = \hat{\mathbf{z}}r\,dr\,d\phi$	$d\mathbf{s}_R = \hat{\mathbf{R}}R^2\sin\theta\,d\theta\,d\phi$ $d\mathbf{s}_\theta = \hat{\boldsymbol{\theta}}R\sin\theta\,dR\,d\phi$ $d\mathbf{s}_\phi = \hat{\boldsymbol{\phi}}R\,dR\,d\theta$
Differential volume $dV =$	$dx\,dy\,dz$	$r\,dr\,d\phi\,dz$	$R^2\sin\theta\,dR\,d\theta\,d\phi$

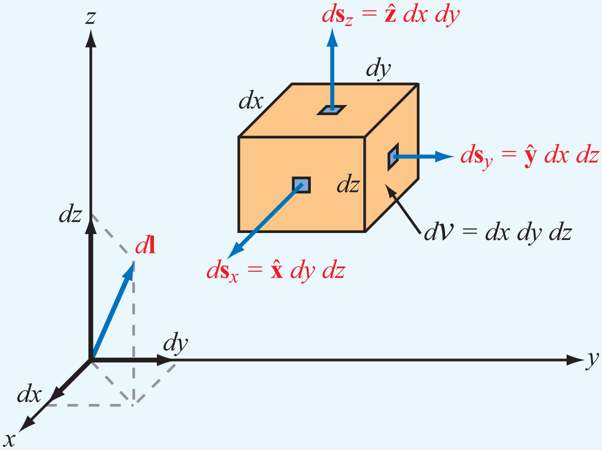

Figure 3-8 Differential length, area, and volume in Cartesian coordinates.

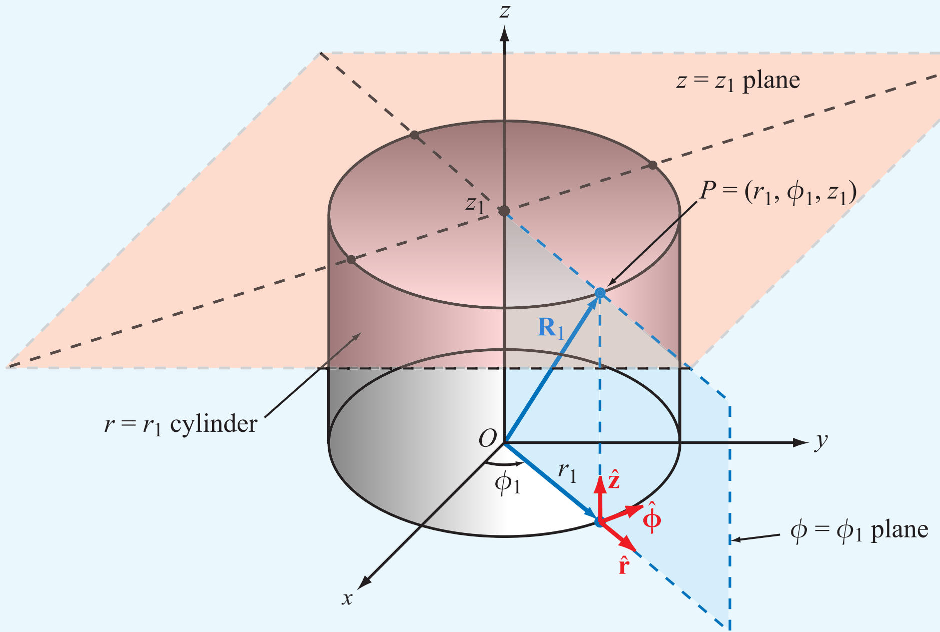

Figure 3-9 Point $P(r_1, \phi_1, z_1)$ in cylindrical coordinates; r_1 is the radial distance from the origin in the x–y plane, ϕ_1 is the angle in the x–y plane measured from the x axis toward the y axis, and z_1 is the vertical distance from the x–y plane.

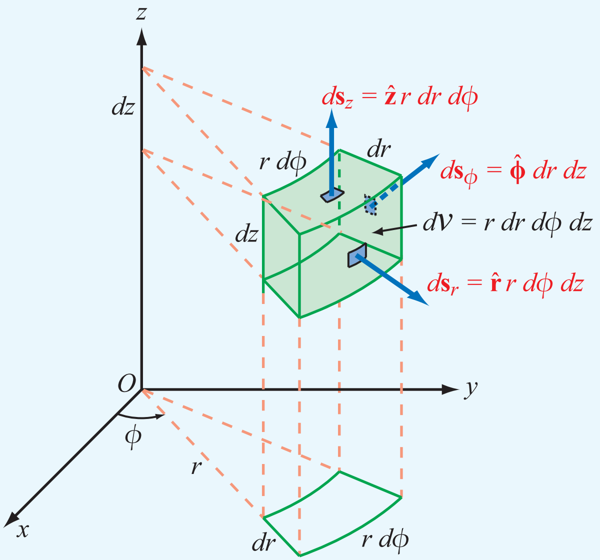

Figure 3-10 Differential areas and volume in cylindrical coordinates.

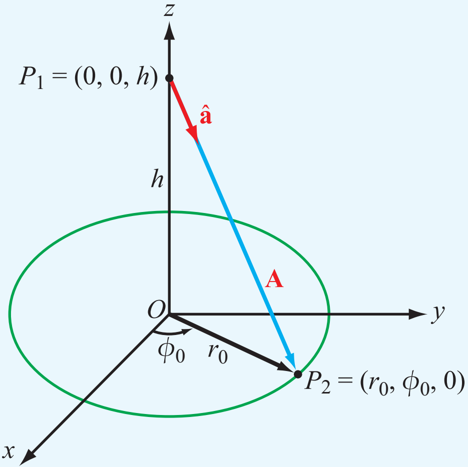

Figure 3-11 Geometry of Example 3-3.

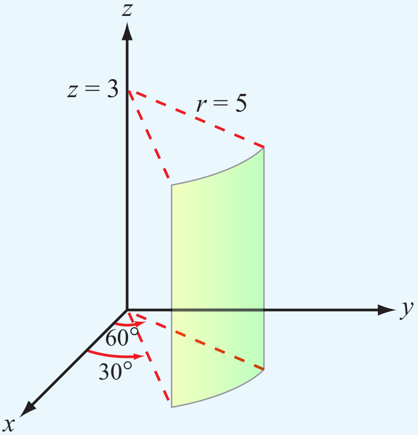

Figure 3-12 Cylindrical surface of Example 3-4.

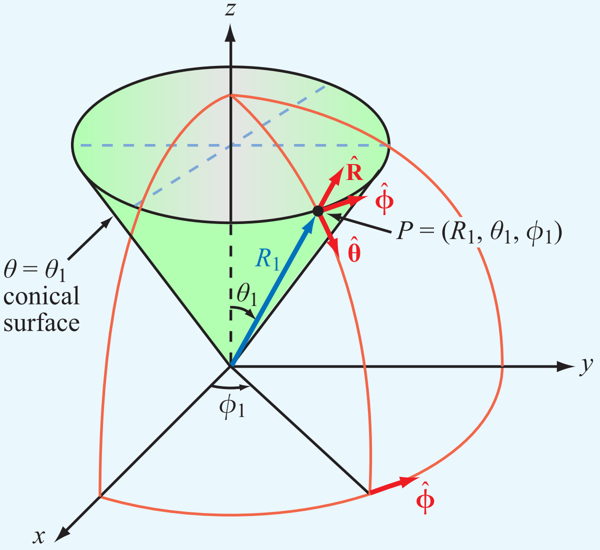

Figure 3-13 Point $P(R_1, \theta_1, \phi_1)$ in spherical coordinates.

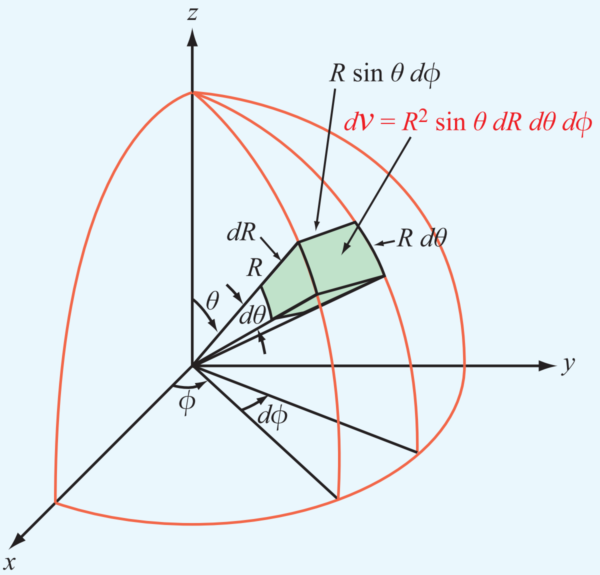

Figure 3-14 Differential volume in spherical coordinates.

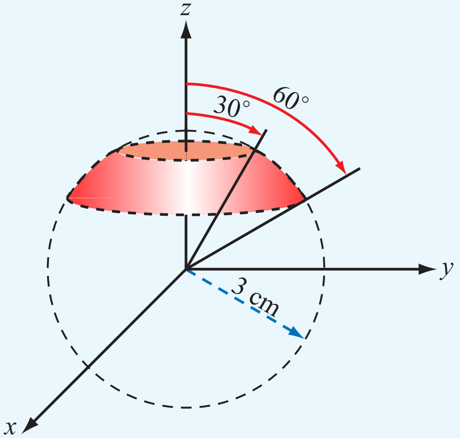

Figure 3-15 Spherical strip of Example 3-5.

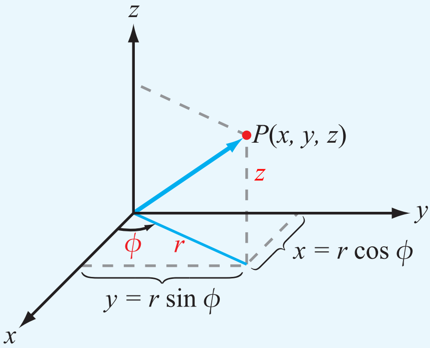

Figure 3-16 Interrelationships between Cartesian coordinates (x, y, z) and cylindrical coordinates (r, ϕ, z).

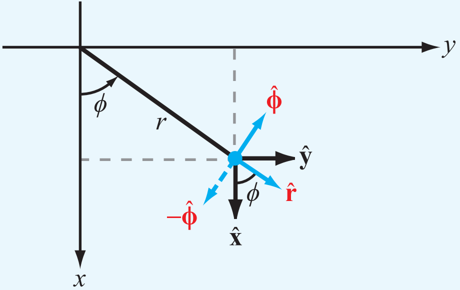

Figure 3-17 Interrelationships between base vectors $(\hat{\mathbf{x}}, \hat{\mathbf{y}})$ and $(\hat{\mathbf{r}}, \hat{\boldsymbol{\phi}})$.

Table 3-2 Coordinate transformation relations.

Transformation	Coordinate Variables	Unit Vectors	Vector Components
Cartesian to cylindrical	$r = \sqrt[+]{x^2 + y^2}$ $\phi = \tan^{-1}(y/x)$ $z = z$	$\hat{\mathbf{r}} = \hat{\mathbf{x}} \cos\phi + \hat{\mathbf{y}} \sin\phi$ $\hat{\boldsymbol{\phi}} = -\hat{\mathbf{x}} \sin\phi + \hat{\mathbf{y}} \cos\phi$ $\hat{\mathbf{z}} = \hat{\mathbf{z}}$	$A_r = A_x \cos\phi + A_y \sin\phi$ $A_\phi = -A_x \sin\phi + A_y \cos\phi$ $A_z = A_z$
Cylindrical to Cartesian	$x = r\cos\phi$ $y = r\sin\phi$ $z = z$	$\hat{\mathbf{x}} = \hat{\mathbf{r}} \cos\phi - \hat{\boldsymbol{\phi}} \sin\phi$ $\hat{\mathbf{y}} = \hat{\mathbf{r}} \sin\phi + \hat{\boldsymbol{\phi}} \cos\phi$ $\hat{\mathbf{z}} = \hat{\mathbf{z}}$	$A_x = A_r \cos\phi - A_\phi \sin\phi$ $A_y = A_r \sin\phi + A_\phi \cos\phi$ $A_z = A_z$
Cartesian to spherical	$R = \sqrt[+]{x^2 + y^2 + z^2}$ $\theta = \tan^{-1}[\sqrt[+]{x^2 + y^2}/z]$ $\phi = \tan^{-1}(y/x)$	$\hat{\mathbf{R}} = \hat{\mathbf{x}} \sin\theta\cos\phi + \hat{\mathbf{y}} \sin\theta\sin\phi + \hat{\mathbf{z}} \cos\theta$ $\hat{\boldsymbol{\theta}} = \hat{\mathbf{x}} \cos\theta\cos\phi + \hat{\mathbf{y}} \cos\theta\sin\phi - \hat{\mathbf{z}} \sin\theta$ $\hat{\boldsymbol{\phi}} = -\hat{\mathbf{x}} \sin\phi + \hat{\mathbf{y}} \cos\phi$	$A_R = A_x \sin\theta\cos\phi + A_y \sin\theta\sin\phi + A_z \cos\theta$ $A_\theta = A_x \cos\theta\cos\phi + A_y \cos\theta\sin\phi - A_z \sin\theta$ $A_\phi = -A_x \sin\phi + A_y \cos\phi$
Spherical to Cartesian	$x = R\sin\theta\cos\phi$ $y = R\sin\theta\sin\phi$ $z = R\cos\theta$	$\hat{\mathbf{x}} = \hat{\mathbf{R}} \sin\theta\cos\phi + \hat{\boldsymbol{\theta}} \cos\theta\cos\phi - \hat{\boldsymbol{\phi}} \sin\phi$ $\hat{\mathbf{y}} = \hat{\mathbf{R}} \sin\theta\sin\phi + \hat{\boldsymbol{\theta}} \cos\theta\sin\phi + \hat{\boldsymbol{\phi}} \cos\phi$ $\hat{\mathbf{z}} = \hat{\mathbf{R}} \cos\theta - \hat{\boldsymbol{\theta}} \sin\theta$	$A_x = A_R \sin\theta\cos\phi + A_\theta \cos\theta\cos\phi - A_\phi \sin\phi$ $A_y = A_R \sin\theta\sin\phi + A_\theta \cos\theta\sin\phi + A_\phi \cos\phi$ $A_z = A_R \cos\theta - A_\theta \sin\theta$
Cylindrical to spherical	$R = \sqrt[+]{r^2 + z^2}$ $\theta = \tan^{-1}(r/z)$ $\phi = \phi$	$\hat{\mathbf{R}} = \hat{\mathbf{r}} \sin\theta + \hat{\mathbf{z}} \cos\theta$ $\hat{\boldsymbol{\theta}} = \hat{\mathbf{r}} \cos\theta - \hat{\mathbf{z}} \sin\theta$ $\hat{\boldsymbol{\phi}} = \hat{\boldsymbol{\phi}}$	$A_R = A_r \sin\theta + A_z \cos\theta$ $A_\theta = A_r \cos\theta - A_z \sin\theta$ $A_\phi = A_\phi$
Spherical to cylindrical	$r = R\sin\theta$ $\phi = \phi$ $z = R\cos\theta$	$\hat{\mathbf{r}} = \hat{\mathbf{R}} \sin\theta + \hat{\boldsymbol{\theta}} \cos\theta$ $\hat{\boldsymbol{\phi}} = \hat{\boldsymbol{\phi}}$ $\hat{\mathbf{z}} = \hat{\mathbf{R}} \cos\theta - \hat{\boldsymbol{\theta}} \sin\theta$	$A_r = A_R \sin\theta + A_\theta \cos\theta$ $A_\phi = A_\phi$ $A_z = A_R \cos\theta - A_\theta \sin\theta$

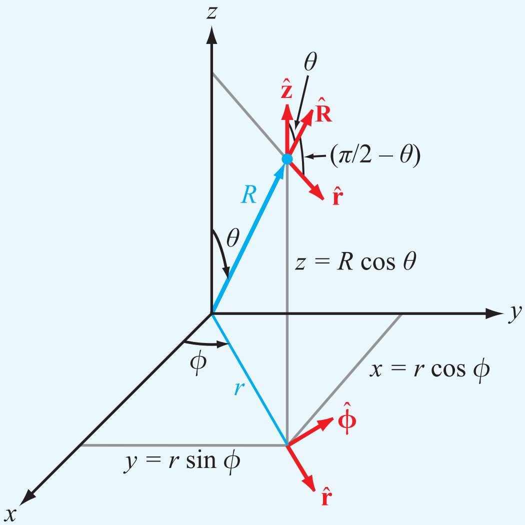

Figure 3-18 Interrelationships between (x, y, z) and (R, θ, ϕ).

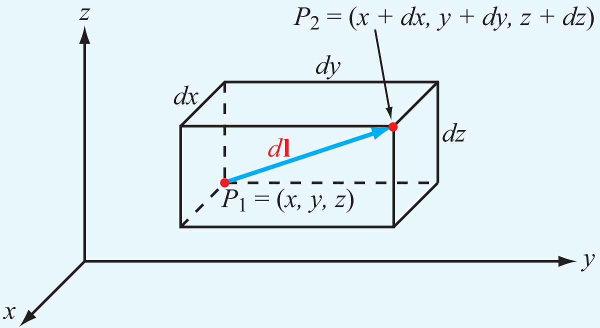

Figure 3-19 Differential distance vector $d\mathbf{l}$ between points P_1 and P_2.

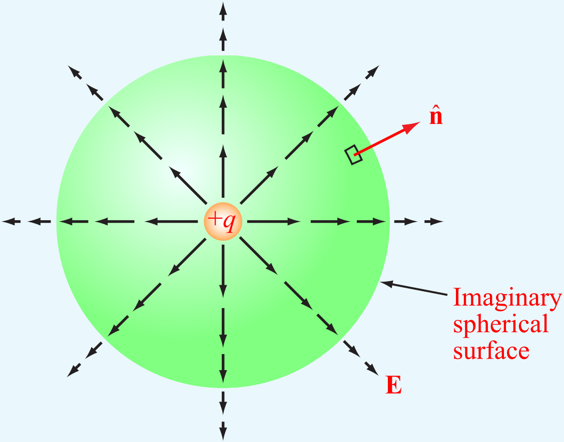

Figure 3-20 Flux lines of the electric field **E** due to a positive charge q.

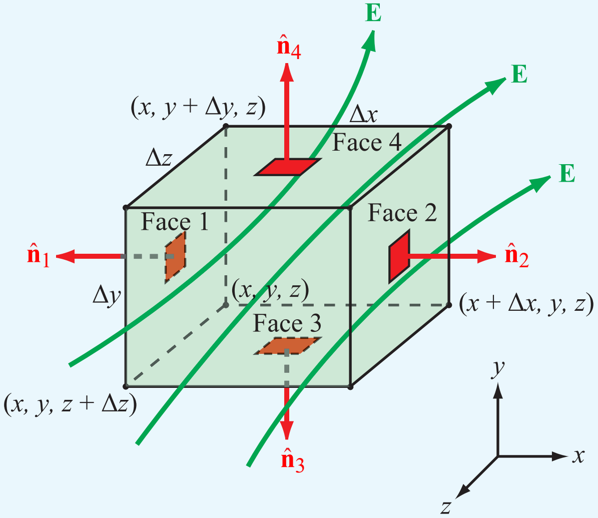

Figure 3-21 Flux lines of a vector field **E** passing through a differential rectangular parallelepiped of volume $\Delta v = \Delta x \, \Delta y \, \Delta z$.

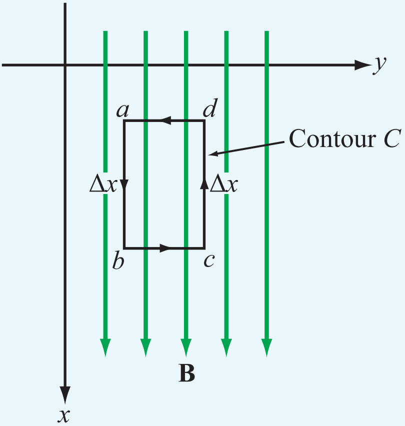

(a) Uniform field

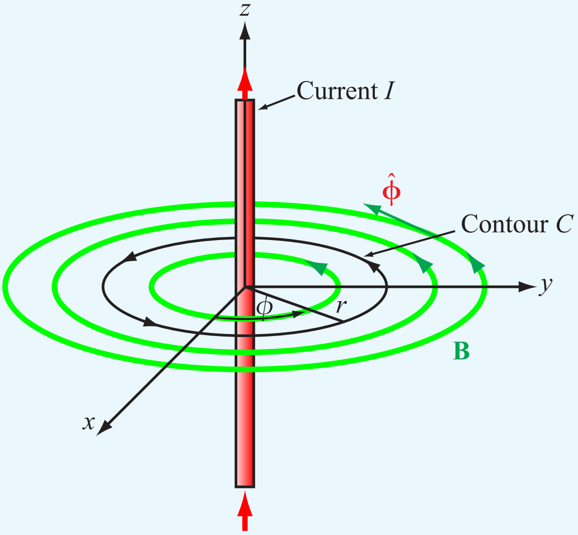

(b) Azimuthal field

Figure 3-22 Circulation is zero for the uniform field in (a), but it is not zero for the azimuthal field in (b).

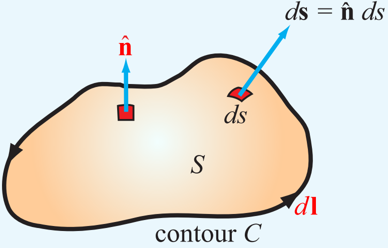

Figure 3-23 The direction of the unit vector $\hat{\mathbf{n}}$ is along the thumb when the other four fingers of the right hand follow $d\mathbf{l}$.

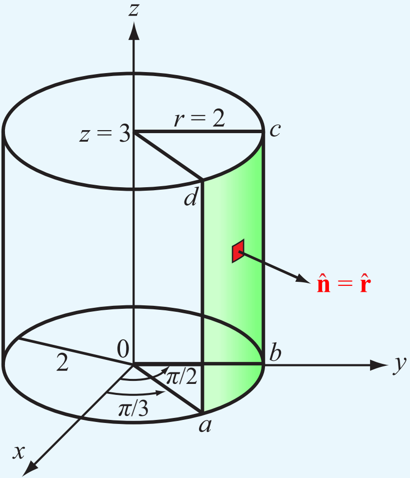

Figure 3-24 Geometry of Example 3-12.

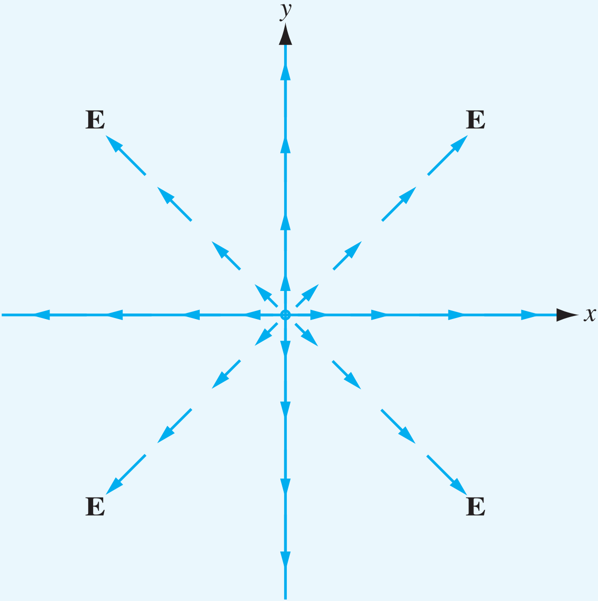

Figure P3.20 Arrow representation for vector field $\mathbf{E} = \hat{\mathbf{r}}\, r$ (Problem 3.20).

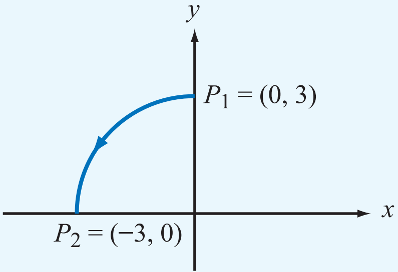

Figure P3.41 Problem 3.41.

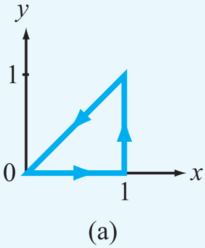

Figure P3.50 Contours for (a) Problem 3.50 and (b) Problem 3.51.

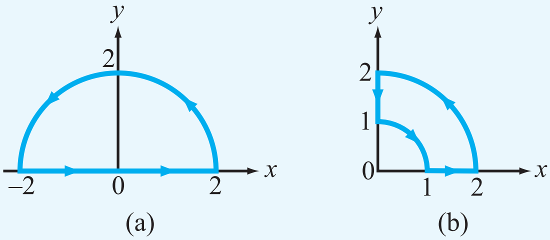

Figure P3.52 Contour paths for (a) Problem 3.52 and (b) Problem 3.53.

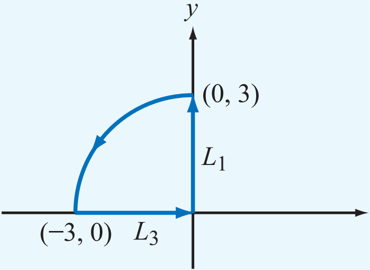

Figure P3.55 Problem 3.55.

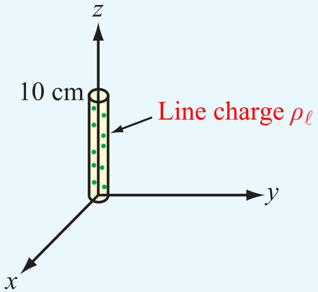

(a) Line charge distribution

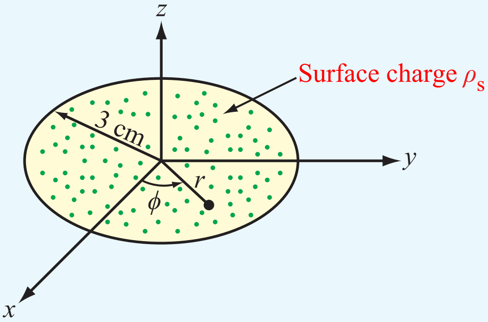

(b) Surface charge distribution

Figure 4-1 Charge distributions for Examples 4-1 and 4-2.

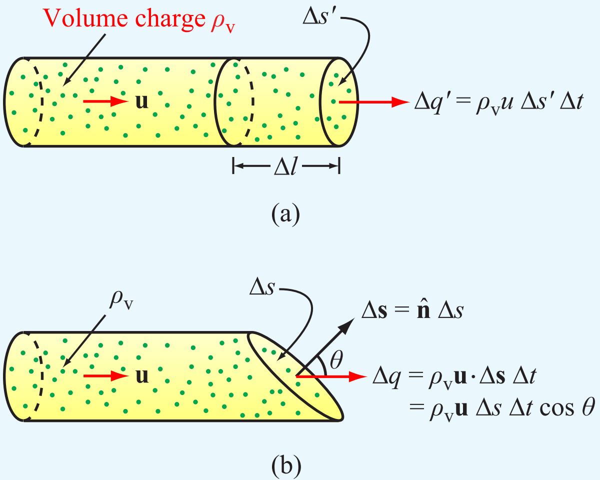

Figure 4-2 Charges with velocity **u** moving through a cross section $\Delta s'$ in (a) and Δs in (b).

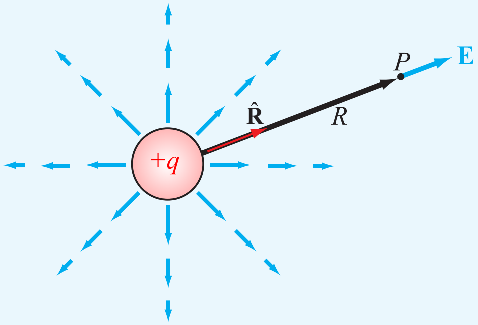

Figure 4-3 Electric-field lines due to a charge q.

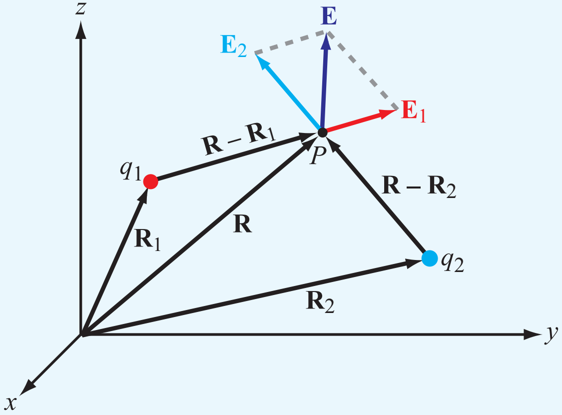

Figure 4-4 The electric field $\mathbf{E}$ at P due to two charges is equal to the vector sum of $\mathbf{E}_1$ and $\mathbf{E}_2$.

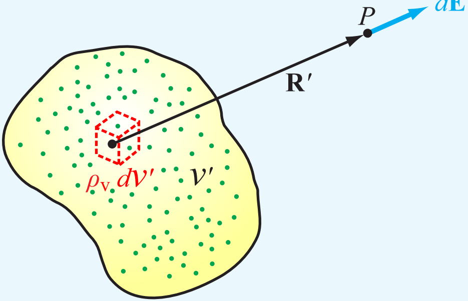

Figure 4-5 Electric field due to a volume charge distribution.

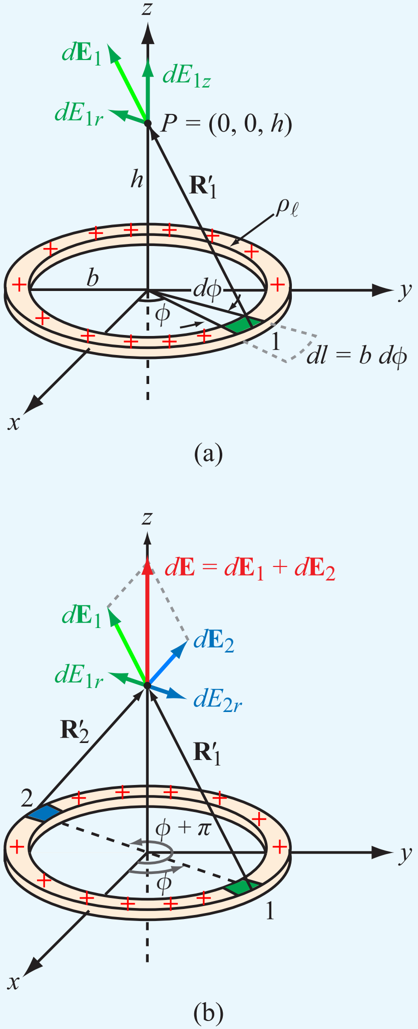

Figure 4-6 Ring of charge with line density ρ_ℓ. (a) The field $d\mathbf{E}_1$ due to infinitesimal segment 1 and (b) the fields $d\mathbf{E}_1$ and $d\mathbf{E}_2$ due to segments at diametrically opposite locations (Example 4-4).

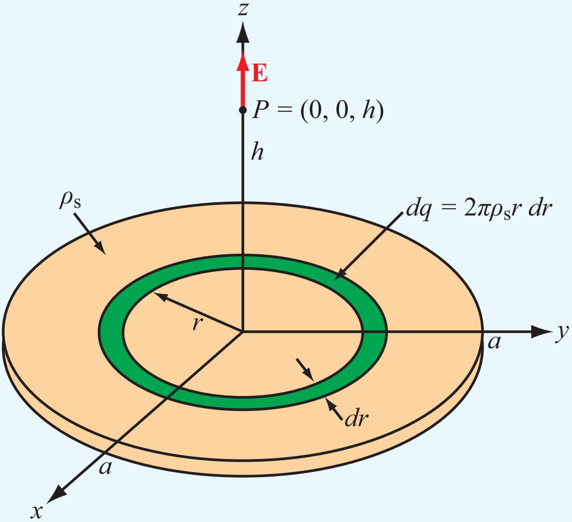

Figure 4-7 Circular disk of charge with surface charge density ρ_s. The electric field at $P = (0, 0, h)$ points along the z direction (Example 4-5).

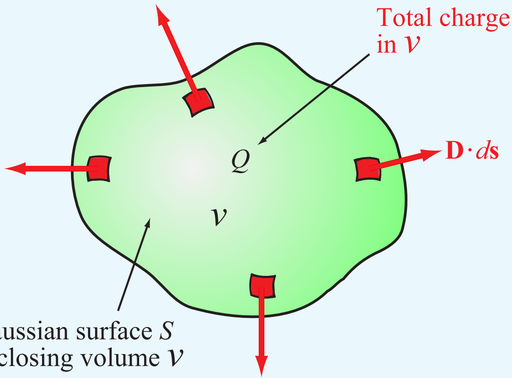

Figure 4-8 The integral form of Gauss's law states that the outward flux of **D** through a surface is proportional to the enclosed charge Q.

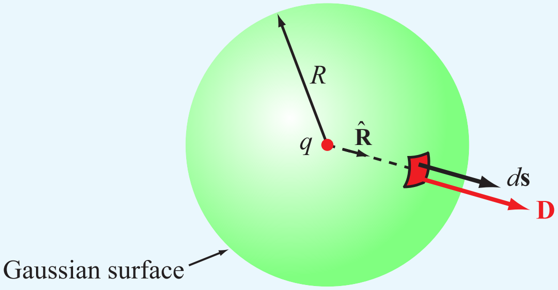

Figure 4-9 Electric field $\mathbf{D}$ due to point charge q.

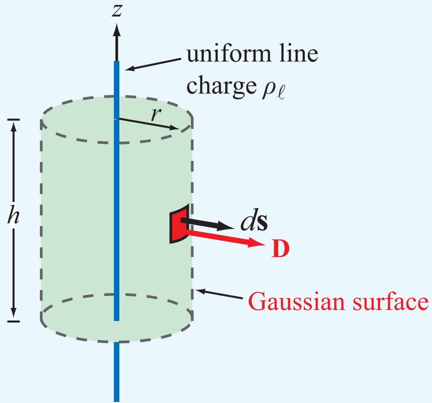

Figure 4-10 Gaussian surface around an infinitely long line of charge (Example 4-6).

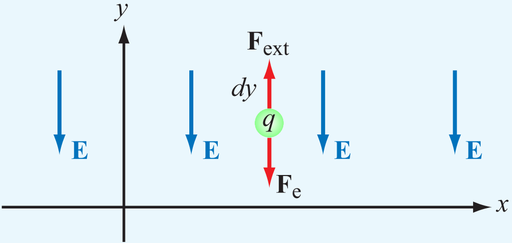

Figure 4-11 Work done in moving a charge q a distance dy against the electric field $\mathbf{E}$ is $dW = qE\,dy$.

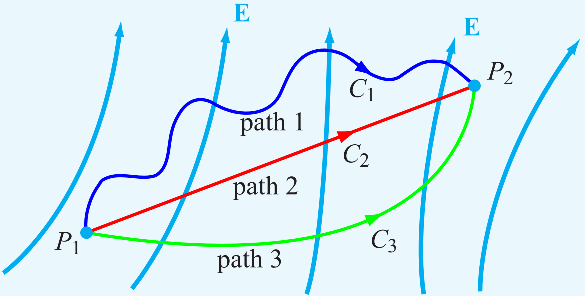

Figure 4-12 In electrostatics, the potential difference between P_2 and P_1 is the same irrespective of the path used for calculating the line integral of the electric field between them.

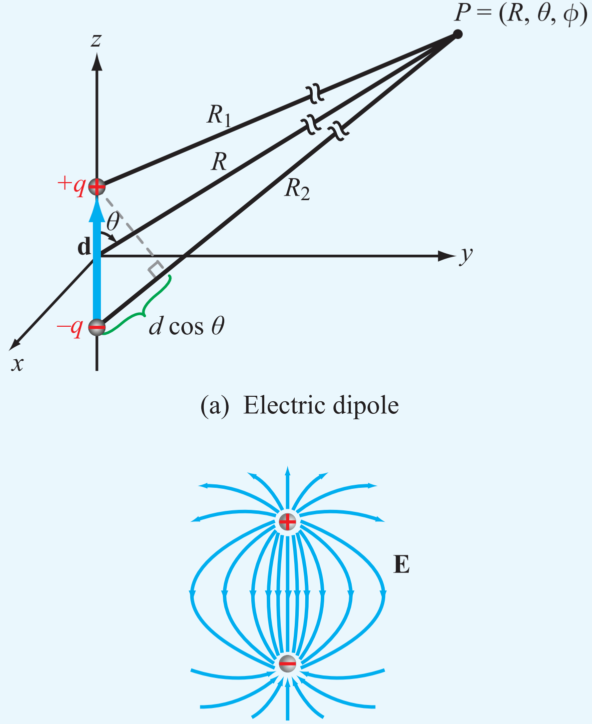

(a) Electric dipole

(b) Electric-field pattern

Figure 4-13 Electric dipole with dipole moment $\mathbf{p} = q\mathbf{d}$ (Example 4-7).

Table 4-1 Conductivity of some common materials at 20 °C.

Material	Conductivity, σ (S/m)
Conductors	
Silver	6.2×10^{7}
Copper	5.8×10^{7}
Gold	4.1×10^{7}
Aluminum	3.5×10^{7}
Iron	10^{7}
Mercury	10^{6}
Carbon	3×10^{4}
Semiconductors	
Pure germanium	2.2
Pure silicon	4.4×10^{-4}
Insulators	
Glass	10^{-12}
Paraffin	10^{-15}
Mica	10^{-15}
Fused quartz	10^{-17}

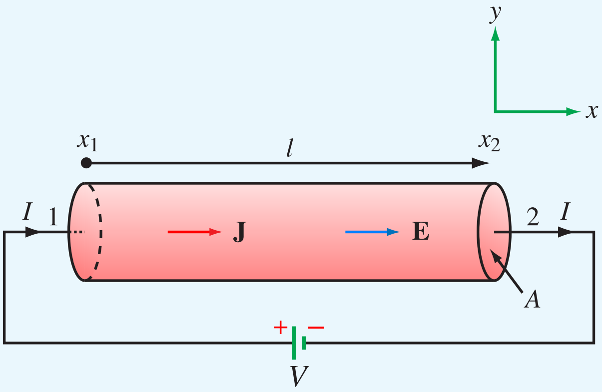

Figure 4-14 Linear resistor of cross section A and length l connected to a dc voltage source V.

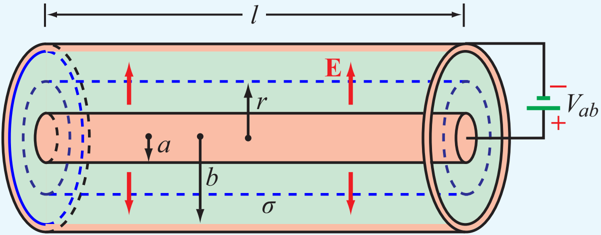

Figure 4-15 Coaxial cable of Example 4-9.

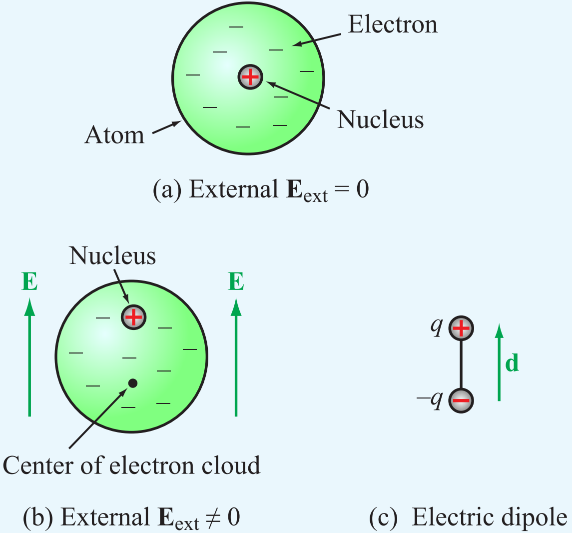

Figure 4-16 In the absence of an external electric field **E**, the center of the electron cloud is co-located with the center of the nucleus, but when a field is applied, the two centers are separated by a distance d.

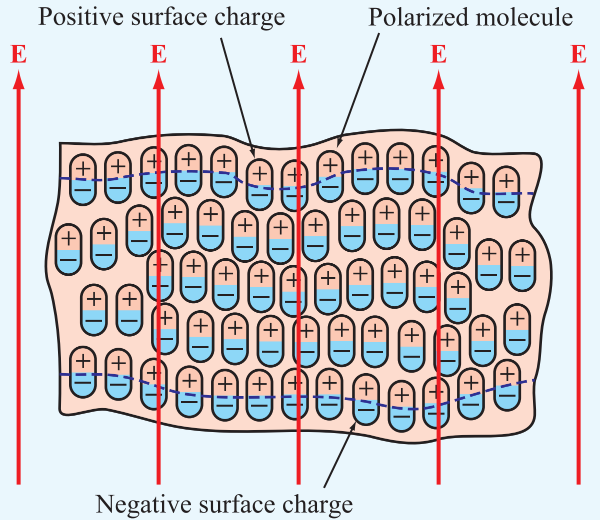

Figure 4-17 A dielectric medium polarized by an external electric field **E**.

Table 4-2 **Relative permittivity (dielectric constant) and dielectric strength of common materials.**

Material	Relative Permittivity, ε_r	Dielectric Strength, E_{ds} (MV/m)
Air (at sea level)	1.0006	3
Petroleum oil	2.1	12
Polystyrene	2.6	20
Glass	4.5–10	25–40
Quartz	3.8–5	30
Bakelite	5	20
Mica	5.4–6	200

$\varepsilon = \varepsilon_r \varepsilon_0$ and $\varepsilon_0 = 8.854 \times 10^{-12}$ F/m.

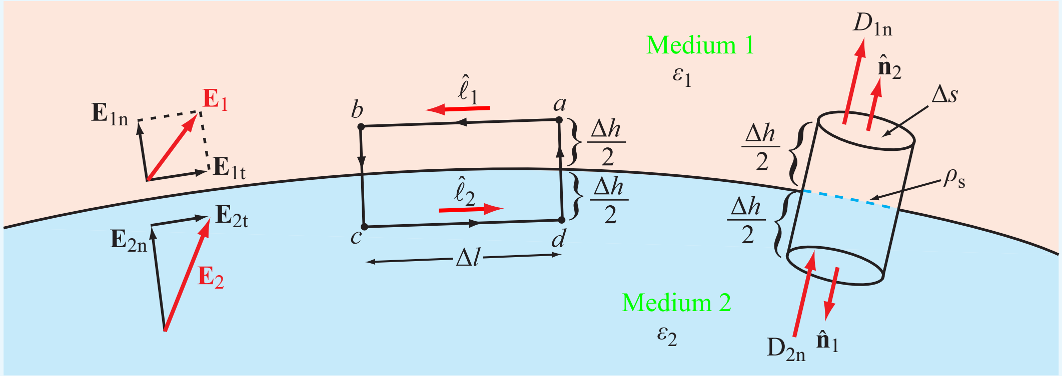

Figure 4-18 Interface between two dielectric media.

Table 4-3 **Boundary conditions for the electric fields.**

Field Component	Any Two Media	Medium 1 Dielectric ε_1	Medium 2 Conductor
Tangential E	$\mathbf{E}_{1t} = \mathbf{E}_{2t}$	$\mathbf{E}_{1t} = \mathbf{E}_{2t} = 0$	
Tangential D	$\mathbf{D}_{1t}/\varepsilon_1 = \mathbf{D}_{2t}/\varepsilon_2$	$\mathbf{D}_{1t} = \mathbf{D}_{2t} = 0$	
Normal E	$\varepsilon_1 E_{1n} - \varepsilon_2 E_{2n} = \rho_s$	$E_{1n} = \rho_s/\varepsilon_1$	$E_{2n} = 0$
Normal D	$D_{1n} - D_{2n} = \rho_s$	$D_{1n} = \rho_s$	$D_{2n} = 0$

Notes: (1) ρ_s is the surface charge density at the boundary; (2) normal components of $\mathbf{E}_1$, $\mathbf{D}_1$, $\mathbf{E}_2$, and $\mathbf{D}_2$ are along $\hat{\mathbf{n}}_2$, the outward normal unit vector of medium 2.

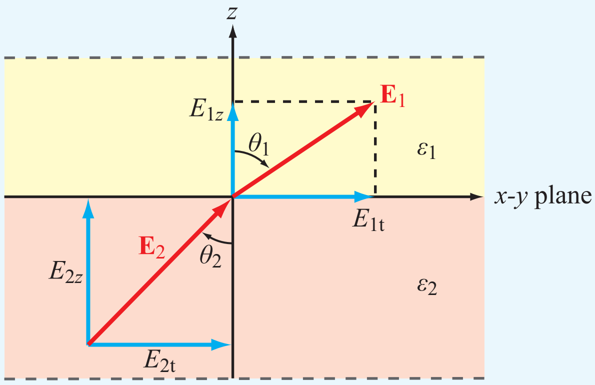

Figure 4-19 Application of boundary conditions at the interface between two dielectric media (Example 4-10).

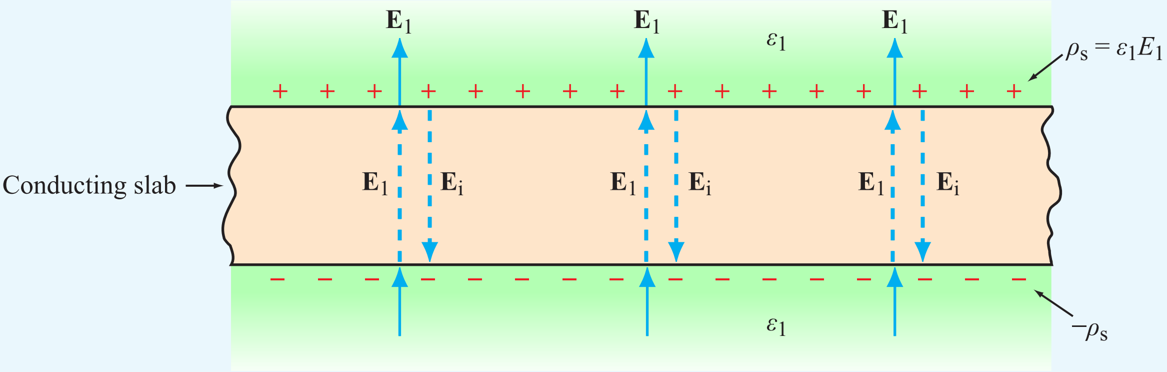

Figure 4-20 When a conducting slab is placed in an external electric field $\mathbf{E}_1$, charges that accumulate on the conductor surfaces induce an internal electric field $\mathbf{E}_i = -\mathbf{E}_1$. Consequently, the total field inside the conductor is zero.

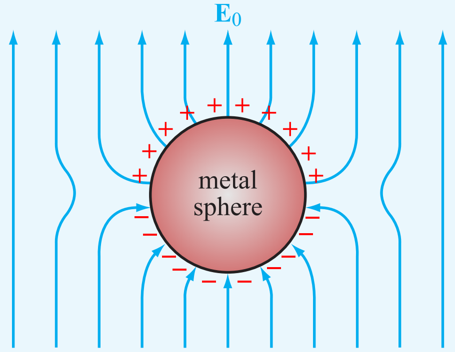

Figure 4-21 Metal sphere placed in an external electric field $\mathbf{E}_0$.

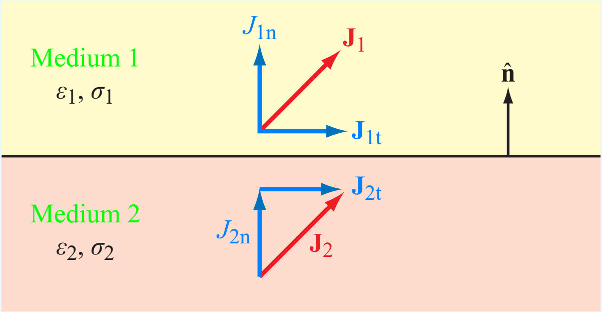

Figure 4-22 Boundary between two conducting media.

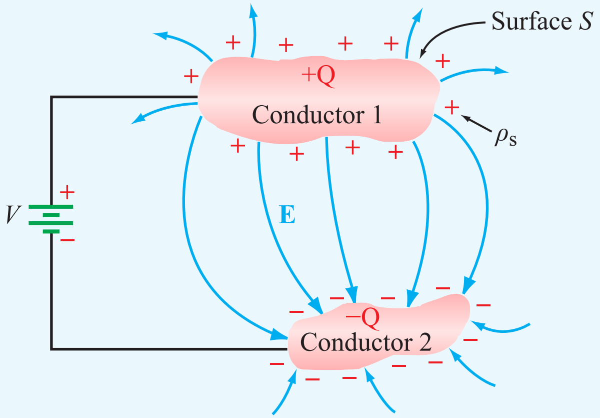

Figure 4-23 A dc voltage source connected to a capacitor composed of two conducting bodies.

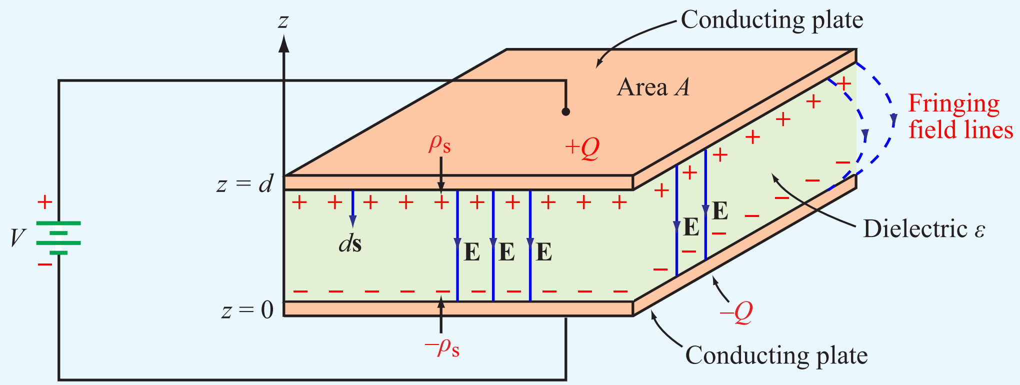

Figure 4-24 A dc voltage source connected to a parallel-plate capacitor (Example 4-11).

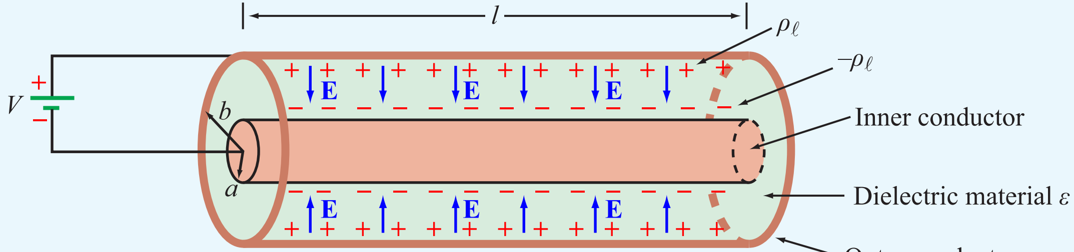

Figure 4-25 Coaxial capacitor filled with insulating material of permittivity ε (Example 4-12).

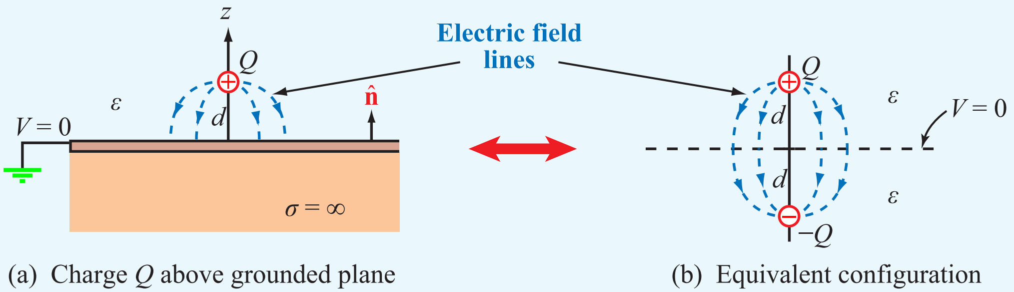

Figure 4-26 By image theory, a charge Q above a grounded perfectly conducting plane is equivalent to Q and its image $-Q$ with the ground plane removed.

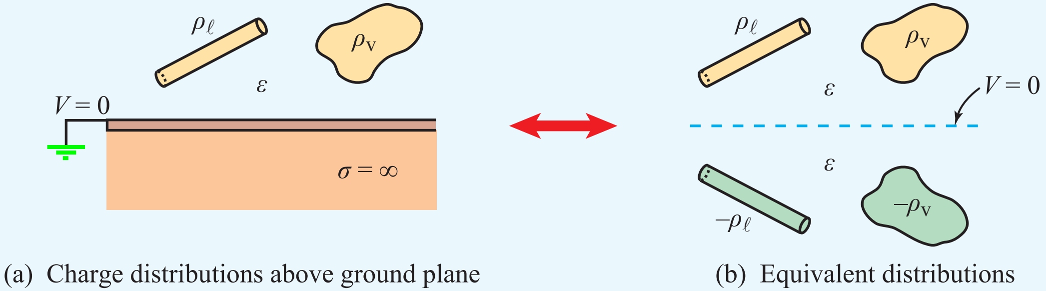

Figure 4-27 Charge distributions above a conducting plane and their image-method equivalents.

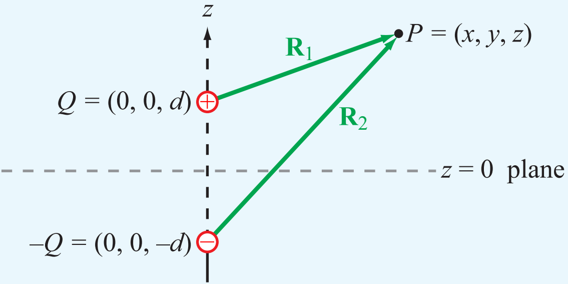

Figure 4-28 Application of the image method for finding **E** at point P (Example 4-13).

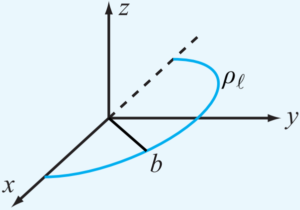

Figure P4.10 Problem 4.10.

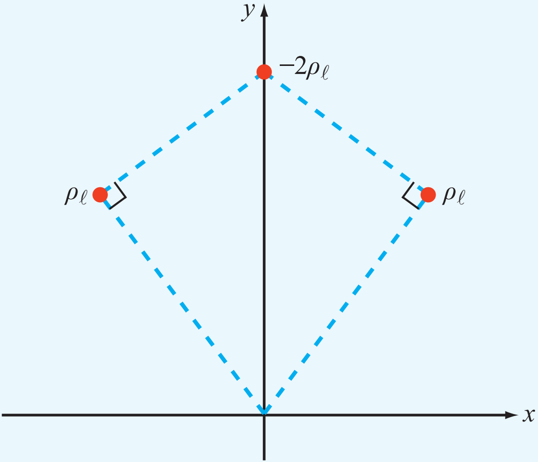

Figure P4.19 Kite-shaped arrangment of line charges for Problem 4.19.

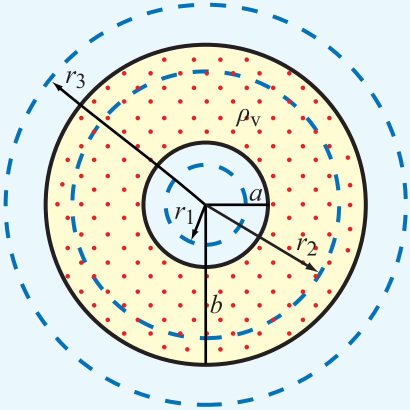

Figure P4.29 Problem 4.29.

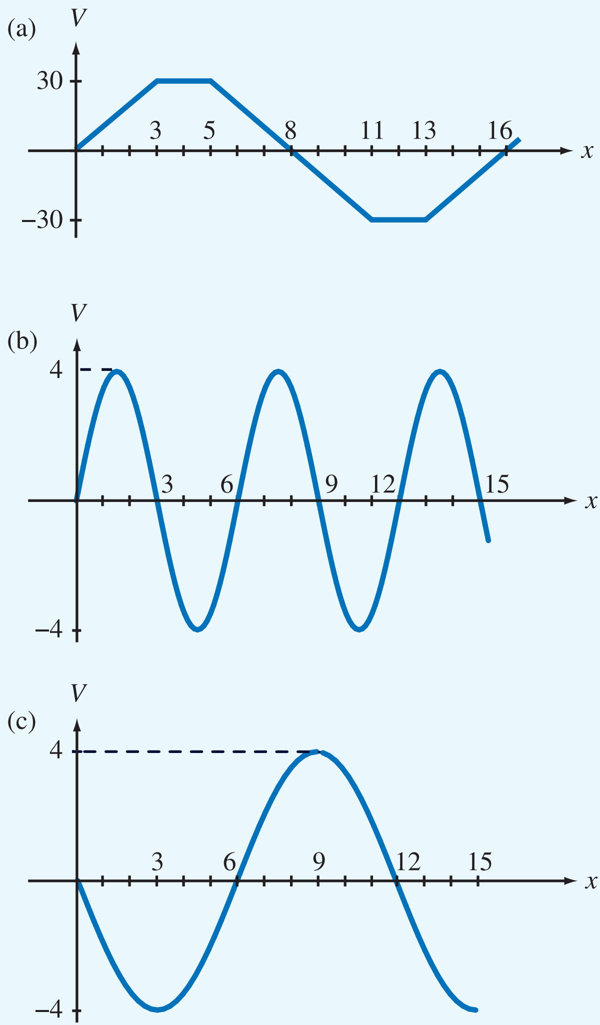

Figure P4.36 Electric potential distributions of Problem 4.36.

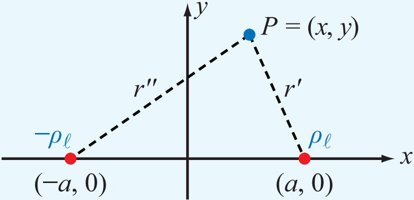

Figure P4.37 Problem 4.37.

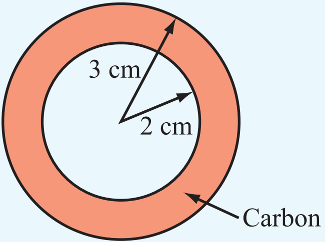

Figure P4.45 Cross-section of hollow cylinder of Problem 4.45.

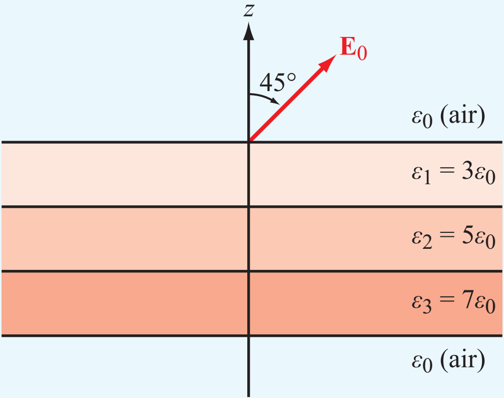

Figure P4.51 Dielectric slabs in Problem 4.51.

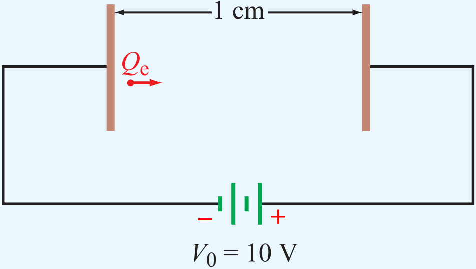

Figure P4.54 Electron between charged plates of Problem 4.54.

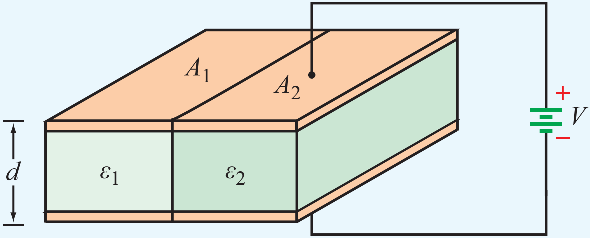

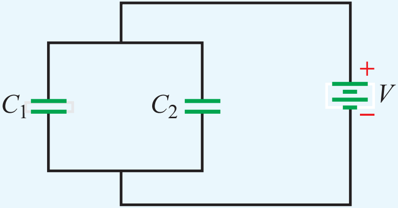

Figure P4.56 (a) Capacitor with parallel dielectric section, and (b) equivalent circuit.

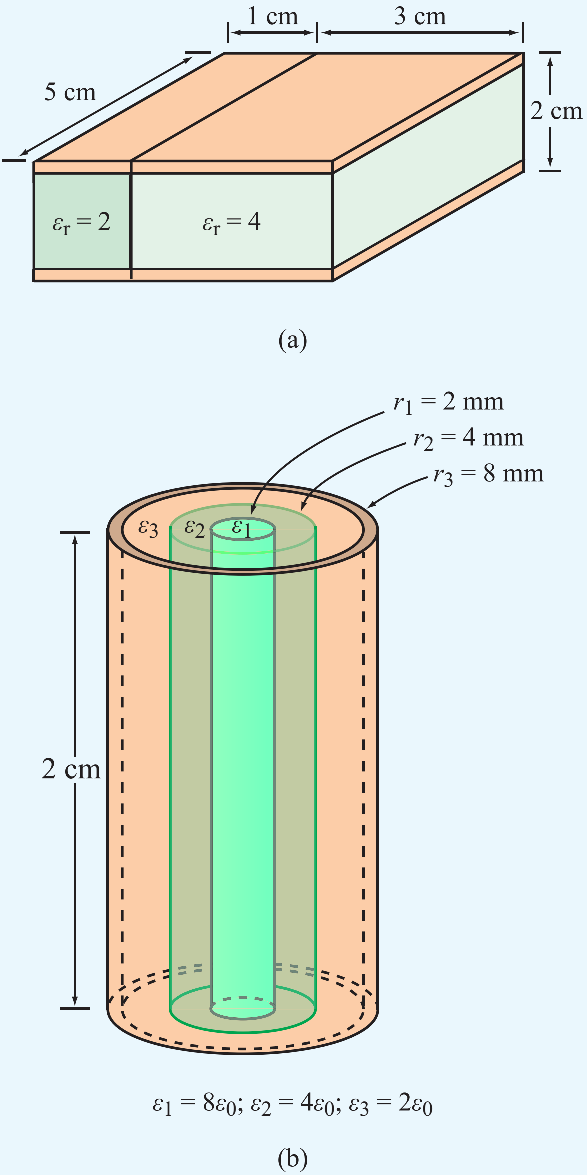

Figure P4.57 Dielectric sections for Problems 4.57 and 4.59.

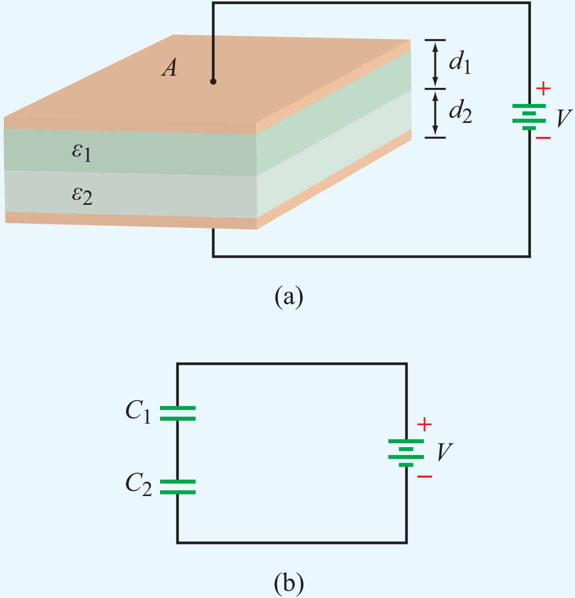

Figure P4.58 (a) Capacitor with parallel dielectric layers, and (b) equivalent circuit (Problem 4.58).

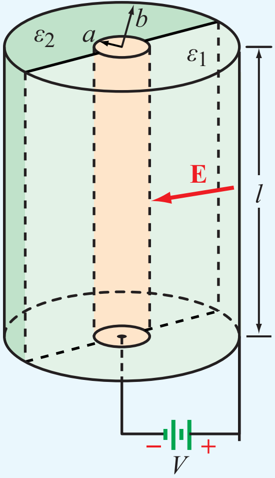

Figure P4.60 Problem 4.60.

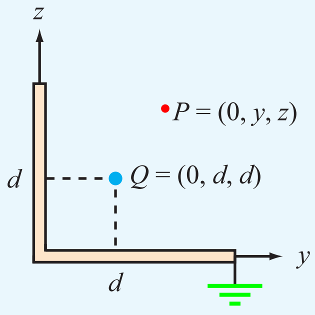

Figure P4.61 Charge Q next to two perpendicular, grounded, conducting half-planes.

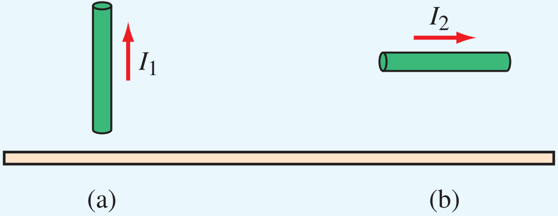

Figure P4.62 Currents above a conducting plane (Problem 4.62).

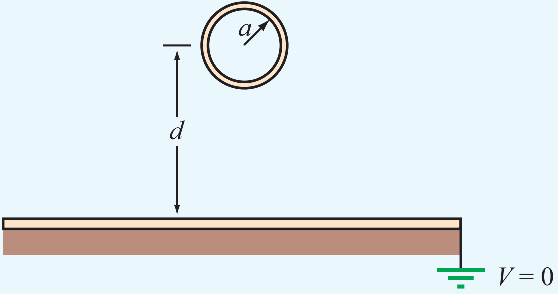

Figure P4.63 Conducting cylinder above a conducting plane (Problem 4.63).

Table 5-1 **Attributes of electrostatics and magnetostatics.**

Attribute	Electrostatics	Magnetostatics
Sources	Stationary charges ρ_{v}	Steady currents $\mathbf{J}$
Fields and Fluxes	$\mathbf{E}$ and $\mathbf{D}$	$\mathbf{H}$ and $\mathbf{B}$
Constitutive parameter(s)	ε and σ	μ
Governing equations		
• **Differential form**	$\nabla \cdot \mathbf{D} = \rho_{\mathrm{v}}$ $\nabla \times \mathbf{E} = 0$	$\nabla \cdot \mathbf{B} = 0$ $\nabla \times \mathbf{H} = \mathbf{J}$
• **Integral form**	$\oint_S \mathbf{D} \cdot d\mathbf{s} = Q$ $\oint_C \mathbf{E} \cdot d\mathbf{l} = 0$	$\oint_S \mathbf{B} \cdot d\mathbf{s} = 0$ $\oint_C \mathbf{H} \cdot d\mathbf{l} = I$
Potential	Scalar V, with $\mathbf{E} = -\nabla V$	Vector $\mathbf{A}$, with $\mathbf{B} = \nabla \times \mathbf{A}$
Energy density	$w_{\mathrm{e}} = \frac{1}{2}\varepsilon E^2$	$w_{\mathrm{m}} = \frac{1}{2}\mu H^2$
Force on charge q	$\mathbf{F}_{\mathrm{e}} = q\mathbf{E}$	$\mathbf{F}_{\mathrm{m}} = q\mathbf{u} \times \mathbf{B}$
Circuit element(s)	C and R	L

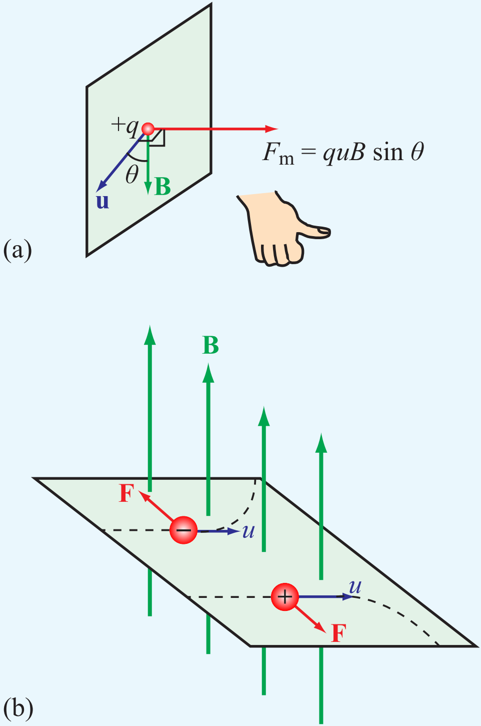

Figure 5-1 The direction of the magnetic force exerted on a charged particle moving in a magnetic field is (a) perpendicular to both **B** and **u** and (b) depends on the charge polarity (positive or negative).

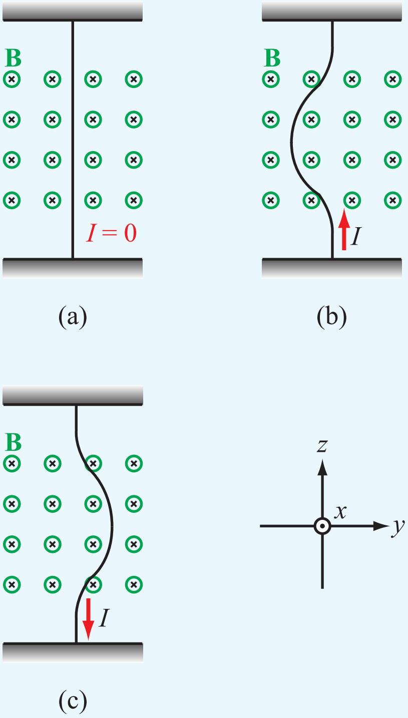

Figure 5-2 When a slightly flexible vertical wire is placed in a magnetic field directed into the page (as denoted by the crosses), it is (a) not deflected when the current through it is zero, (b) deflected to the left when I is upward, and (c) deflected to the right when I is downward.

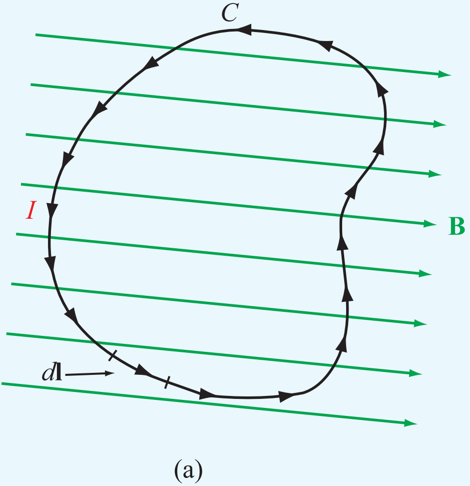

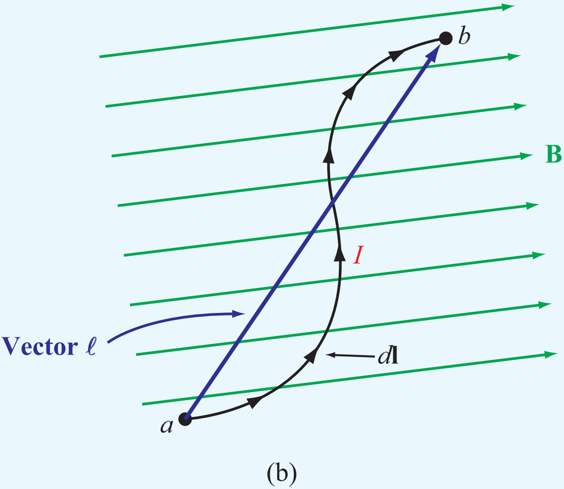

Figure 5-3 In a uniform magnetic field, (a) the net force on a closed current loop is zero because the integral of the displacement vector $d\mathbf{l}$ over a closed contour is zero, and (b) the force on a line segment is proportional to the vector between the end point ($\mathbf{F}_\text{m} = I\boldsymbol{\ell} \times \mathbf{B}$).

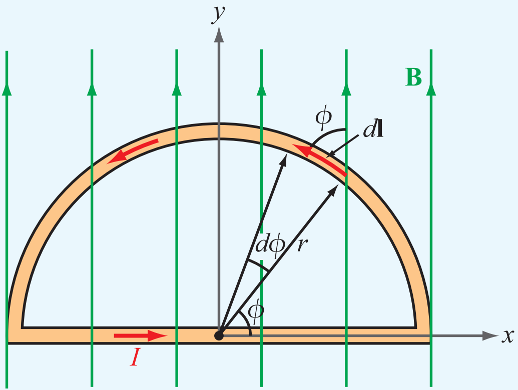

Figure 5-4 Semicircular conductor in a uniform field (Example 5-1).

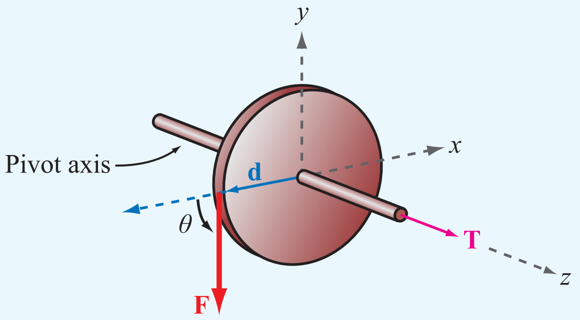

Figure 5-5 The force **F** acting on a circular disk that can pivot along the z axis generates a torque $\mathbf{T} = \mathbf{d} \times \mathbf{F}$ that causes the disk to rotate.

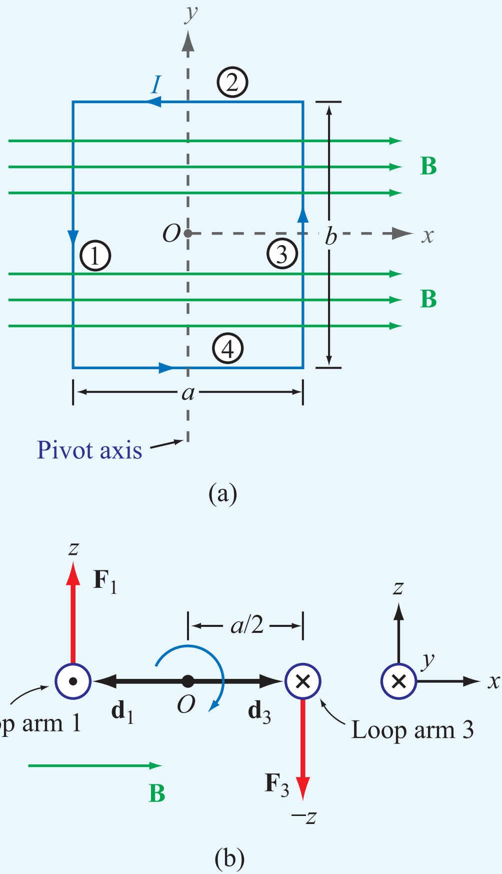

Figure 5-6 Rectangular loop pivoted along the y axis: (a) front view and (b) bottom view. The combination of forces $\mathbf{F}_1$ and $\mathbf{F}_3$ on the loop generates a torque that tends to rotate the loop in a clockwise direction as shown in (b).

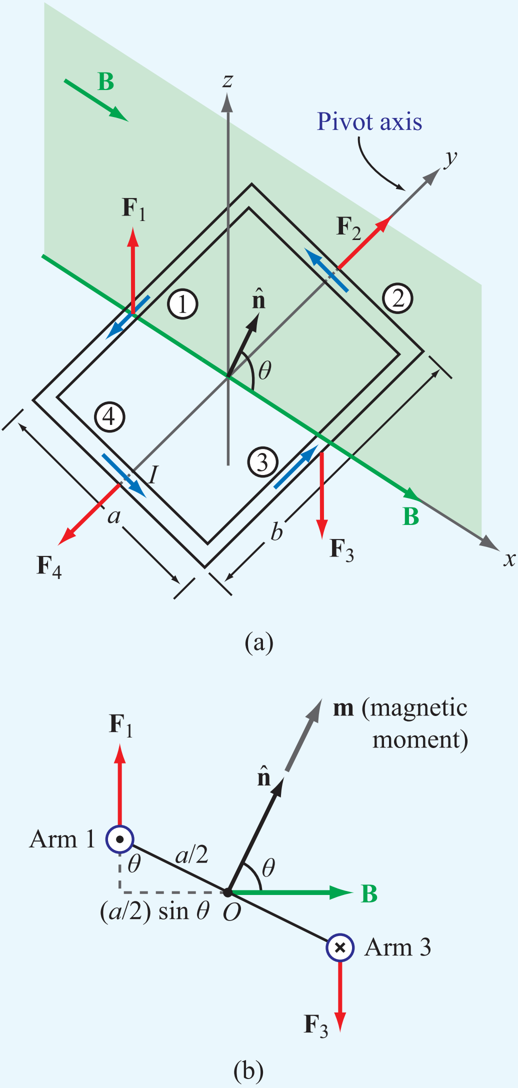

Figure 5-7 Rectangular loop in a uniform magnetic field with flux density **B** whose direction is perpendicular to the rotation axis of the loop, but makes an angle θ with the loop's surface normal $\hat{\mathbf{n}}$.

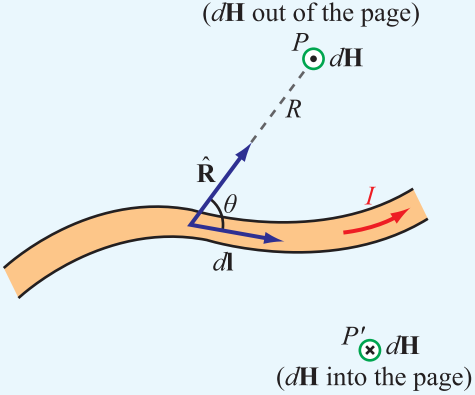

Figure 5-8 Magnetic field $d\mathbf{H}$ generated by a current element $I\,d\mathbf{l}$. The direction of the field induced at point P is opposite to that induced at point P'.

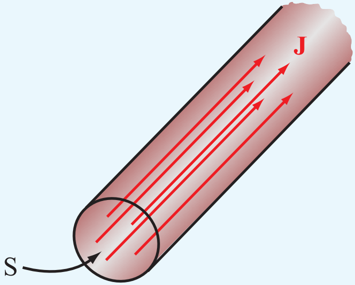

(a) Volume current density **J** in A/m^2

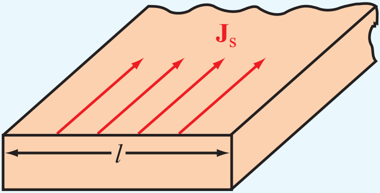

(b) Surface current density $\mathbf{J}_s$ in A/m

Figure 5-9 (a) The total current crossing the cross section S of the cylinder is $I = \int_S \mathbf{J} \cdot d\mathbf{s}$. (b) The total current flowing across the surface of the conductor is $I = \int_l J_s \, dl$.

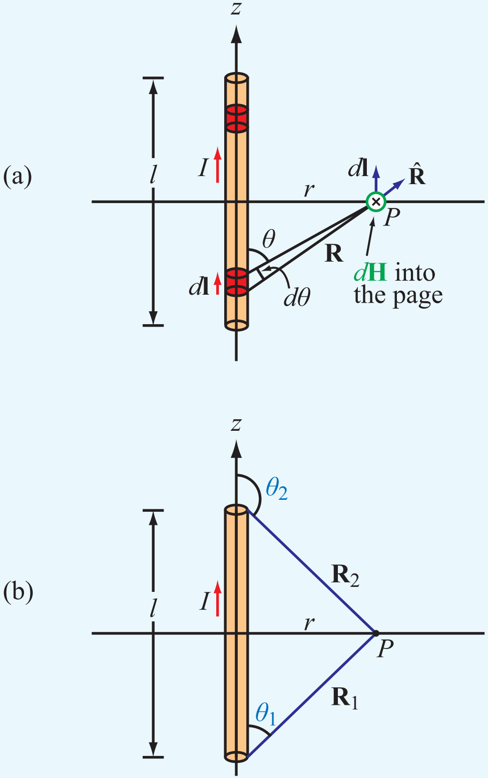

Figure 5-10 Linear conductor of length l carrying a current I. (a) The field $d\mathbf{H}$ at point P due to incremental current element $d\mathbf{l}$. (b) Limiting angles θ_1 and θ_2, each measured between vector $I\,d\mathbf{l}$ and the vector connecting the end of the conductor associated with that angle to point P (Example 5-2).

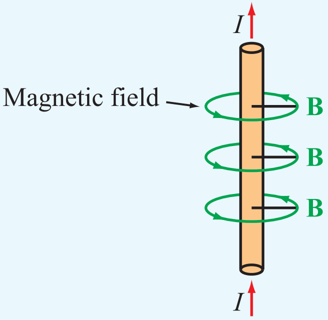

Figure 5-11 Magnetic field surrounding a long, linear current-carrying conductor.

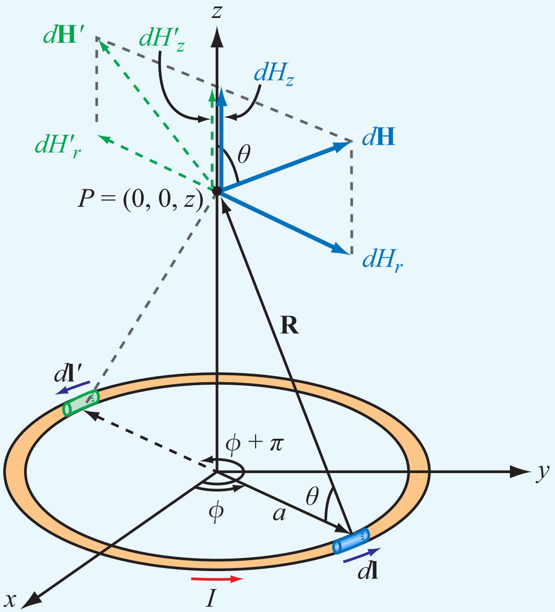

Figure 5-12 Circular loop carrying a current I (Example 5-3).

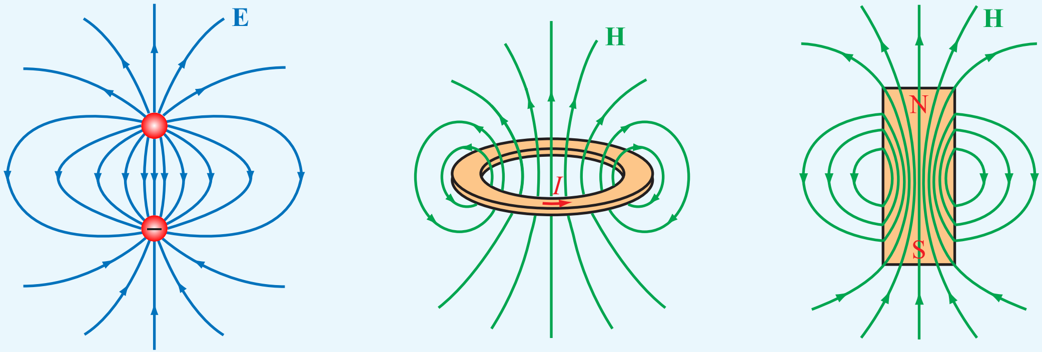

(a) Electric dipole (b) Magnetic dipole (c) Bar magnet

Figure 5-13 Patterns of (a) the electric field of an electric dipole, (b) the magnetic field of a magnetic dipole, and (c) the magnetic field of a bar magnet. Far away from the sources, the field patterns are similar in all three cases.

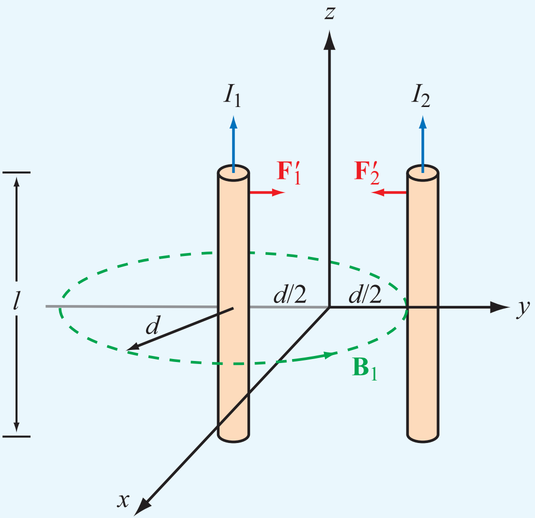

Figure 5-14 Magnetic forces on parallel current-carrying conductors.

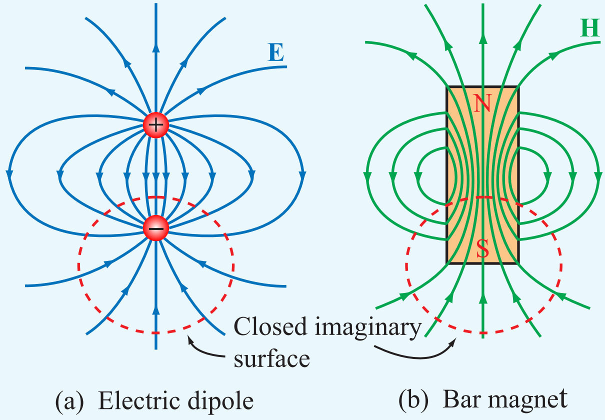

Figure 5-15 Whereas (a) the net electric flux through a closed surface surrounding a charge is not zero, (b) the net magnetic flux through a closed surface surrounding one of the poles of a magnet is zero.

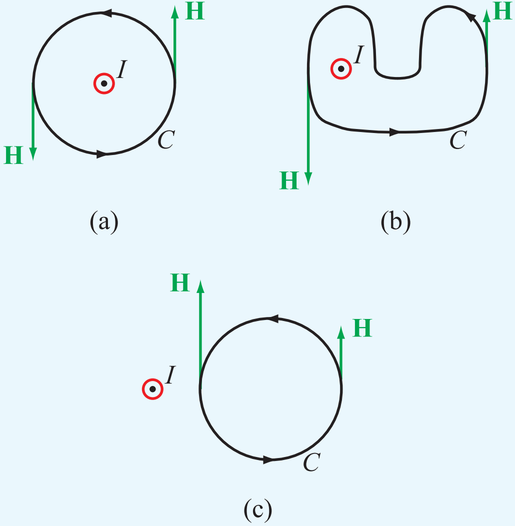

Figure 5-16 Ampère's law states that the line integral of **H** around a closed contour C is equal to the current traversing the surface bounded by the contour. This is true for contours (a) and (b), but the line integral of **H** is zero for the contour in (c) because the current I (denoted by the symbol $\odot$) is not enclosed by the contour C.

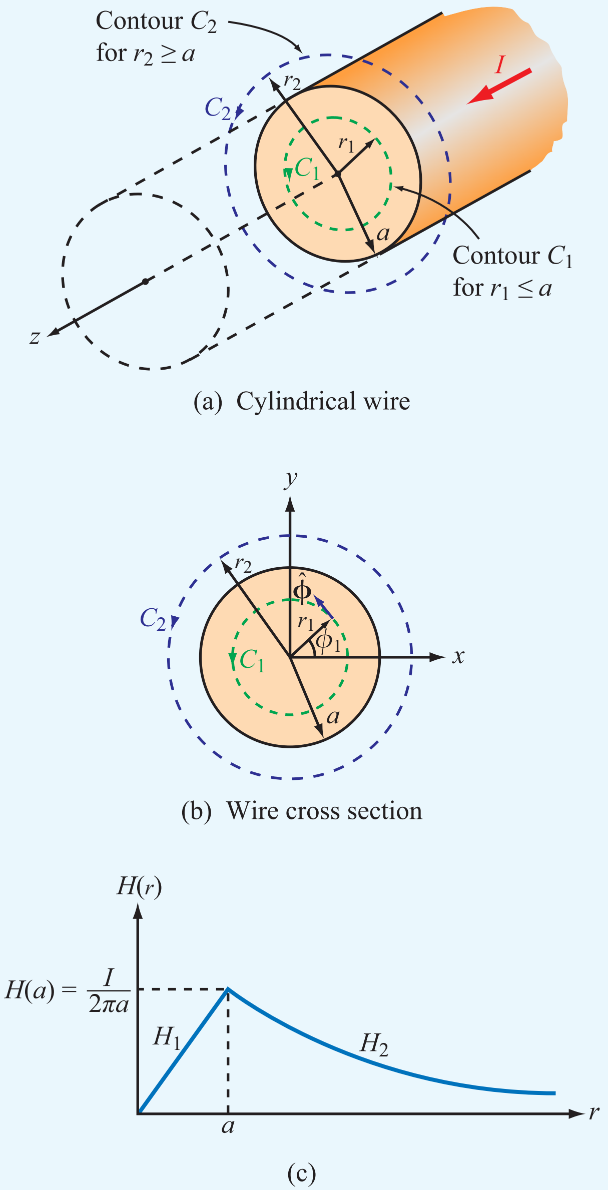

Figure 5-17 Infinitely long wire of radius a carrying a uniform current I along the $+z$ direction: (a) general configuration showing contours C_1 and C_2; (b) cross-sectional view; and (c) a plot of H versus r (Example 5-4).

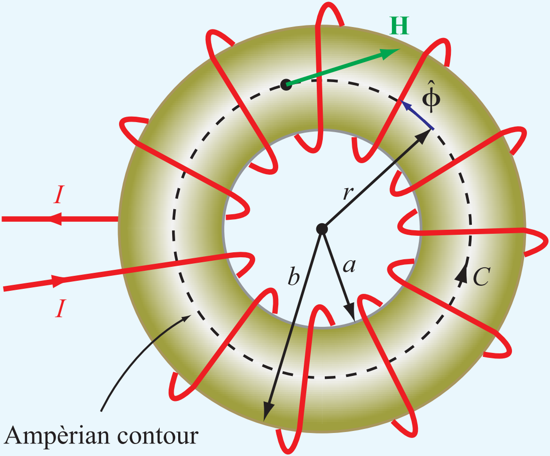

Figure 5-18 Toroidal coil with inner radius a and outer radius b. The wire loops usually are much more closely spaced than shown in the figure (Example 5-5).

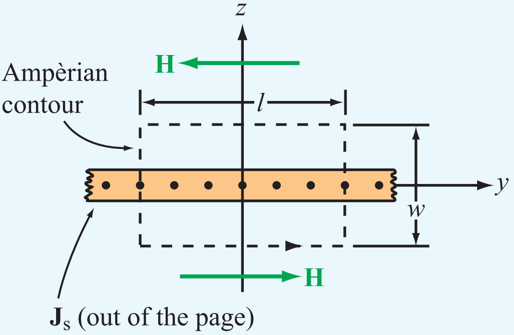

Figure 5-19 A thin current sheet in the x–y plane carrying a surface current density $\mathbf{J}_s = \hat{\mathbf{x}} J_s$ (Example 5-6).

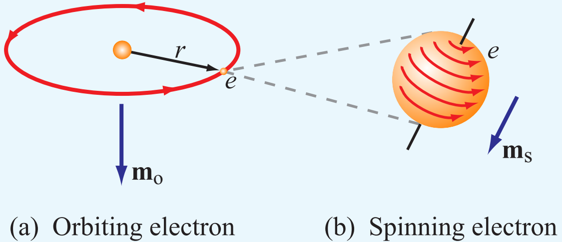

Figure 5-20 An electron generates (a) an orbital magnetic moment $\mathbf{m}_o$ as it rotates around the nucleus and (b) a spin magnetic moment $\mathbf{m}_s$, as it spins about its own axis.

Table 5-2 **Properties of magnetic materials.**

	Diamagnetism	**Paramagnetism**	**Ferromagnetism**
Permanent magnetic dipole moment	No	Yes, but weak	Yes, and strong
Primary magnetization mechanism	Electron orbital magnetic moment	Electron spin magnetic moment	Magnetized domains
Direction of induced magnetic field (relative to external field)	Opposite	Same	Hysteresis [see **Fig. 5-22**]
Common substances	Bismuth, copper, diamond, gold, lead, mercury, silver, silicon	Aluminum, calcium, chromium, magnesium, niobium, platinum, tungsten	Iron, nickel, cobalt
Typical value of χ_m **Typical value of μ_r**	$\approx -10^{-5}$ ≈ 1	$\approx 10^{-5}$ ≈ 1	$\lvert\chi_m\rvert \gg 1$ and hysteretic $\lvert\mu_r\rvert \gg 1$ and hysteretic

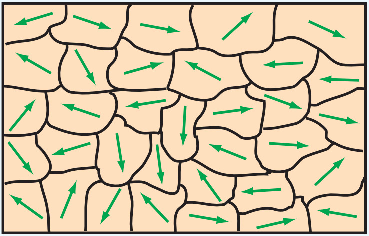

(a) Unmagnetized domains

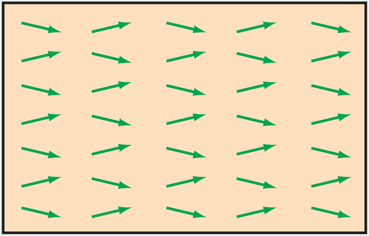

(b) Magnetized domains

Figure 5-21 Comparison of (a) unmagnetized and (b) magnetized domains in a ferromagnetic material.

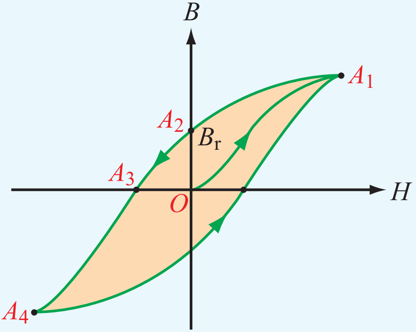

Figure 5-22 Typical hysteresis curve for a ferromagnetic material.

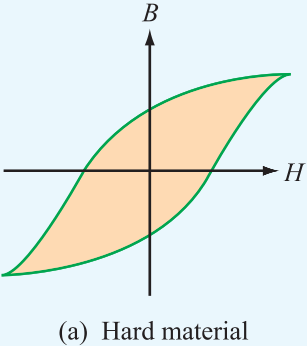

Figure 5-23 Comparison of hysteresis curves for (a) a hard ferromagnetic material and (b) a soft ferromagnetic material.

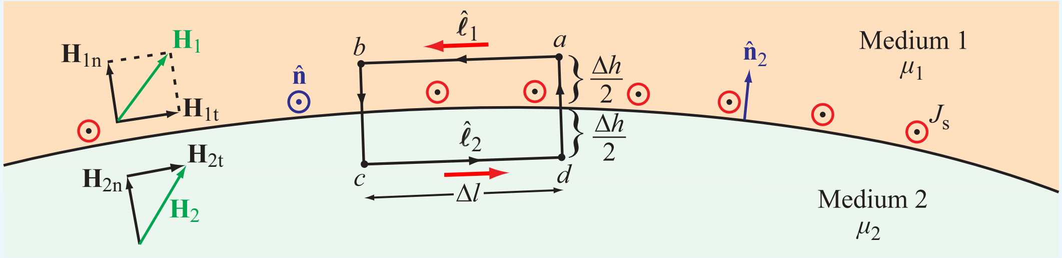

Figure 5-24 Boundary between medium 1 with μ_1 and medium 2 with μ_2.

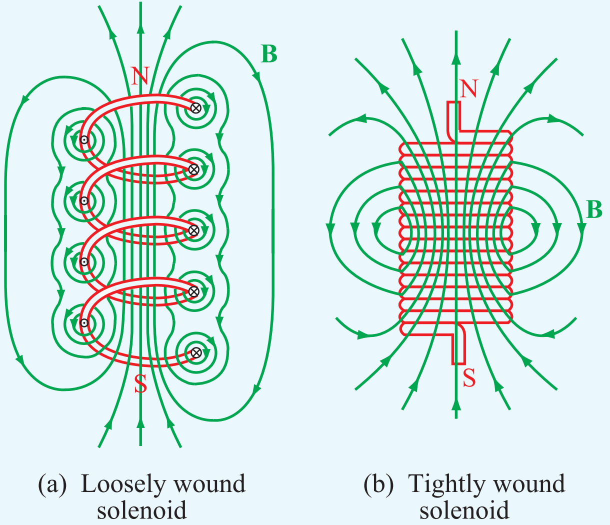

Figure 5-25 Magnetic field lines of (a) a loosely wound solenoid and (b) a tightly wound solenoid.

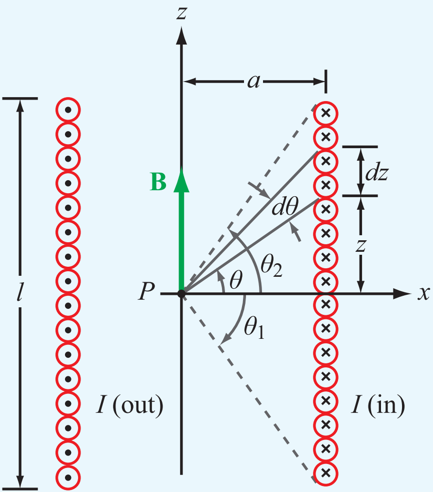

Figure 5-26 Solenoid cross section showing geometry for calculating **H** at a point P on the solenoid axis.

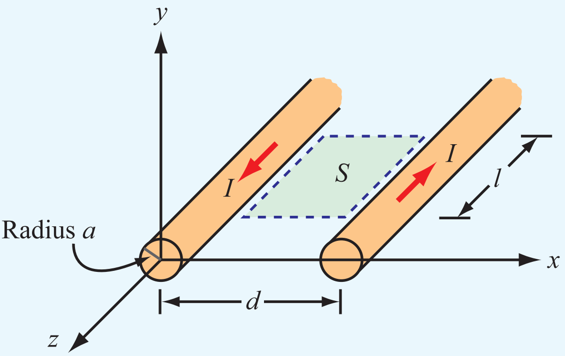

(a) Parallel-wire transmission line

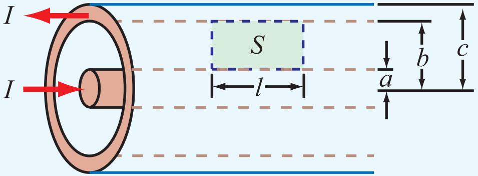

(b) Coaxial transmission line

Figure 5-27 To compute the inductance per unit length of a two-conductor transmission line, we need to determine the magnetic flux through the area S between the conductors.

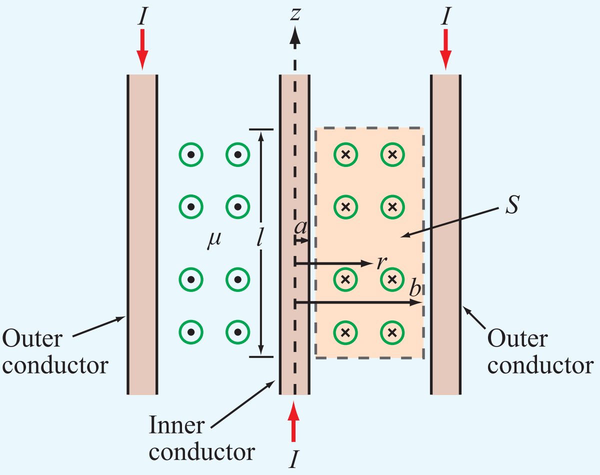

Figure 5-28 Cross-sectional view of coaxial transmission line (Example 5-7). ⊙ and ⊗ denote **H** field out of and into the page, respectively.

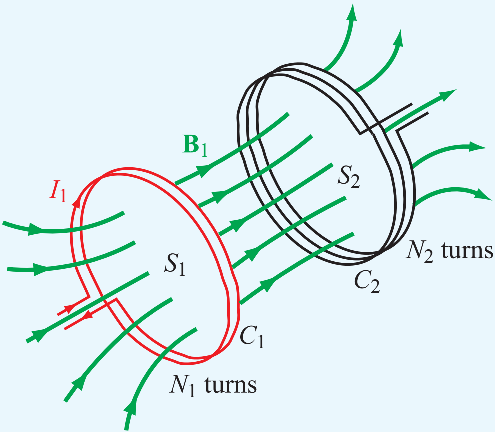

Figure 5-29 Magnetic field lines generated by current I_1 in loop 1 linking surface S_2 of loop 2.

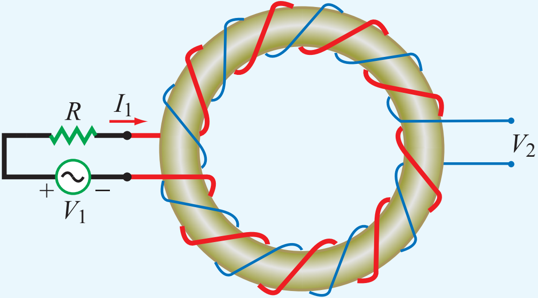

Figure 5-30 Toroidal coil with two windings used as a transformer.

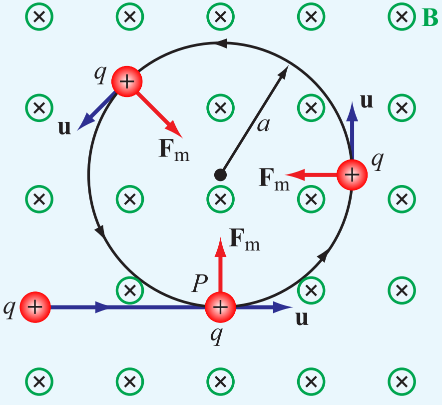

Figure P5.2 Particle of charge q projected with velocity $\mathbf{u}$ into a medium with a uniform field $\mathbf{B}$ perpendicular to $\mathbf{u}$ (Problem 5.2).

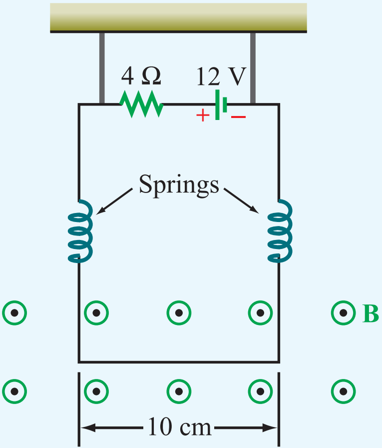

Figure P5.3 Configuration of Problem 5.3.

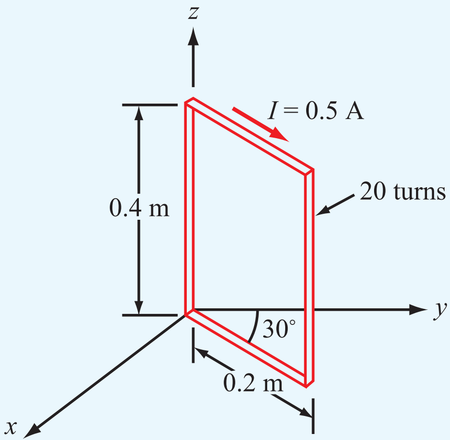

Figure P5.4 Hinged rectangular loop of Problem 5.4.

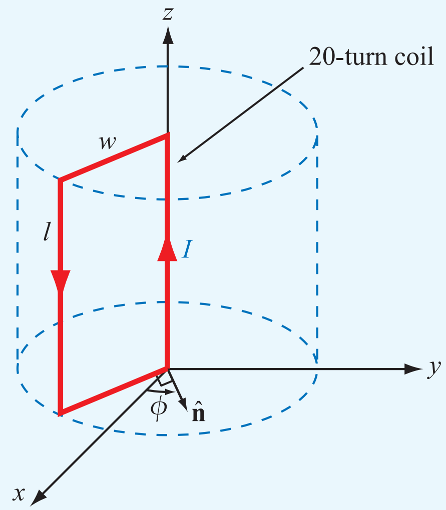

Figure P5.6 Rectangular loop of Problem 5.6.

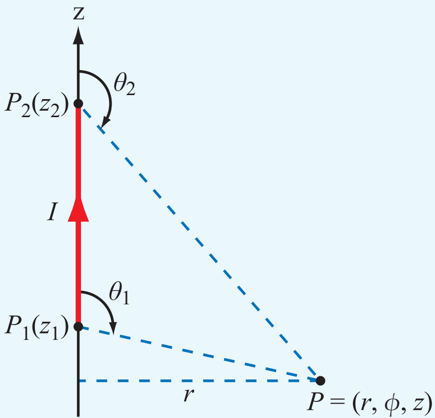

Figure P5.8 Current-carrying linear conductor of Problem 5.8.

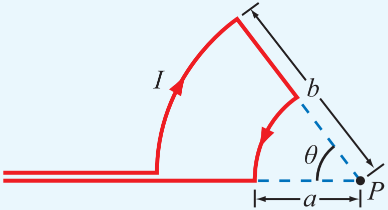

Figure P5.9 Configuration of Problem 5.9.

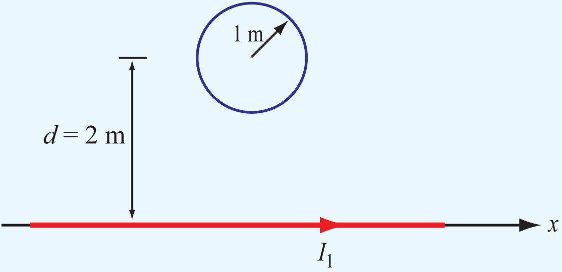

Figure P5.11 Circular loop next to a linear current (Problem 5.11).

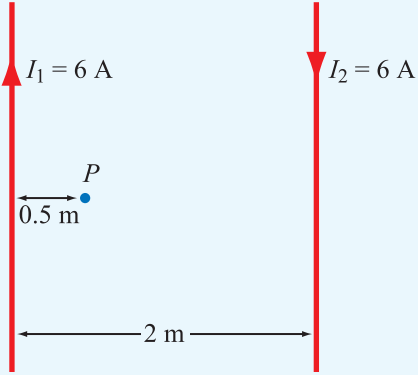

Figure P5.12 Arrangement for Problem 5.12.

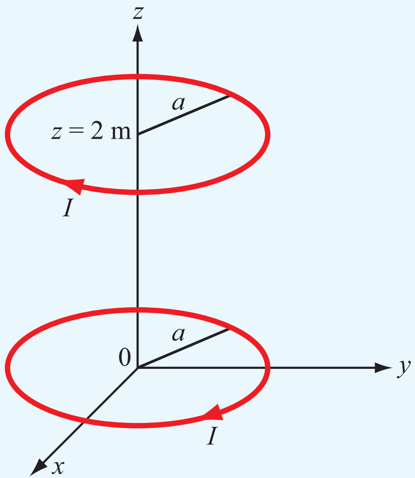

Figure P5.14 Parallel circular loops of Problem 5.14.

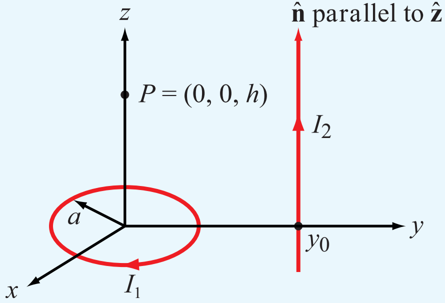

Figure P5.15 Problem 5.15.

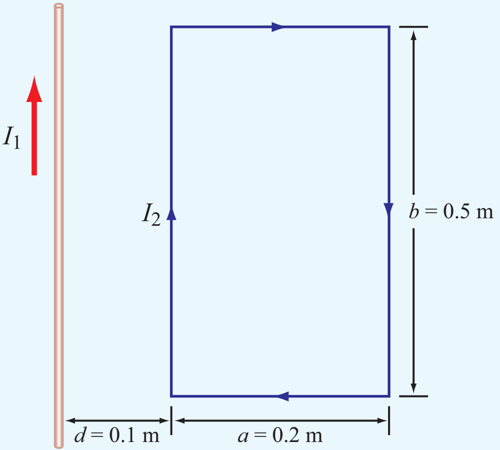

Figure P5.16 Current loop next to a conducting wire (Problem 5.16).

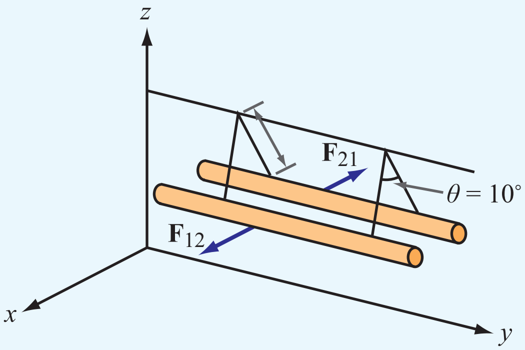

Figure P5.17 Parallel conductors supported by strings (Problem 5.17).

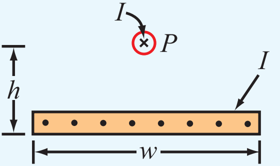

Figure P5.18 A linear current source above a current sheet (Problem 5.18).

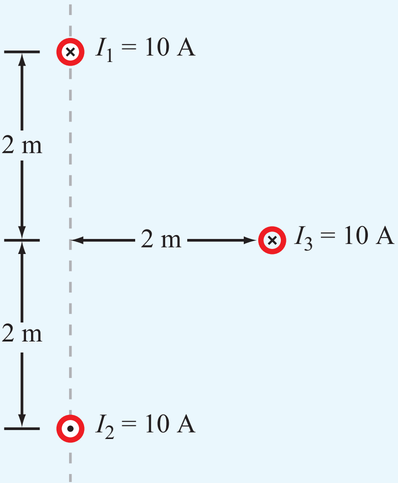

Figure P5.19 Three parallel wires of Problem 5.19.

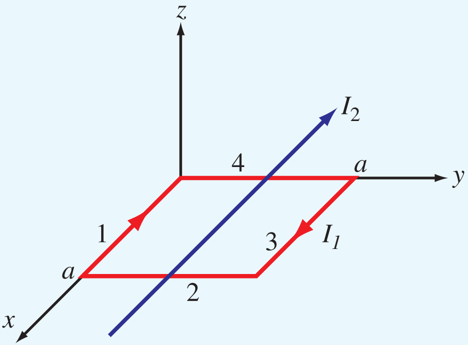

Figure P5.20 Long wire carrying current I_2, just above a square loop carrying I_1 (Problem 5.20).

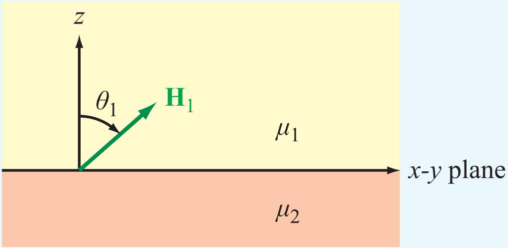

Figure P5.32 Adjacent magnetic media (Problem 5.32).

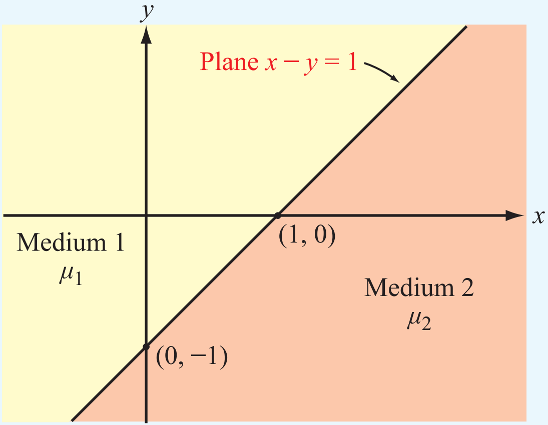

Figure P5.34 Magnetic media separated by the plane $x - y = 1$ (Problem 5.34).

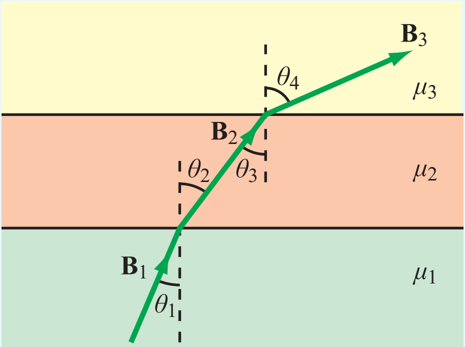

Figure P5.36 Three magnetic media with parallel interfaces (Problem 5.36).

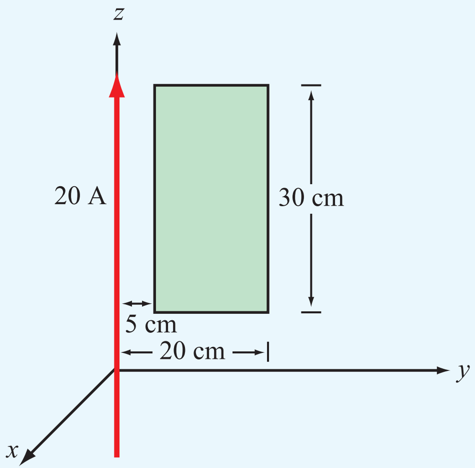

Figure P5.40 Loop and wire arrangement for Problem 5.40.

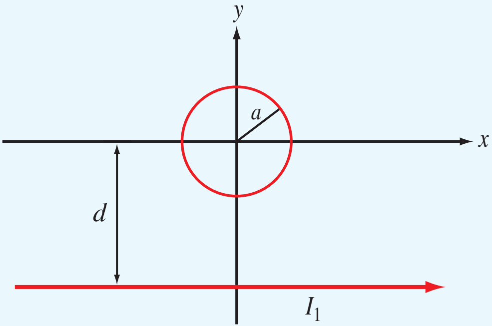

Figure P5.41 Linear conductor with current I_1 next to a circular loop of radius a at distance d (Problem 5.41).

Table 6-1 Maxwell's equations.

Reference	Differential Form	Integral Form	
Gauss's law	$\nabla \cdot \mathbf{D} = \rho_{\mathrm{v}}$	$\oint_S \mathbf{D} \cdot d\mathbf{s} = Q$	(6.1)
Faraday's law	$\nabla \times \mathbf{E} = -\dfrac{\partial \mathbf{B}}{\partial t}$	$\oint_C \mathbf{E} \cdot d\mathbf{l} = -\int_S \dfrac{\partial \mathbf{B}}{\partial t} \cdot d\mathbf{s}$	(6.2)*
No magnetic charges (Gauss's law for magnetism)	$\nabla \cdot \mathbf{B} = 0$	$\oint_S \mathbf{B} \cdot d\mathbf{s} = 0$	(6.3)
Ampère's law	$\nabla \times \mathbf{H} = \mathbf{J} + \dfrac{\partial \mathbf{D}}{\partial t}$	$\oint_C \mathbf{H} \cdot d\mathbf{l} = \int_S \left(\mathbf{J} + \dfrac{\partial \mathbf{D}}{\partial t} \right) \cdot d\mathbf{s}$	(6.4)

*For a stationary surface S.

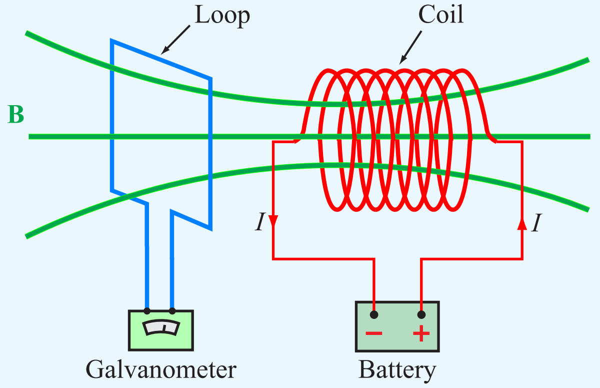

Figure 6-1 The galvanometer (predecessor of the ammeter) shows a deflection whenever the magnetic flux passing through the square loop changes with time.

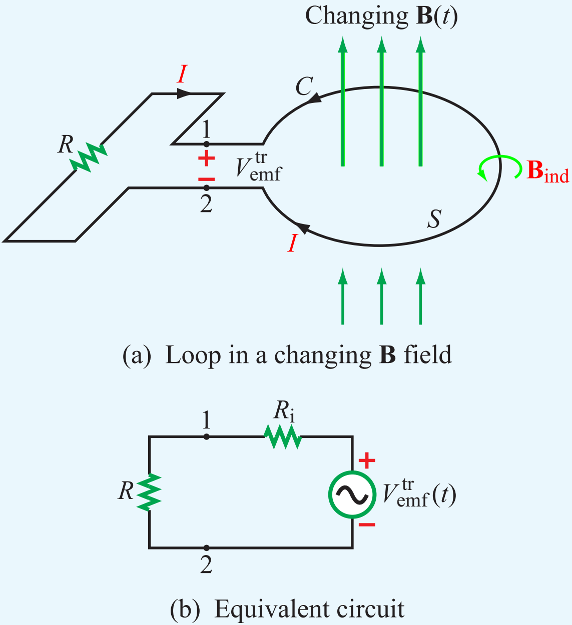

Figure 6-2 (a) Stationary circular loop in a changing magnetic field $\mathbf{B}(t)$, and (b) its equivalent circuit.

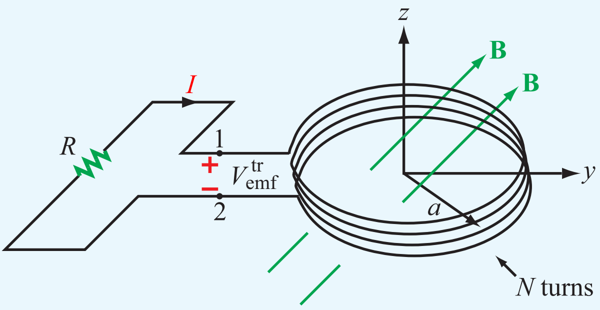

Figure 6-3 Circular loop with N turns in the x–y plane. The magnetic field is $\mathbf{B} = B_0(\hat{\mathbf{y}}2 + \hat{\mathbf{z}}3)\sin\omega t$ (Example 6-1).

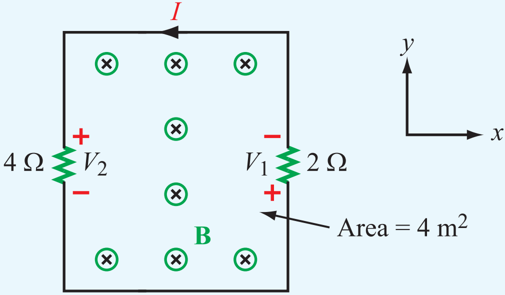

Figure 6-4 Circuit for Example 6-2.

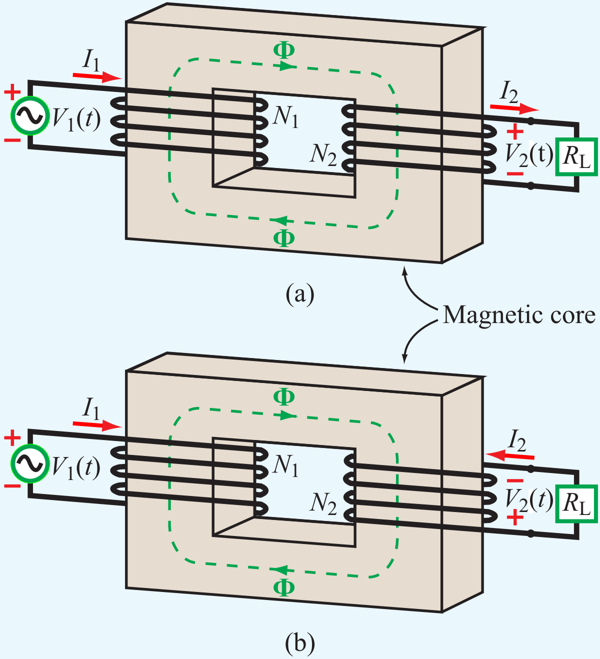

Figure 6-5 In a transformer, the directions of I_1 and I_2 are such that the flux Φ generated by one of them is opposite to that generated by the other. The direction of the secondary winding in (b) is opposite to that in (a), and so are the direction of I_2 and the polarity of V_2.

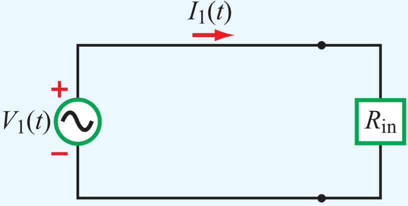

Figure 6-6 Equivalent circuit for the primary side of the transformer.

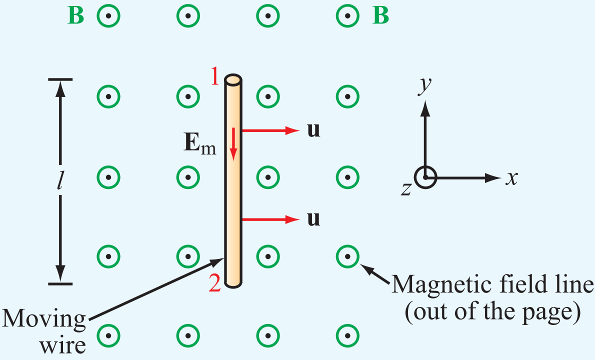

Figure 6-7 Conducting wire moving with velocity **u** in a static magnetic field.

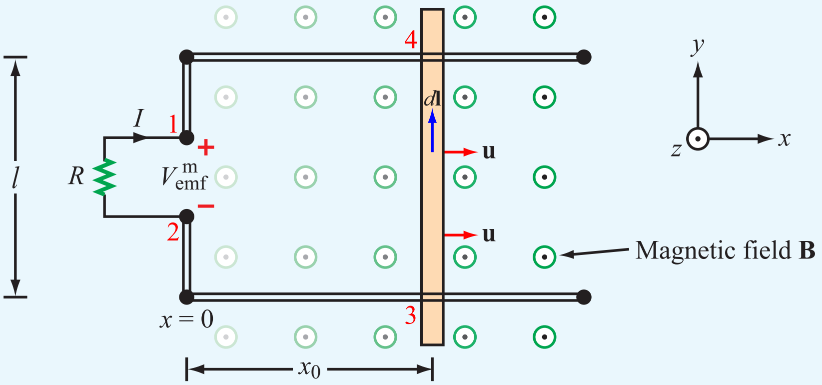

Figure 6-8 Sliding bar with velocity $\mathbf{u}$ in a magnetic field that increases linearly with x; that is, $\mathbf{B} = \hat{\mathbf{z}}B_0x$ (Example 6-3).

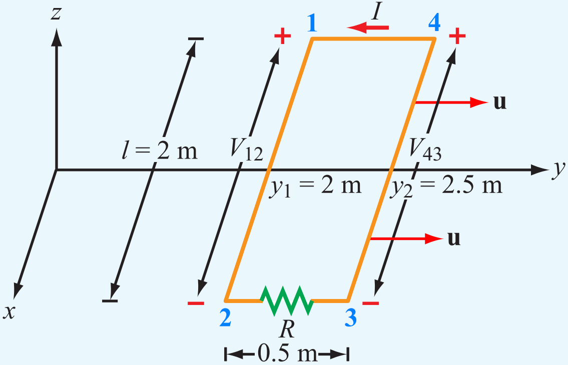

Figure 6-9 Moving loop of Example 6-4.

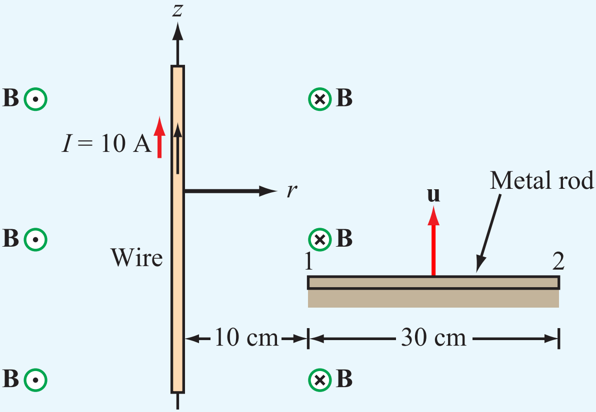

Figure 6-10 Moving rod of Example 6-5.

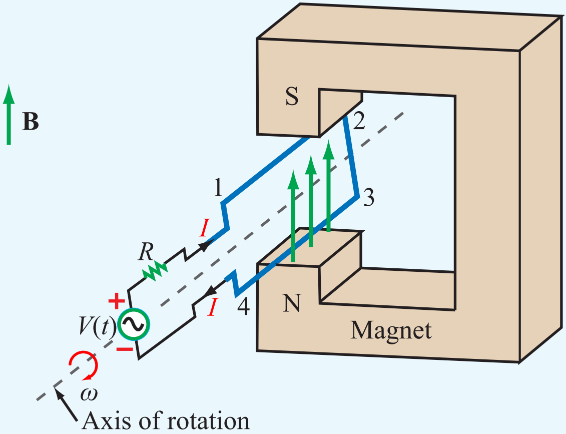

(a) ac motor

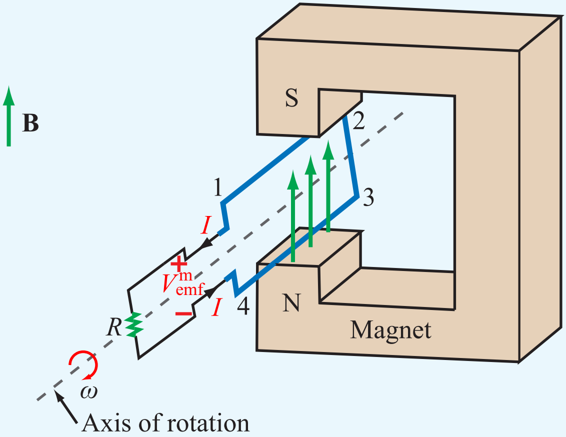

(b) ac generator

Figure 6-11 Principles of the ac motor and the ac generator. In (a) the magnetic torque on the wires causes the loop to rotate, and in (b) the rotating loop generates an emf.

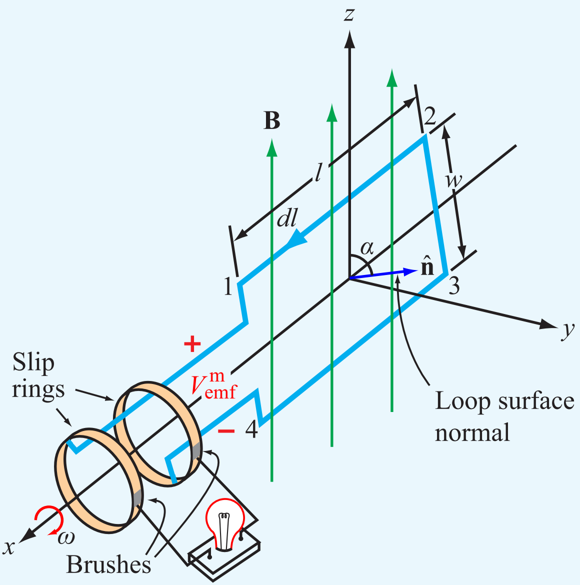

Figure 6-12 A loop rotating in a magnetic field induces an emf.

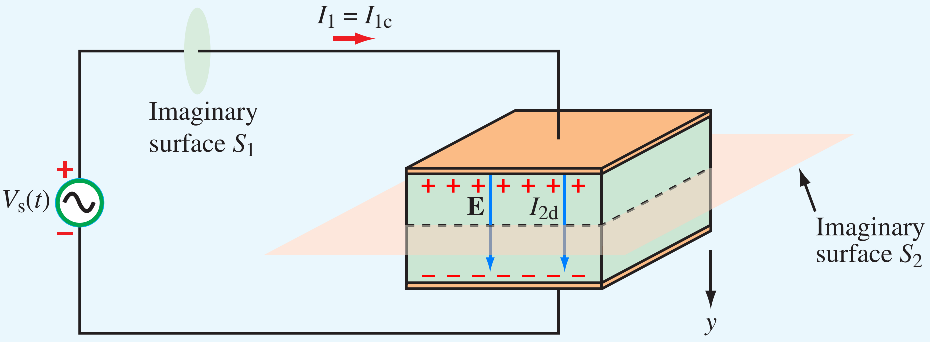

Figure 6-13 The displacement current I_{2d} in the insulating material of the capacitor is equal to the conducting current I_{1c} in the wire.

Table 6-2 Boundary conditions for the electric and magnetic fields.

Field Components	General Form	Medium 1 Dielectric	Medium 2 Dielectric	Medium 1 Dielectric	Medium 2 Conductor
Tangential E	$\hat{\mathbf{n}}_2 \times (\mathbf{E}_1 - \mathbf{E}_2) = 0$	$E_{1t} = E_{2t}$		$E_{1t} = E_{2t} = 0$	
Normal D	$\hat{\mathbf{n}}_2 \cdot (\mathbf{D}_1 - \mathbf{D}_2) = \rho_s$	$D_{1n} - D_{2n} = \rho_s$		$D_{1n} = \rho_s$	$D_{2n} = 0$
Tangential H	$\hat{\mathbf{n}}_2 \times (\mathbf{H}_1 - \mathbf{H}_2) = \mathbf{J}_s$	$H_{1t} = H_{2t}$		$H_{1t} = J_s$	$H_{2t} = 0$
Normal B	$\hat{\mathbf{n}}_2 \cdot (\mathbf{B}_1 - \mathbf{B}_2) = 0$	$B_{1n} = B_{2n}$		$B_{1n} = B_{2n} = 0$	

Notes: (1) ρ_s is the surface charge density at the boundary; (2) $\mathbf{J}_s$ is the surface current density at the boundary; (3) normal components of all fields are along $\hat{\mathbf{n}}_2$, the outward unit vector of medium 2; (4) $E_{1t} = E_{2t}$ implies that the tangential components are equal in magnitude and parallel in direction; (5) direction of $\mathbf{J}_s$ is orthogonal to $(\mathbf{H}_1 - \mathbf{H}_2)$.

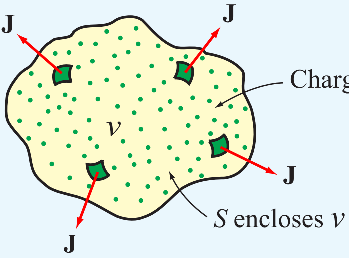

Figure 6-14 The total current flowing out of a volume $\mathcal{V}$ is equal to the flux of the current density **J** through the surface S, which in turn is equal to the rate of decrease of the charge enclosed in $\mathcal{V}$.

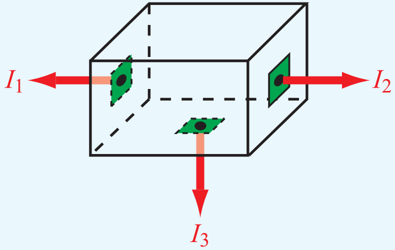

Figure 6-15 Kirchhoff's current law states that the algebraic sum of all the currents flowing out of a junction is zero.

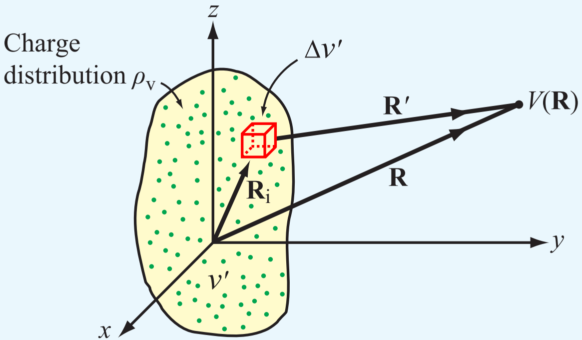

Figure 6-16 Electric potential $V(\mathbf{R})$ due to a charge distribution ρ_v over a volume v'.

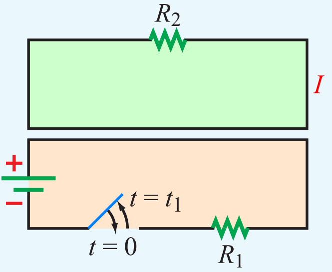

Figure P6.1 Loops of Problem 6.1.

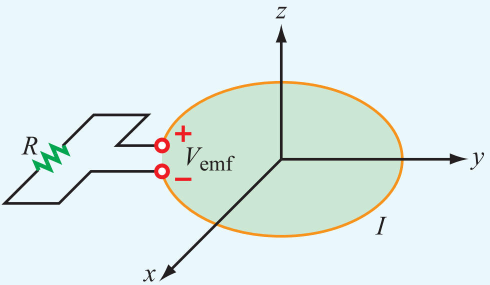

Figure P6.2 Loop of Problem 6.2.

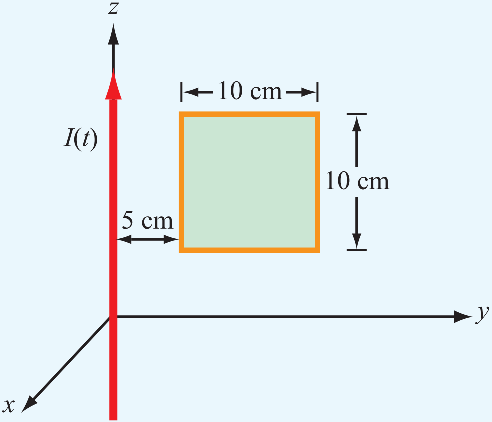

Figure P6.6 Loop coplanar with long wire (Problem 6.6).

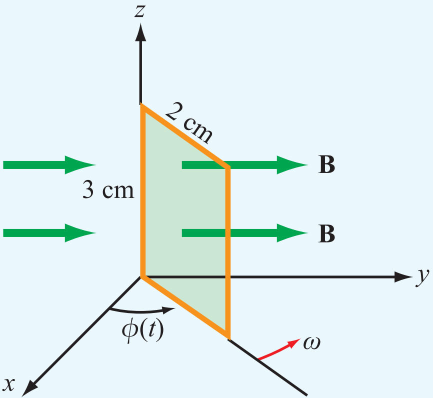

Figure P6.7 Rotating loop in a magnetic field (Problem 6.7).

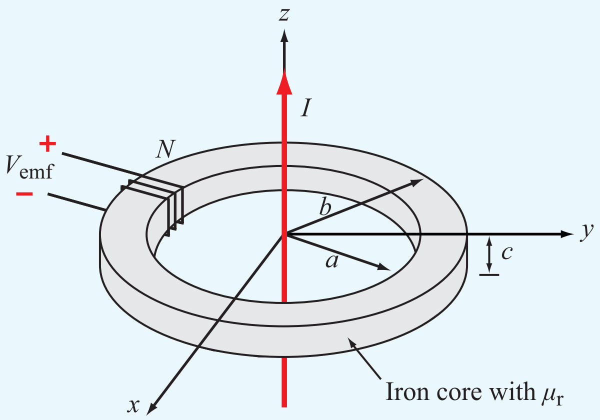

Figure P6.8 Problem 6.8.

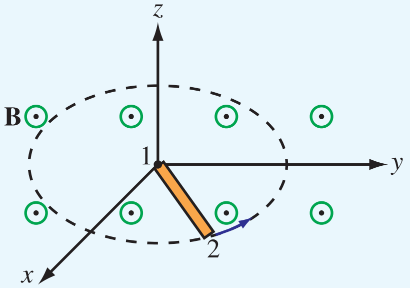

Figure P6.10 Rotating rod of Problem 6.10.

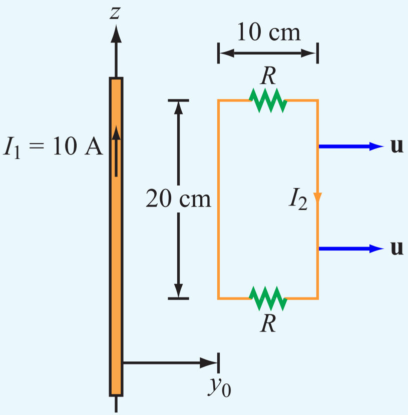

Figure P6.11 Moving loop of Problem 6.11.

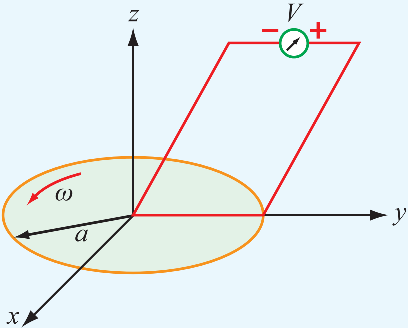

Figure P6.13 Rotating circular disk in a magnetic field (Problem 6.13).

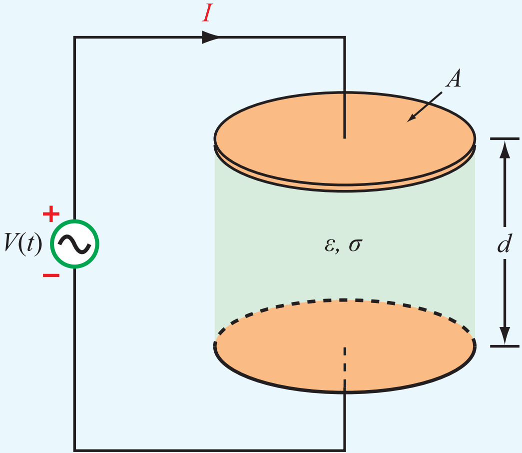

Figure P6.16 Parallel-plate capacitor containing a lossy dielectric material (Problem 6.16).

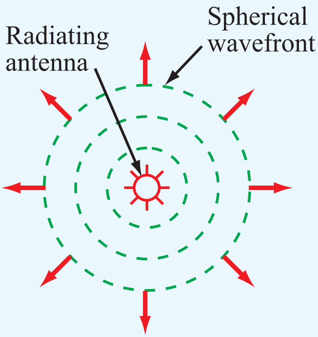

(a) Spherical wave

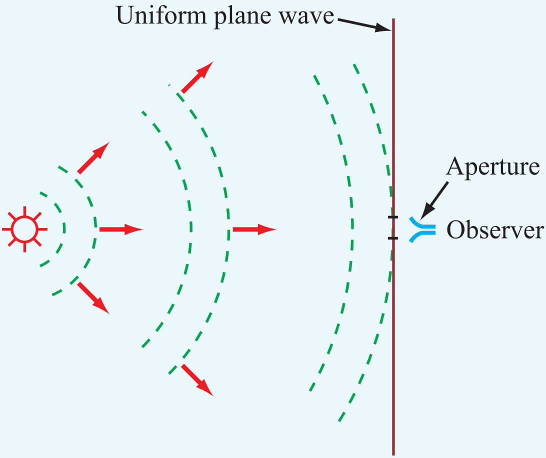

(b) Plane-wave approximation

Figure 7-1 Waves radiated by an EM source, such as a light bulb or an antenna, have spherical wavefronts, as in (a); to a distant observer, however, the wavefront across the observer's aperture appears approximately planar, as in (b).

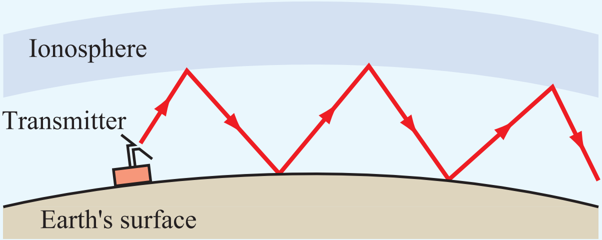

Figure 7-2 The atmospheric layer bounded by the ionosphere at the top and Earth's surface at the bottom forms a guiding structure for the propagation of radio waves in the HF band.

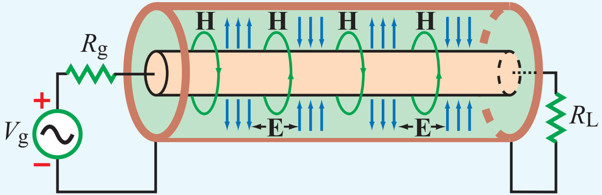

Figure 7-3 A guided electromagnetic wave traveling in a coaxial transmission line consists of time-varying electric and magnetic fields in the dielectric medium between the inner and outer conductors.

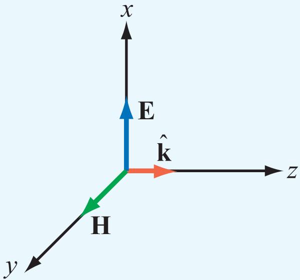

Figure 7-4 A transverse electromagnetic (TEM) wave propagating in the direction $\hat{\mathbf{k}} = \hat{\mathbf{z}}$. For all TEM waves, $\hat{\mathbf{k}}$ is parallel to $\mathbf{E} \times \mathbf{H}$.

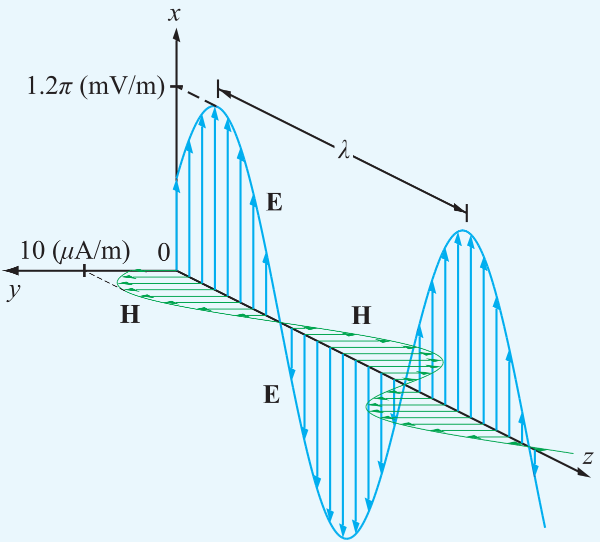

Figure 7-5 Spatial variations of **E** and **H** at $t = 0$ for the plane wave of Example 7-1.

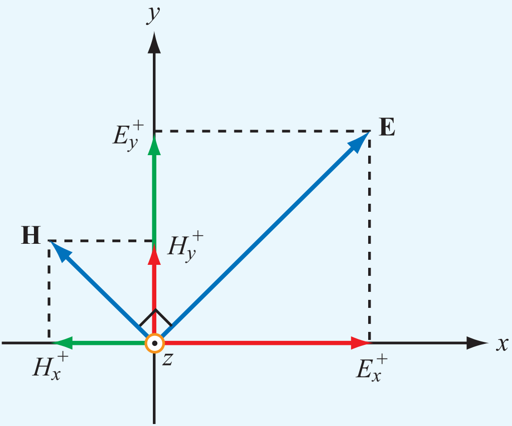

Figure 7-6 The wave $(\mathbf{E}, \mathbf{H})$ is equivalent to the sum of two waves, one with fields (E_x^+, H_y^+) and another with (E_y^+, H_x^+), with both traveling in the $+z$ direction.

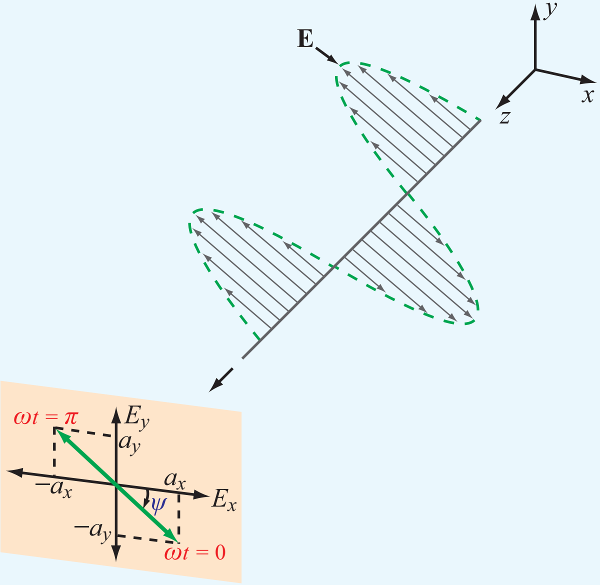

Figure 7-7 Linearly polarized wave traveling in the $+z$ direction (out of the page).

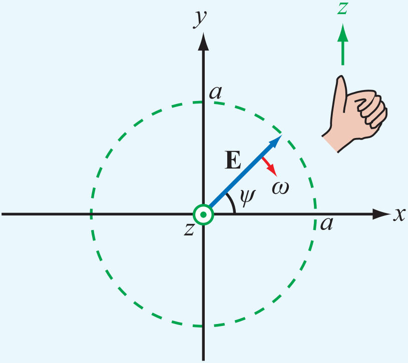

(a) LHC polarization

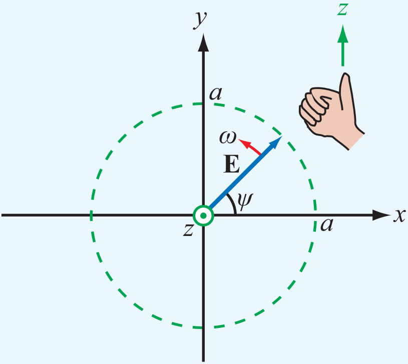

(b) RHC polarization

Figure 7-8 Circularly polarized plane waves propagating in the $+z$ direction (out of the page).

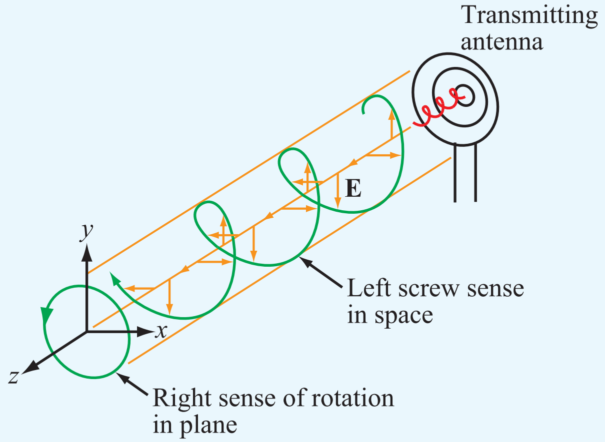

Figure 7-9 Right-hand circularly polarized wave radiated by a helical antenna.

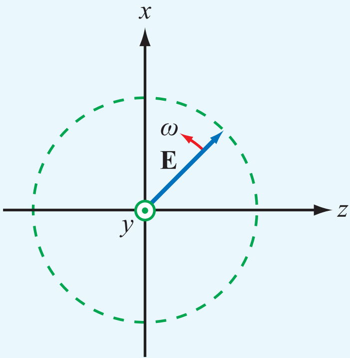

Figure 7-10 Right-hand circularly polarized wave of Example 7-2.

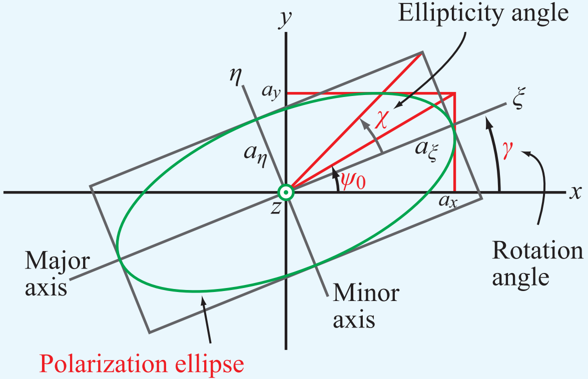

Figure 7-11 Polarization ellipse in the x–y plane, with the wave traveling in the z direction (out of the page).

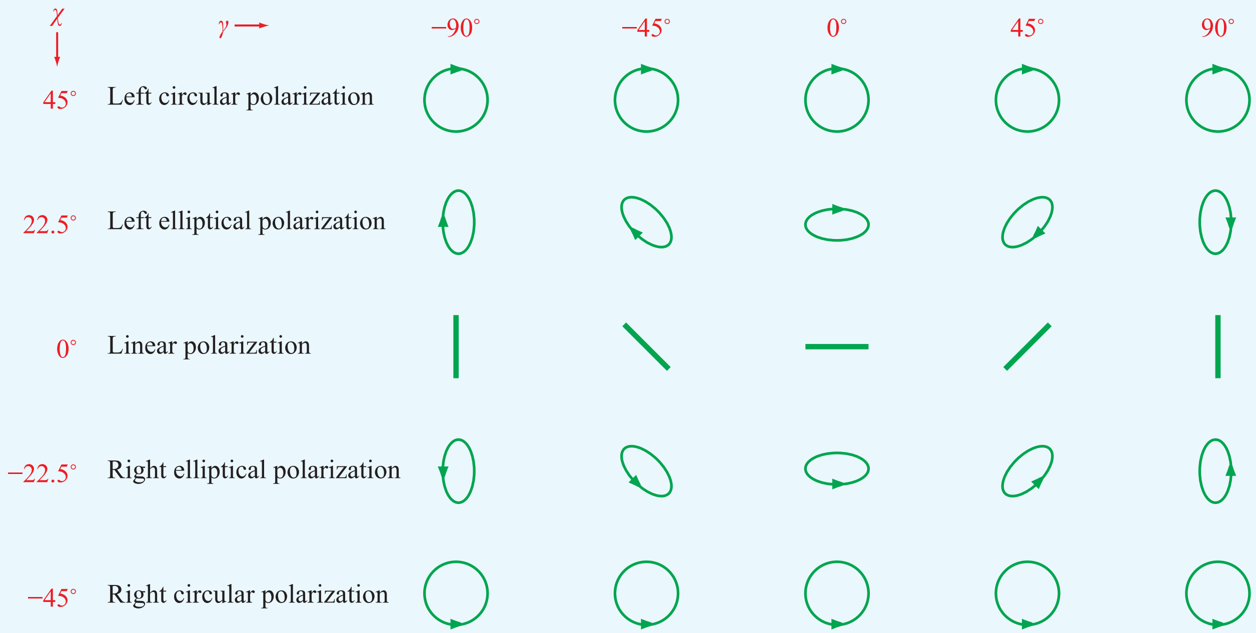

Figure 7-12 Polarization states for various combinations of the polarization angles (γ, χ) for a wave traveling out of the page.

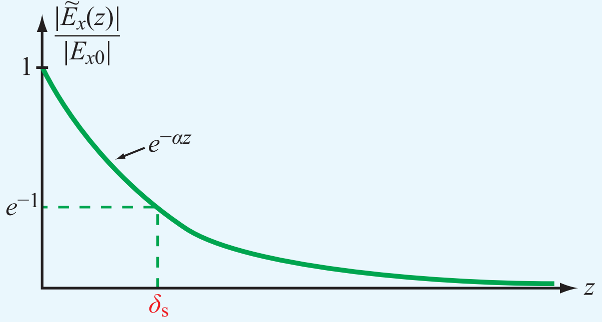

Figure 7-13 Attenuation of the magnitude of $\widetilde{E}_x(z)$ with distance z. The skin depth δ_s is the value of z at which $|\widetilde{E}_x(z)|/|E_{x0}| = e^{-1}$, or $z = \delta_s = 1/\alpha$.

Table 7-1 **Expressions for α, β, η_c, u_p, and λ for various types of media.**

	Any Medium	Lossless Medium $(\sigma = 0)$	Low-loss Medium $(\varepsilon''/\varepsilon' \ll 1)$	Good Conductor $(\varepsilon''/\varepsilon' \gg 1)$	Units
$\alpha =$	$\omega \left[\frac{\mu\varepsilon'}{2} \left[\sqrt{1 + \left(\frac{\varepsilon''}{\varepsilon'}\right)^2} - 1 \right] \right]^{1/2}$	0	$\frac{\sigma}{2}\sqrt{\frac{\mu}{\varepsilon}}$	$\sqrt{\pi f \mu \sigma}$	(Np/m)
$\beta =$	$\omega \left[\frac{\mu\varepsilon'}{2} \left[\sqrt{1 + \left(\frac{\varepsilon''}{\varepsilon'}\right)^2} + 1 \right] \right]^{1/2}$	$\omega\sqrt{\mu\varepsilon}$	$\omega\sqrt{\mu\varepsilon}$	$\sqrt{\pi f \mu \sigma}$	(rad/m)
$\eta_c =$	$\sqrt{\frac{\mu}{\varepsilon'}} \left(1 - j\frac{\varepsilon''}{\varepsilon'}\right)^{-1/2}$	$\sqrt{\frac{\mu}{\varepsilon}}$	$\sqrt{\frac{\mu}{\varepsilon}}$	$(1+j)\frac{\alpha}{\sigma}$	(Ω)
$u_p =$	ω/β	$1/\sqrt{\mu\varepsilon}$	$1/\sqrt{\mu\varepsilon}$	$\sqrt{4\pi f/\mu\sigma}$	(m/s)
$\lambda =$	$2\pi/\beta = u_p/f$	u_p/f	u_p/f	u_p/f	(m)

Notes: $\varepsilon' = \varepsilon$; $\varepsilon'' = \sigma/\omega$; in free space, $\varepsilon = \varepsilon_0$, $\mu = \mu_0$; in practice, a material is considered a low-loss medium if $\varepsilon''/\varepsilon' = \sigma/\omega\varepsilon < 0.01$ and a good conducting medium if $\varepsilon''/\varepsilon' > 100$.

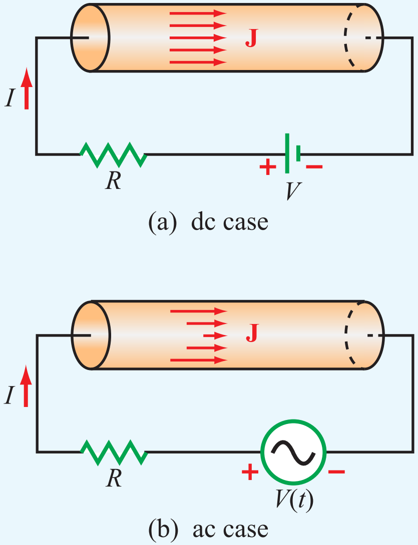

Figure 7-14 Current density **J** in a conducting wire is (a) uniform across its cross section in the dc case, but (b) in the ac case, **J** is highest along the wire's perimeter.

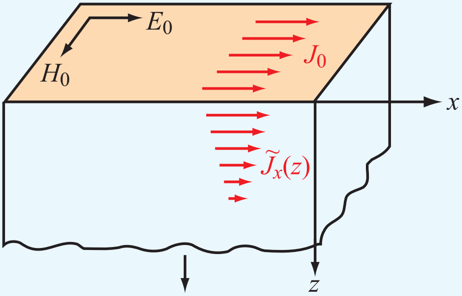

(a) Exponentially decaying $\widetilde{J}_x(z)$

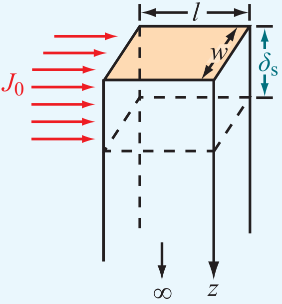

(b) Equivalent J_0 over skin depth δ_s

Figure 7-15 Exponential decay of current density $\widetilde{J}_x(z)$ with z in a solid conductor. The total current flowing through (a) a section of width w extending between $z = 0$ and $z = \infty$ is equivalent to (b) a constant current density J_0 flowing through a section of depth δ_s.

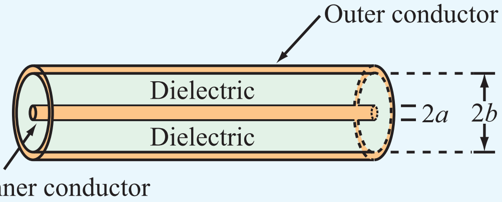

(a) Coaxial cable

(b) Equivalent inner conductor

Figure 7-16 The inner conductor of the coaxial cable in (a) is represented in (b) by a planar conductor of width $2\pi a$ and depth δ_s, as if its skin has been cut along its length on the bottom side and then unfurled into a planar geometry.

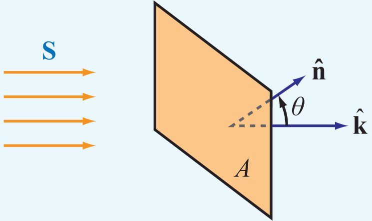

Figure 7-17 EM power flow through an aperture.

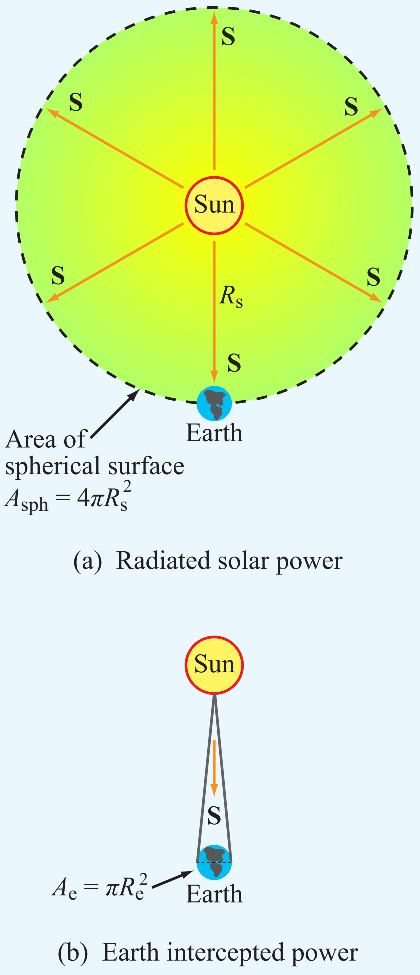

Figure 7-18 Solar radiation intercepted by (a) a spherical surface of radius R_s, and (b) Earth's surface (Example 7-5).

Table 7-2 Power ratios in natural numbers and in decibels.

G	G [dB]
10^x	$10x$ dB
4	6 dB
2	3 dB
1	0 dB
0.5	-3 dB
0.25	-6 dB
0.1	-10 dB
10^{-3}	-30 dB

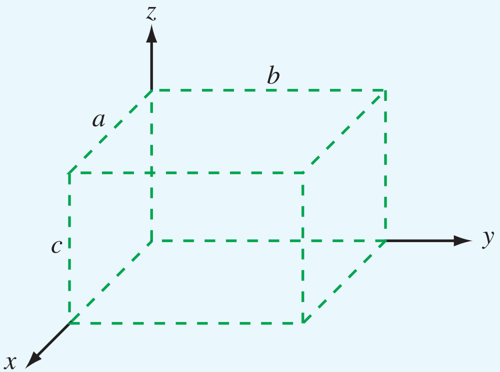

Figure P7.39 Imaginary rectangular box of Problems 7.39 and 7.40.

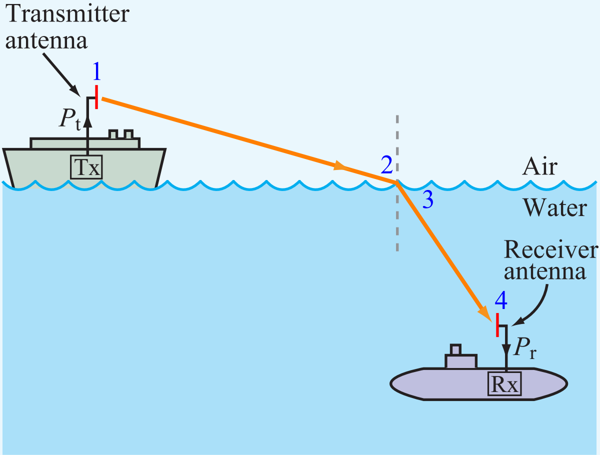

Figure 8-1 Signal path between a shipboard transmitter (Tx) and a submarine receiver (Rx).

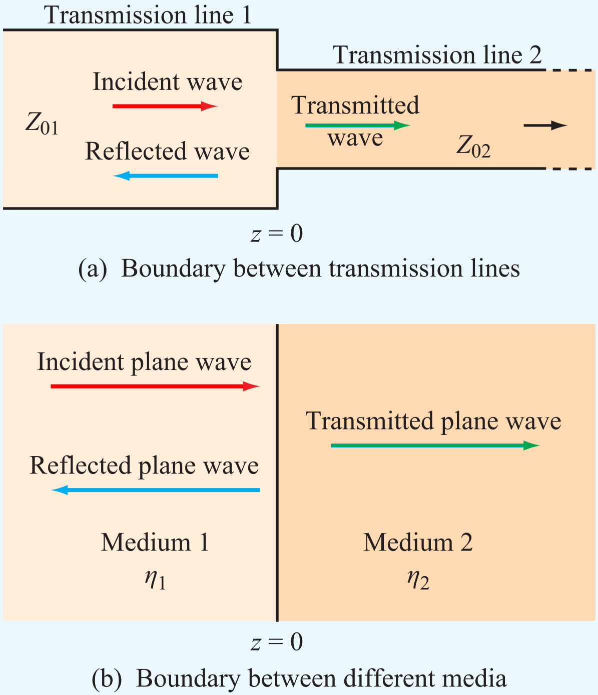

Figure 8-2 Discontinuity between two different transmission lines is analogous to that between two dissimilar media.

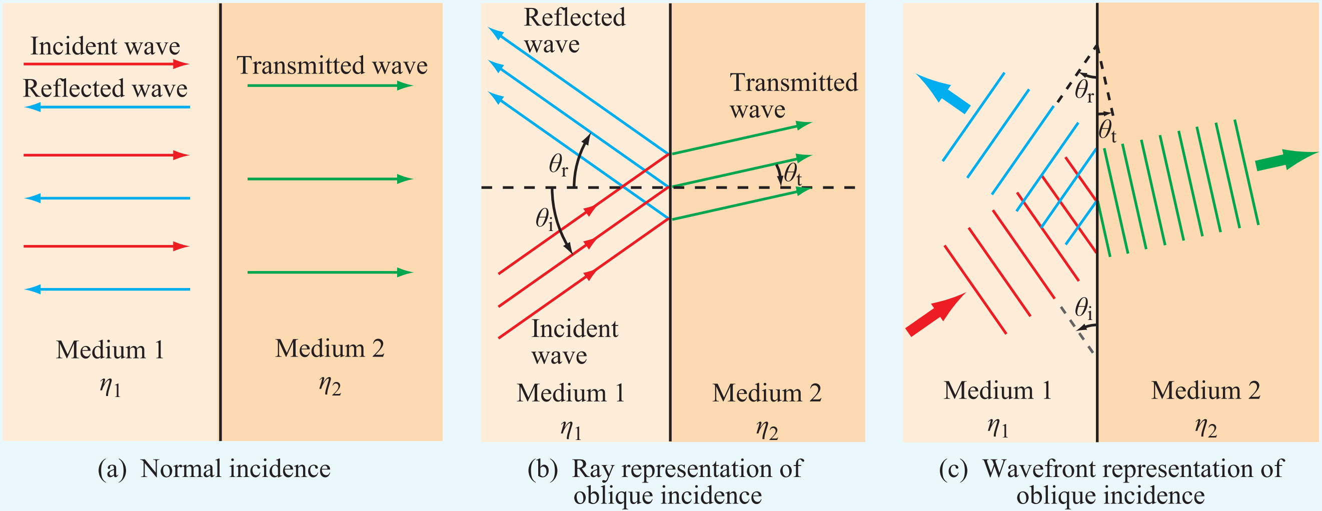

Figure 8-3 Ray representation of wave reflection and transmission at (a) normal incidence and (b) oblique incidence, and (c) wavefront representation of oblique incidence.

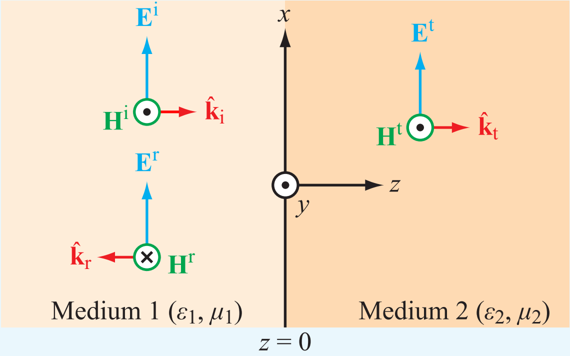

(a) Boundary between dielectric media

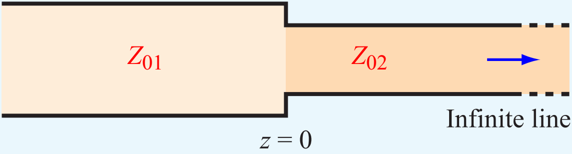

(b) Transmission-line analogue

Figure 8-4 The two dielectric media separated by the *x*–*y* plane in (a) can be represented by the transmission-line analogue in (b).

Table 8-1 **Analogy between plane-wave equations for normal incidence and transmission-line equations, both under lossless conditions.**

Plane Wave [Fig. 8-4(a)]		Transmission Line [Fig. 8-4(b)]	
$\widetilde{\mathbf{E}}_1(z) = \hat{\mathbf{x}} E_0^{\mathrm{i}} (e^{-jk_1 z} + \Gamma e^{jk_1 z})$	(8.11a)	$\widetilde{V}_1(z) = V_0^+ (e^{-j\beta_1 z} + \Gamma e^{j\beta_1 z})$	(8.11b)
$\widetilde{\mathbf{H}}_1(z) = \hat{\mathbf{y}} \dfrac{E_0^{\mathrm{i}}}{\eta_1} (e^{-jk_1 z} - \Gamma e^{jk_1 z})$	(8.12a)	$\tilde{I}_1(z) = \dfrac{V_0^+}{Z_{01}} (e^{-j\beta_1 z} - \Gamma e^{j\beta_1 z})$	(8.12b)
$\widetilde{\mathbf{E}}_2(z) = \hat{\mathbf{x}} \tau E_0^{\mathrm{i}} e^{-jk_2 z}$	(8.13a)	$\widetilde{V}_2(z) = \tau V_0^+ e^{-j\beta_2 z}$	(8.13b)
$\widetilde{\mathbf{H}}_2(z) = \hat{\mathbf{y}} \tau \dfrac{E_0^{\mathrm{i}}}{\eta_2}\, e^{-jk_2 z}$	(8.14a)	$\tilde{I}_2(z) = \tau \dfrac{V_0^+}{Z_{02}}\, e^{-j\beta_2 z}$	(8.14b)
$\Gamma = (\eta_2 - \eta_1)/(\eta_2 + \eta_1)$		$\Gamma = (Z_{02} - Z_{01})/(Z_{02} + Z_{01})$	
$\tau = 1 + \Gamma$		$\tau = 1 + \Gamma$	
$k_1 = \omega\sqrt{\mu_1 \varepsilon_1}\,, \qquad k_2 = \omega\sqrt{\mu_2 \varepsilon_2}$		$\beta_1 = \omega\sqrt{\mu_1 \varepsilon_1}\,, \qquad \beta_2 = \omega\sqrt{\mu_2 \varepsilon_2}$	
$\eta_1 = \sqrt{\mu_1/\varepsilon_1}\,, \qquad \eta_2 = \sqrt{\mu_2/\varepsilon_2}$		Z_{01} and Z_{02} depend on transmission-line parameters	

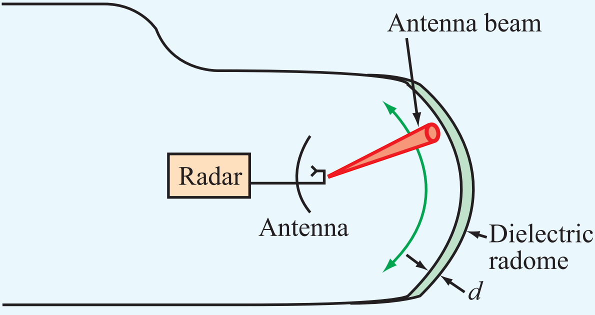

Figure 8-5 Antenna beam “looking” through an aircraft radome of thickness d (Example 8-1).

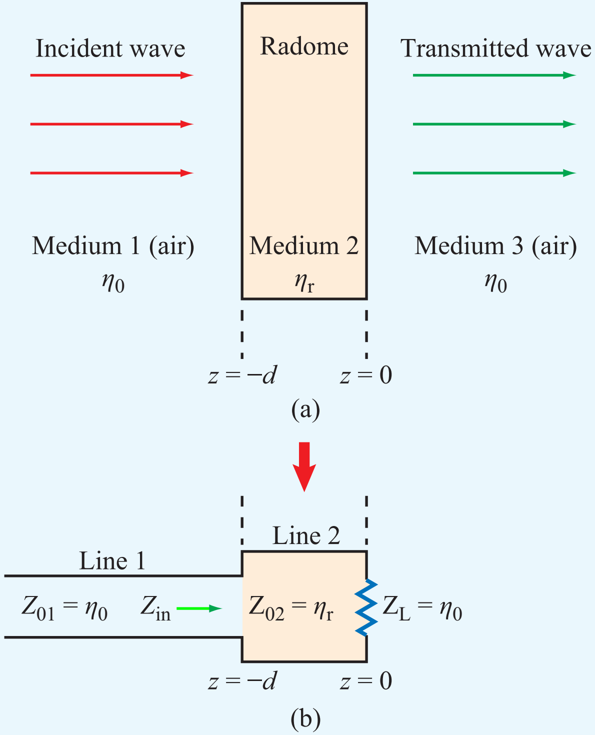

Figure 8-6 (a) Planar section of the radome of **Fig. 8-5** at an expanded scale and (b) its transmission-line equivalent model (Example 8-1).

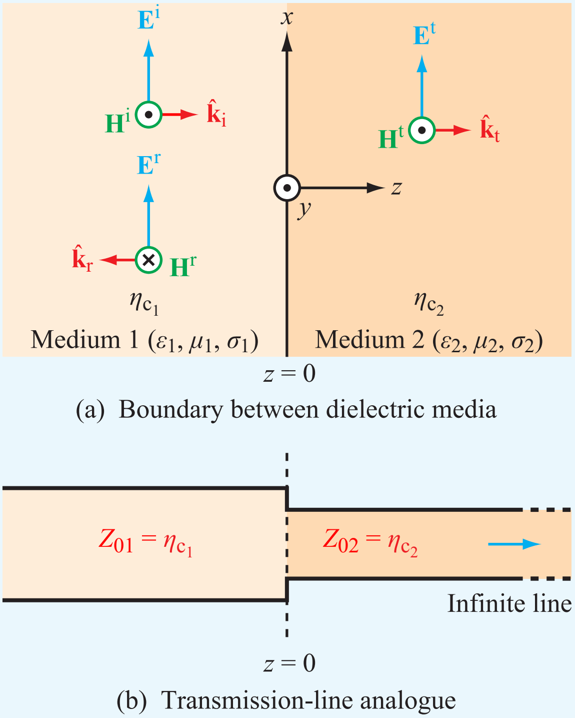

Figure 8-7 Normal incidence at a planar boundary between two lossy media.

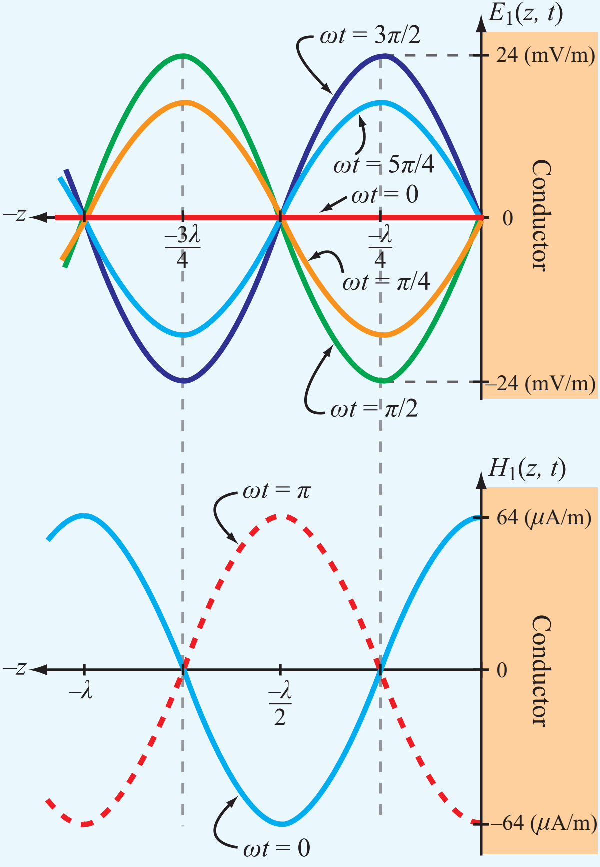

Figure 8-8 Wave patterns for fields $E_1(z,t)$ and $H_1(z,t)$ of Example 8-3.

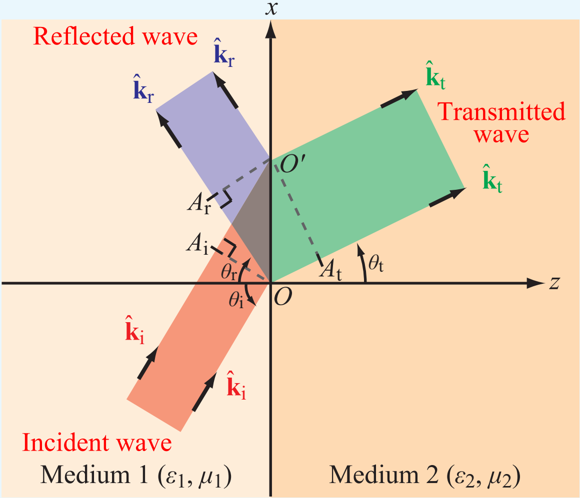

Figure 8-9 Wave reflection and refraction at a planar boundary between different media.

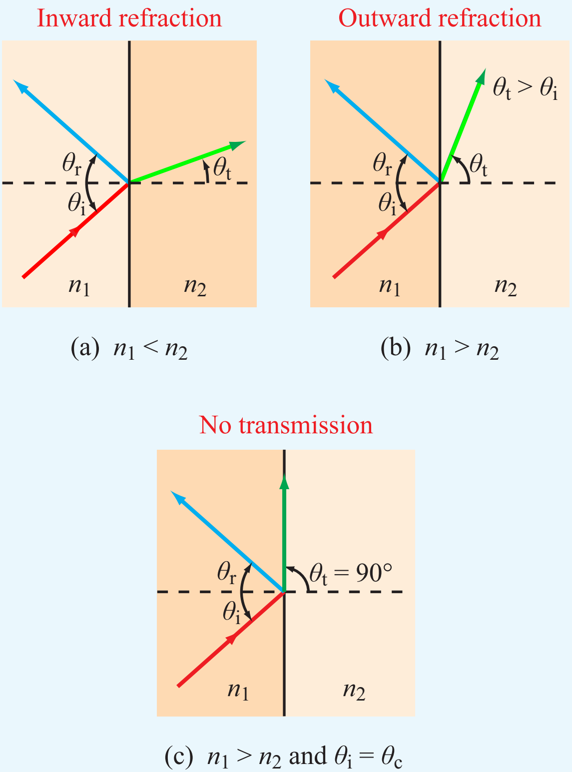

Figure 8-10 Snell's laws state that $\theta_r = \theta_i$ and $\sin\theta_t = (n_1/n_2)\sin\theta_i$. Refraction is (a) inward if $n_1 < n_2$ and (b) outward if $n_1 > n_2$; and (c) the refraction angle is $90°$ if $n_1 > n_2$ and θ_i is equal to or greater than the critical angle $\theta_c = \sin^{-1}(n_2/n_1)$.

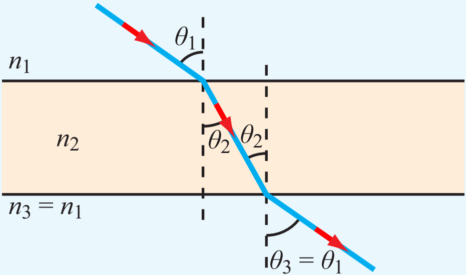

Figure 8-11 The exit angle θ_3 is equal to the incidence angle θ_1 if the dielectric slab has parallel boundaries and is surrounded by media with the same index of refraction on both sides (Example 8-4).

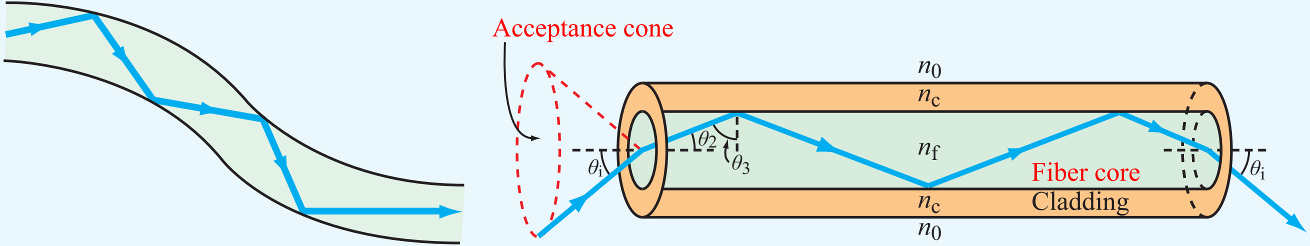

(a) Optical fiber (b) Successive internal reflections

Figure 8-12 Waves can be guided along optical fibers as long as the reflection angles exceed the critical angle for total internal reflection.

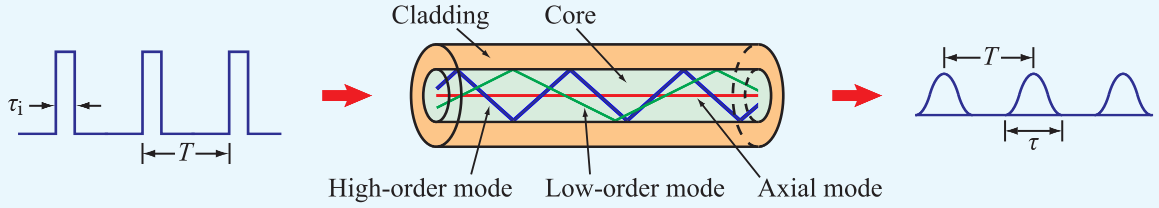

Figure 8-13 Distortion of rectangular pulses caused by modal dispersion in optical fibers.

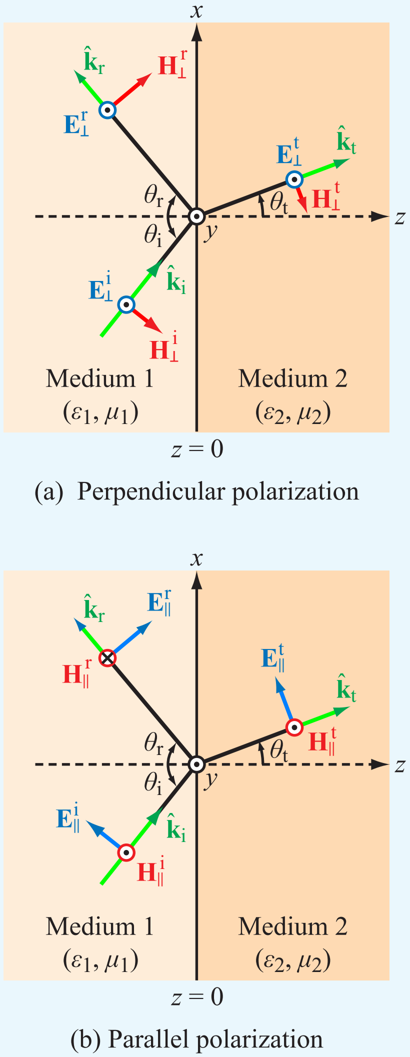

Figure 8-14 The plane of incidence is the plane containing the direction of wave travel, $\hat{\mathbf{k}}_i$, and the surface normal to the boundary. In the present case the plane of incidence containing $\hat{\mathbf{k}}_i$ and $\hat{\mathbf{z}}$ coincides with the plane of the paper. A wave is (a) perpendicularly polarized when its electric field vector is perpendicular to the plane of incidence and (b) parallel polarized when its electric field vector lies in the plane of incidence.

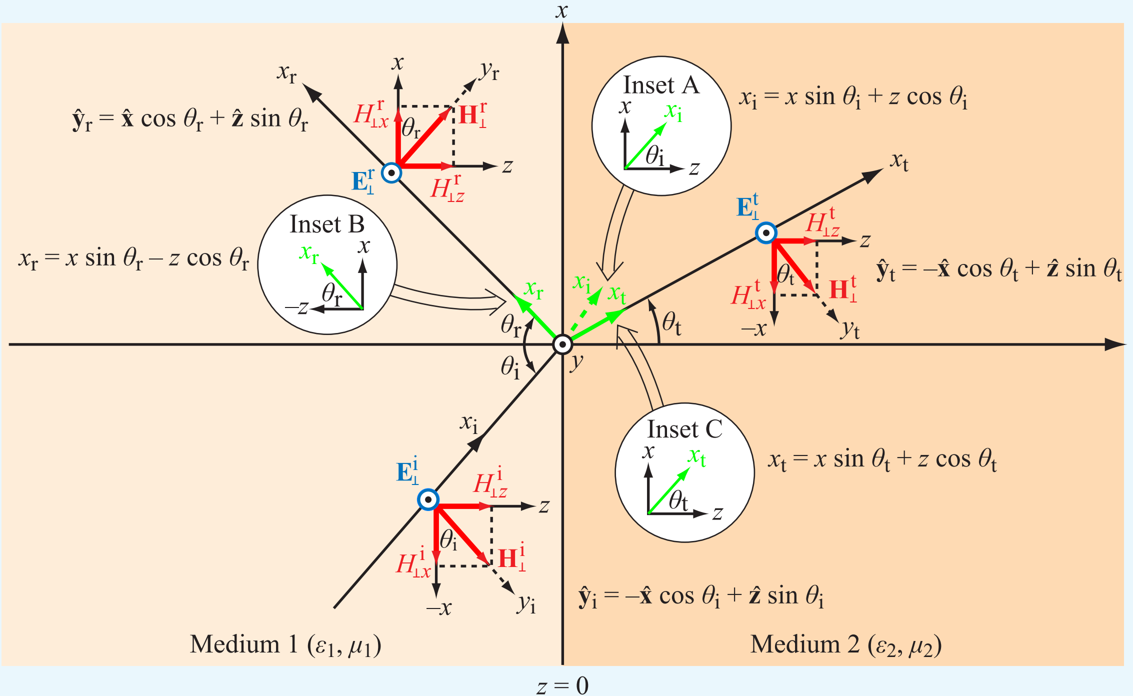

Figure 8-15 Perpendicularly polarized plane wave incident at an angle θ_i upon a planar boundary.

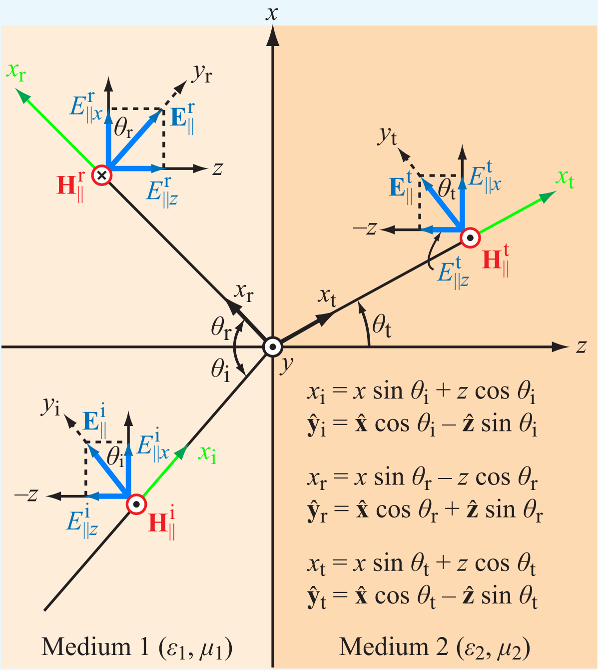

Figure 8-16 Parallel-polarized plane wave incident at an angle θ_i upon a planar boundary.

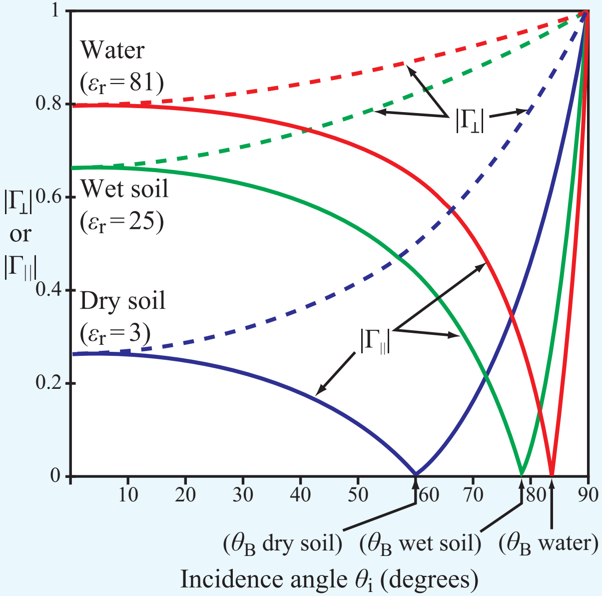

Figure 8-17 Plots for $|\Gamma_\perp|$ and $|\Gamma_\parallel|$ as a function of θ_i for a dry soil surface, a wet-soil surface, and a water surface. For each surface, $|\Gamma_\parallel| = 0$ at the Brewster angle.

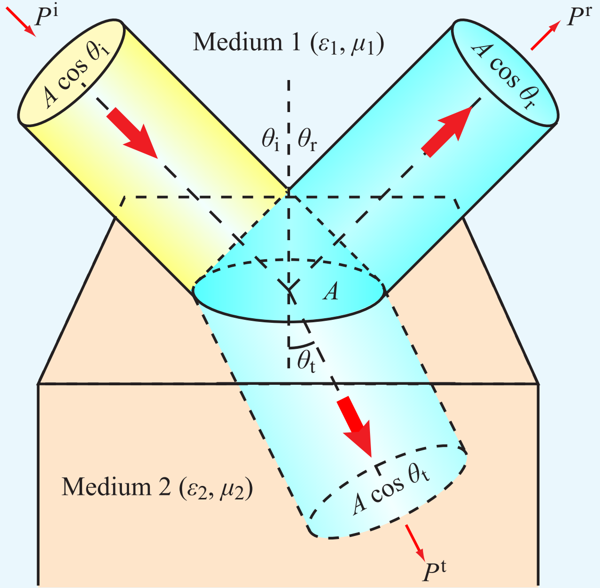

Figure 8-18 Reflection and transmission of an incident circular beam illuminating a spot of size A on the interface.

Table 8-2 **Expressions for Γ, τ, R, and T for wave incidence from a medium with intrinsic impedance η_1 onto a medium with intrinsic impedance η_2. Angles θ_i and θ_t are the angles of incidence and transmission, respectively.**

Property	Normal Incidence $\theta_\mathrm{i} = \theta_\mathrm{t} = 0$	Perpendicular Polarization	Parallel Polarization
Reflection coefficient	$\Gamma = \dfrac{\eta_2 - \eta_1}{\eta_2 + \eta_1}$	$\Gamma_\perp = \dfrac{\eta_2 \cos\theta_\mathrm{i} - \eta_1 \cos\theta_\mathrm{t}}{\eta_2 \cos\theta_\mathrm{i} + \eta_1 \cos\theta_\mathrm{t}}$	$\Gamma_\parallel = \dfrac{\eta_2 \cos\theta_\mathrm{t} - \eta_1 \cos\theta_\mathrm{i}}{\eta_2 \cos\theta_\mathrm{t} + \eta_1 \cos\theta_\mathrm{i}}$
Transmission coefficient	$\tau = \dfrac{2\eta_2}{\eta_2 + \eta_1}$	$\tau_\perp = \dfrac{2\eta_2 \cos\theta_\mathrm{i}}{\eta_2 \cos\theta_\mathrm{i} + \eta_1 \cos\theta_\mathrm{t}}$	$\tau_\parallel = \dfrac{2\eta_2 \cos\theta_\mathrm{i}}{\eta_2 \cos\theta_\mathrm{t} + \eta_1 \cos\theta_\mathrm{i}}$
Relation of Γ to τ	$\tau = 1 + \Gamma$	$\tau_\perp = 1 + \Gamma_\perp$	$\tau_\parallel = (1 + \Gamma_\parallel)\, \dfrac{\cos\theta_\mathrm{i}}{\cos\theta_\mathrm{t}}$
Reflectivity	$R = \lvert\Gamma\rvert^2$	$R_\perp = \lvert\Gamma_\perp\rvert^2$	$R_\parallel = \lvert\Gamma_\parallel\rvert^2$
Transmissivity	$T = \lvert\tau\rvert^2 \left(\dfrac{\eta_1}{\eta_2}\right)$	$T_\perp = \lvert\tau_\perp\rvert^2\, \dfrac{\eta_1 \cos\theta_\mathrm{t}}{\eta_2 \cos\theta_\mathrm{i}}$	$T_\parallel = \lvert\tau_\parallel\rvert^2\, \dfrac{\eta_1 \cos\theta_\mathrm{t}}{\eta_2 \cos\theta_\mathrm{i}}$
Relation of R to T	$T = 1 - R$	$T_\perp = 1 - R_\perp$	$T_\parallel = 1 - R_\parallel$

Notes: (1) $\sin\theta_\mathrm{t} = \sqrt{\mu_1\varepsilon_1/\mu_2\varepsilon_2}\,\sin\theta_\mathrm{i}$; (2) $\eta_1 = \sqrt{\mu_1/\varepsilon_1}$; (3) $\eta_2 = \sqrt{\mu_2/\varepsilon_2}$; (4) for nonmagnetic media, $\eta_2/\eta_1 = n_1/n_2$.

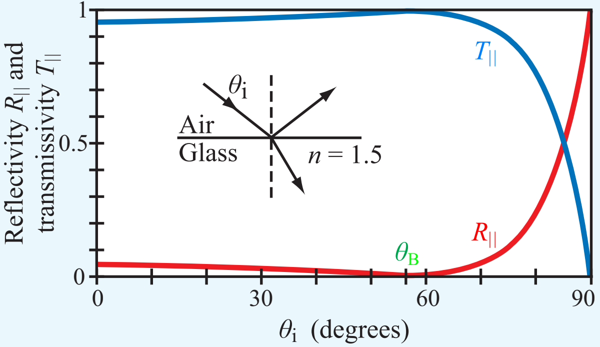

Figure 8-19 Angular plots for $(R_\parallel, T_\parallel)$ for an air–glass interface.

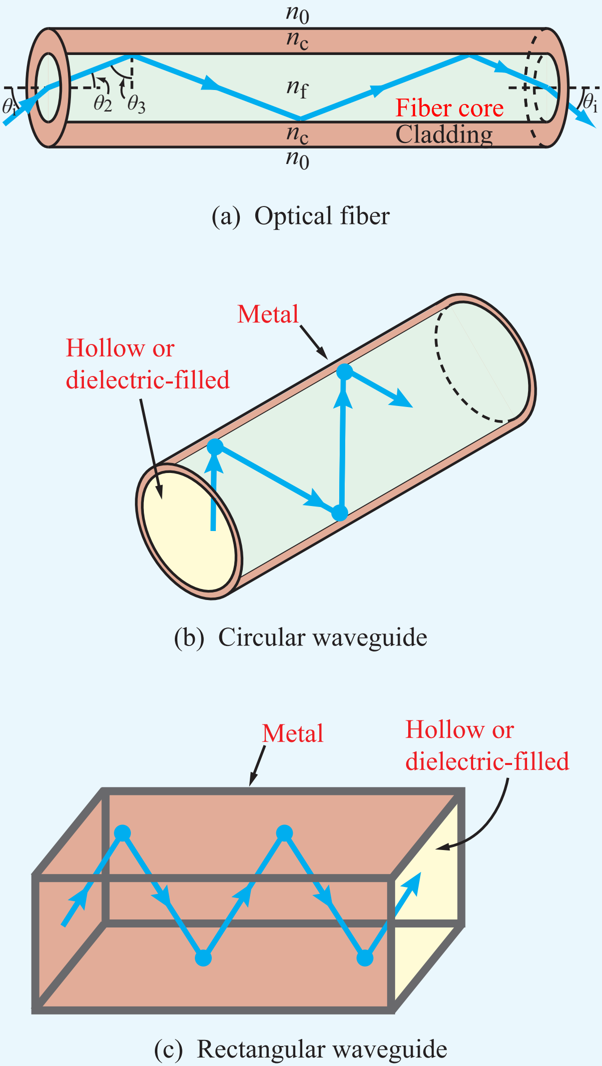

Figure 8-20 Wave travel by successive reflections in (a) an optical fiber, (b) a circular metal waveguide, and (c) a rectangular metal waveguide.

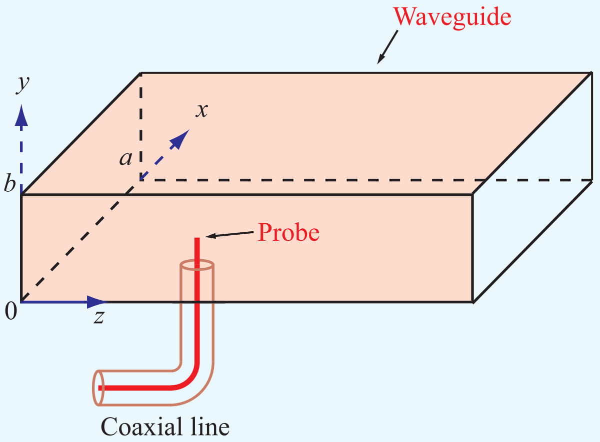

(a) Coax-to-waveguide coupler

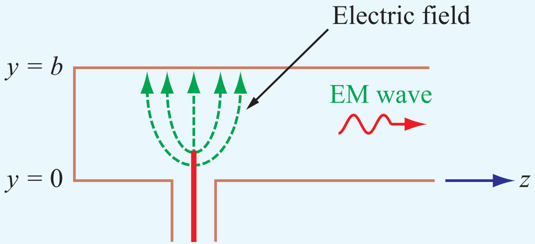

(b) Cross-sectional view at $x = a/2$

Figure 8-21 The inner conductor of a coaxial cable can excite an EM wave in the waveguide.

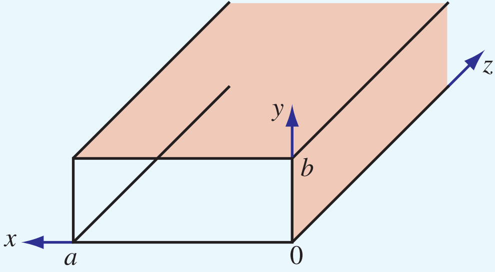

Figure 8-22 Waveguide coordinate system.

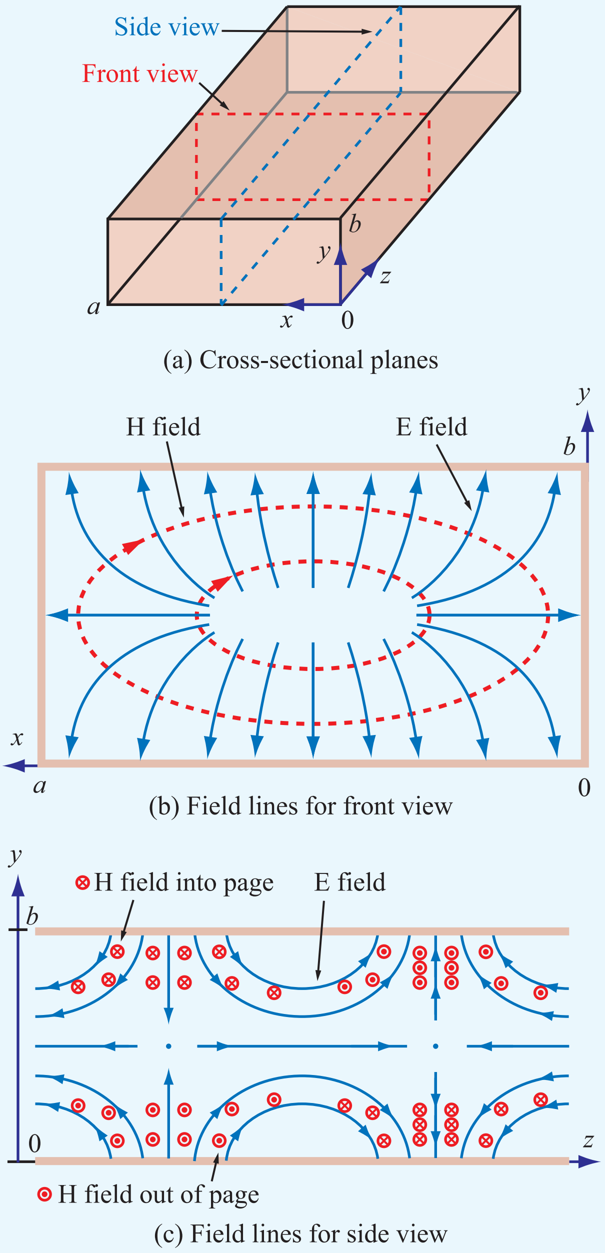

Figure 8-23 TM$_{11}$ electric and magnetic field lines across two cross-sectional planes.

Table 8-3 **Wave properties for TE and TM modes in a rectangular waveguide with dimensions $a \times b$, filled with a dielectric material with constitutive parameters ε and μ. The TEM case, shown for reference, pertains to plane-wave propagation in an unbounded medium.**

Rectangular Waveguides		Plane Wave
TE Modes	**TM Modes**	**TEM Mode**
$\widetilde{E}_x = \frac{j\omega\mu}{k_c^2}\left(\frac{n\pi}{b}\right) H_0 \cos\left(\frac{m\pi x}{a}\right) \sin\left(\frac{n\pi y}{b}\right)\ e^{-j\beta z}$	$\widetilde{E}_x = \frac{-j\beta}{k_c^2}\left(\frac{m\pi}{a}\right) E_0 \cos\left(\frac{m\pi x}{a}\right) \sin\left(\frac{n\pi y}{b}\right)\ e^{-j\beta z}$	$\widetilde{E}_x = E_{x0} e^{-j\beta z}$
$\widetilde{E}_y = \frac{-j\omega\mu}{k_c^2}\left(\frac{m\pi}{a}\right) H_0 \sin\left(\frac{m\pi x}{a}\right) \cos\left(\frac{n\pi y}{b}\right)\ e^{-j\beta z}$	$\widetilde{E}_y = \frac{-j\beta}{k_c^2}\left(\frac{n\pi}{b}\right) E_0 \sin\left(\frac{m\pi x}{a}\right) \cos\left(\frac{n\pi y}{b}\right)\ e^{-j\beta z}$	$\widetilde{E}_y = E_{y0} e^{-j\beta z}$
$\widetilde{E}_z = 0$	$\widetilde{E}_z = E_0 \sin\left(\frac{m\pi x}{a}\right) \sin\left(\frac{n\pi y}{b}\right)\ e^{-j\beta z}$	$\widetilde{E}_z = 0$
$\widetilde{H}_x = -\widetilde{E}_y / Z_{\mathrm{TE}}$	$\widetilde{H}_x = -\widetilde{E}_y / Z_{\mathrm{TM}}$	$\widetilde{H}_x = -\widetilde{E}_y / \eta$
$\widetilde{H}_y = \widetilde{E}_x / Z_{\mathrm{TE}}$	$\widetilde{H}_y = \widetilde{E}_x / Z_{\mathrm{TM}}$	$\widetilde{H}_y = \widetilde{E}_x / \eta$
$\widetilde{H}_z = H_0 \cos\left(\frac{m\pi x}{a}\right) \cos\left(\frac{n\pi y}{b}\right)\ e^{-j\beta z}$	$\widetilde{H}_z = 0$	$\widetilde{H}_z = 0$
$Z_{\mathrm{TE}} = \eta / \sqrt{1 - (f_c/f)^2}$	$Z_{\mathrm{TM}} = \eta \sqrt{1 - (f_c/f)^2}$	$\eta = \sqrt{\mu/\varepsilon}$
Properties Common to TE and TM Modes		
$f_c = \frac{u_{p_0}}{2}\sqrt{\left(\frac{m}{a}\right)^2 + \left(\frac{n}{b}\right)^2}$		$f_c =$ not applicable
$\beta = k\sqrt{1 - (f_c/f)^2}$		$k = \omega\sqrt{\mu\varepsilon}$
$u_p = \frac{\omega}{\beta} = u_{p_0} / \sqrt{1 - (f_c/f)^2}$		$u_{p_0} = 1/\sqrt{\mu\varepsilon}$

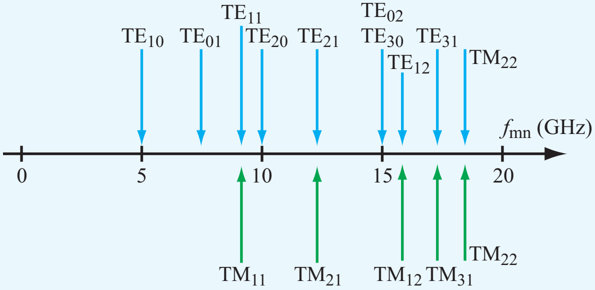

Figure 8-24 Cutoff frequencies for TE and TM modes in a hollow rectangular waveguide with $a = 3$ cm and $b = 2$ cm (Example 8-9).

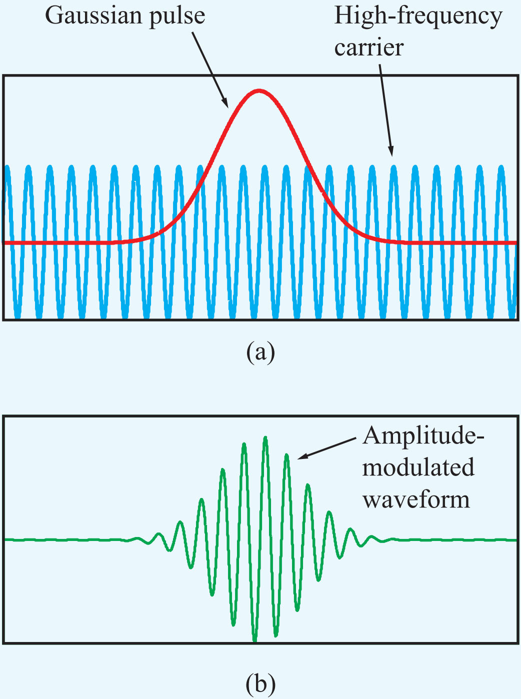

Figure 8-25 The amplitude-modulated high-frequency waveform in (b) is the product of the Gaussian-shaped pulse with the sinusoidal high-frequency carrier in (a).

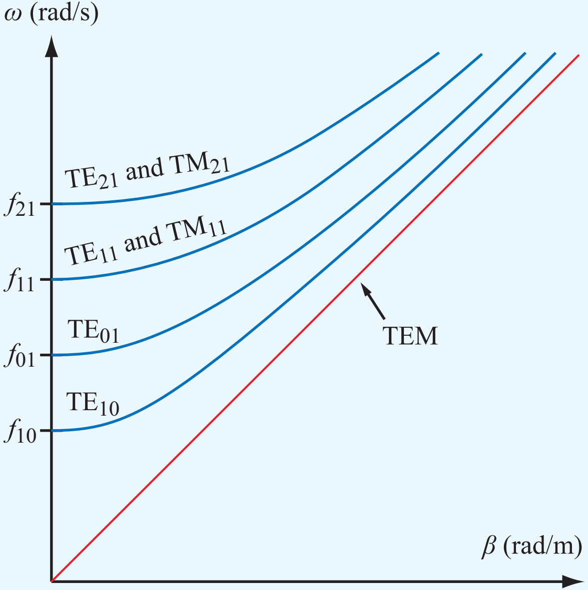

Figure 8-26 ω-β diagram for TE and TM modes in a hollow rectangular waveguide. The straight line pertains to propagation in an unbounded medium or on a TEM transmission line.

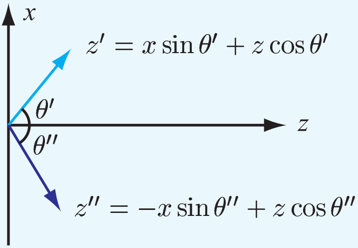

From Eq. (8.118a), $z' = \frac{\pi x}{\beta a} + z$.
Hence, $\theta' = \tan^{-1}(\pi/\beta a)$.

From Eq. (8.118b), $z'' = -\frac{\pi x}{\beta a} + z$.
Hence, $\theta'' = -\tan^{-1}(\pi/\beta a)$.

(a) z' and z'' propagation directions

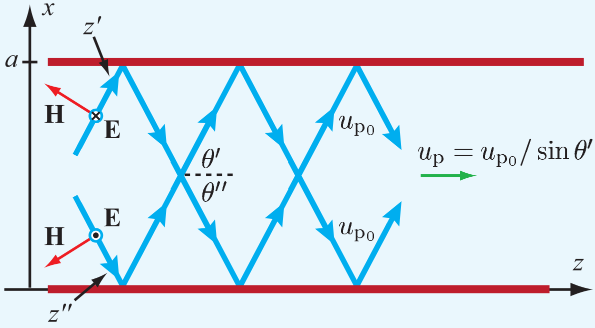

(b) TEM waves

Figure 8-27 The TE_{10} mode can be constructed as the sum of two TEM waves.

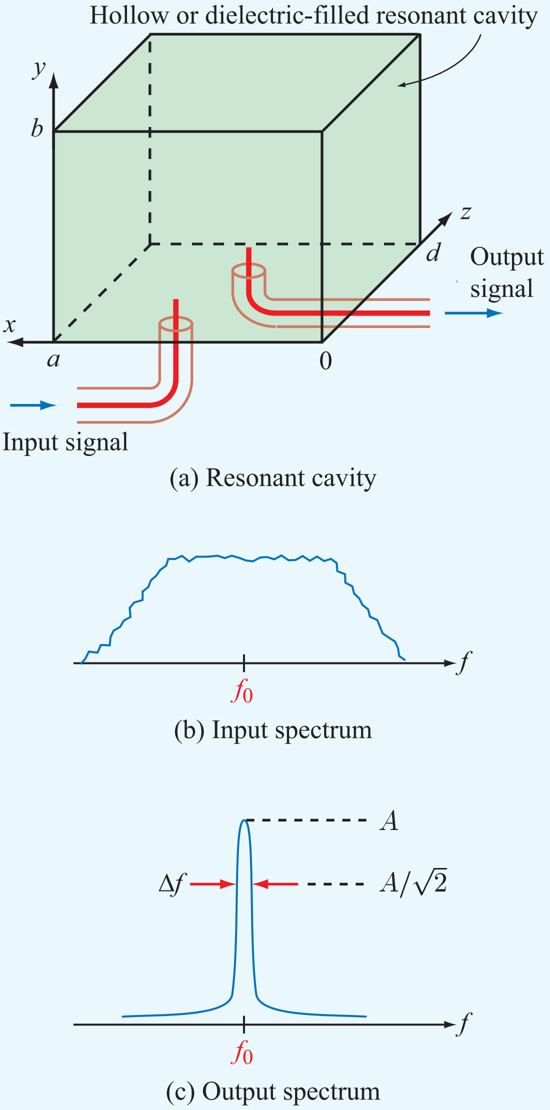

Figure 8-28 A resonant cavity supports a very narrow bandwidth around its resonant frequency f_0.

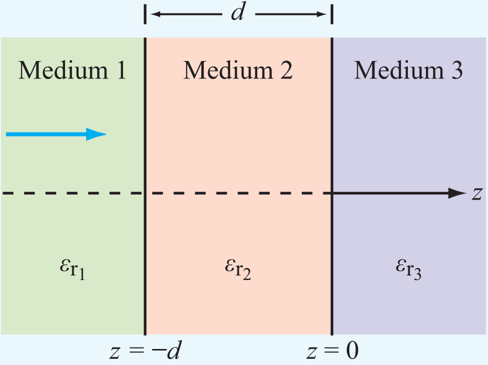

Figure P8.9 Dielectric layers for Problems 8.9 to 8.11.

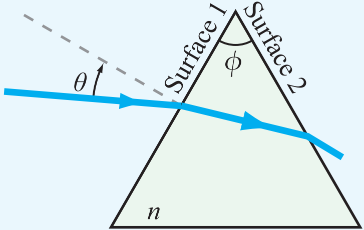

Figure P8.17 Prism of Problem 8.17.

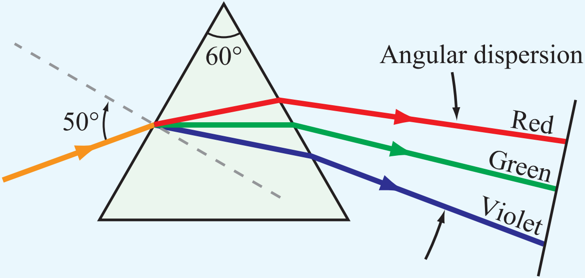

Figure P8.18 Prism of Problem 8.18.

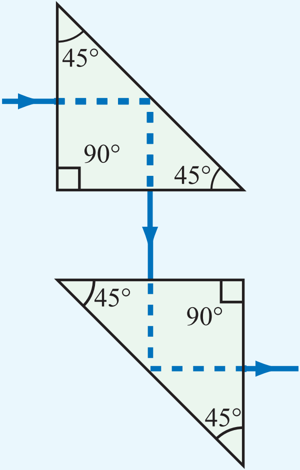

Figure P8.19 Periscope prisms of Problem 8.19.

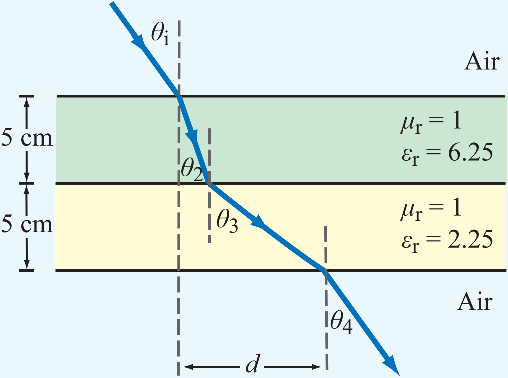

Figure P8.20 Problem P8.20.

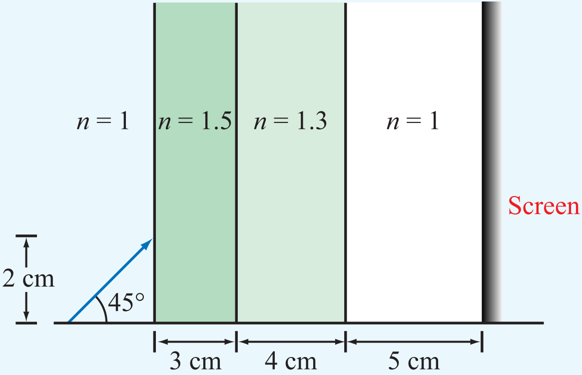

Figure P8.21 Light incident on a screen through a multilayered dielectric (Problem 8.21).

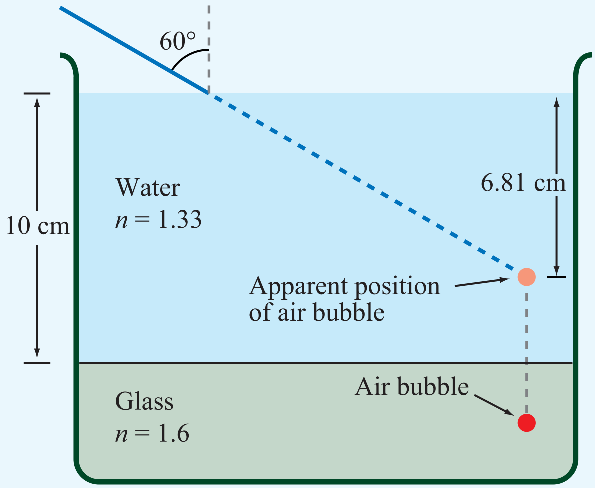

Figure P8.22 Apparent position of the air bubble in Problem 8.22.

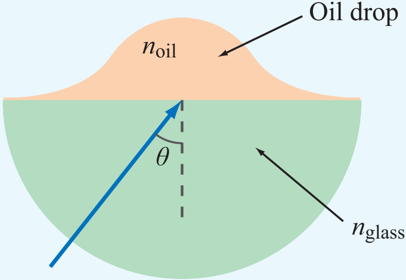

Figure P8.23 Oil drop on the flat surface of a glass semicylinder (Problem 8.23).

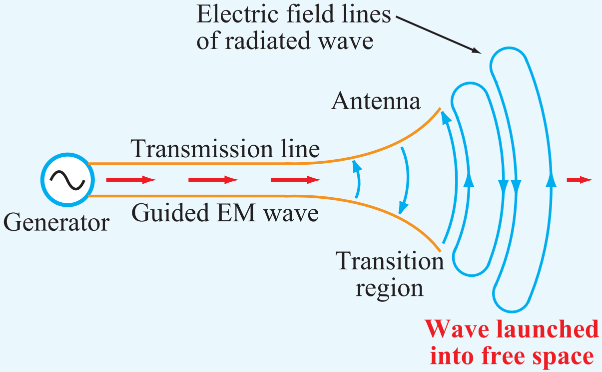

(a) Transmission mode

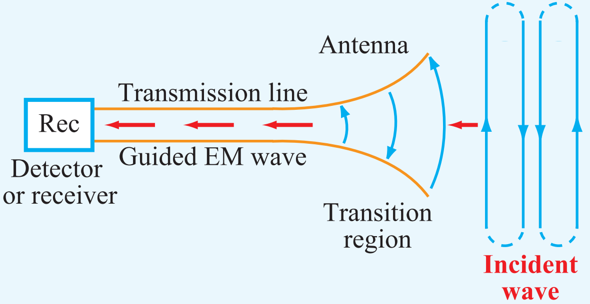

(b) Reception mode

Figure 9-1 Antenna as a transducer between a guided electromagnetic wave and a free-space wave, for both transmission and reception.

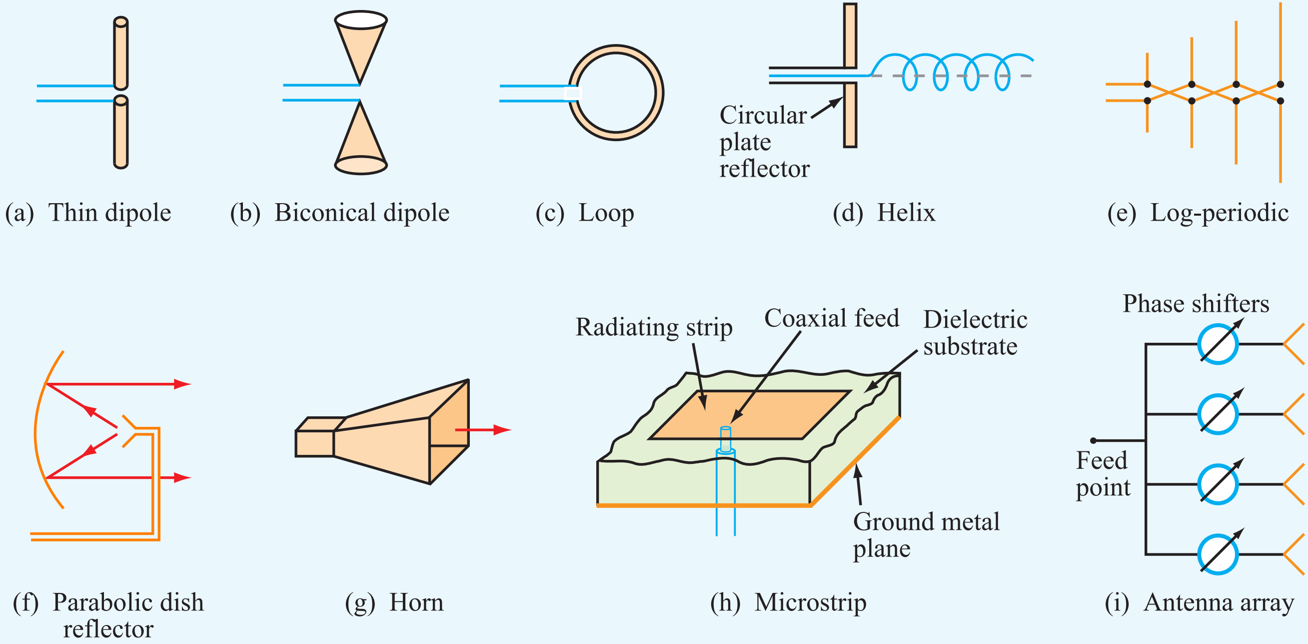

Figure 9-2 Various types of antennas.

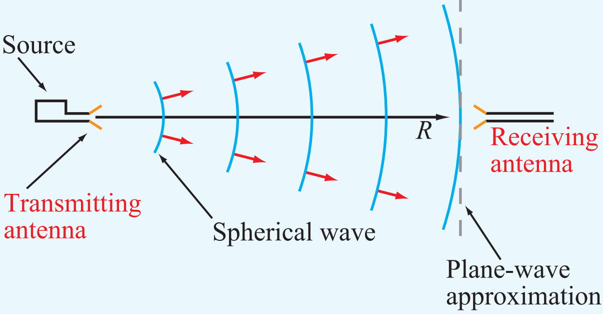

Figure 9-3 Far-field plane-wave approximation.

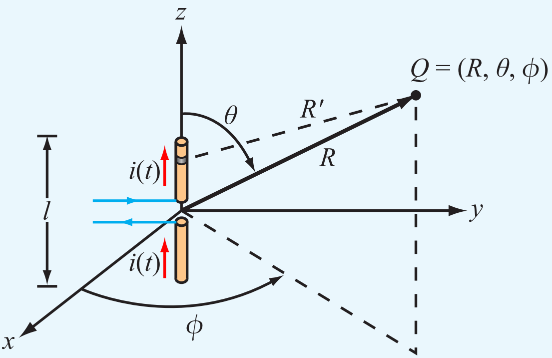

Figure 9-4 Short dipole placed at the origin of a spherical coordinate system.

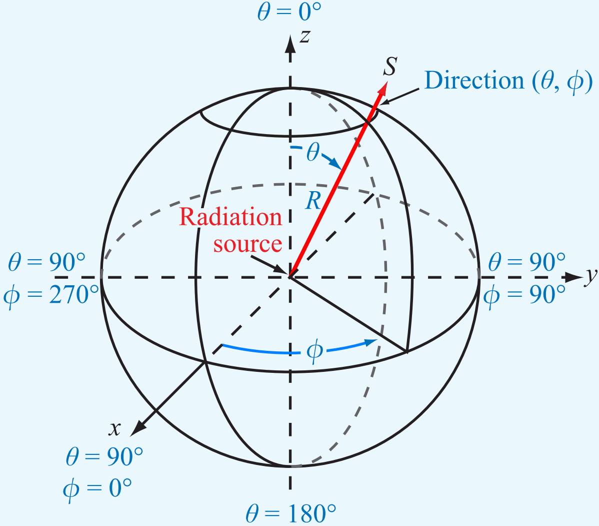

Figure 9-5 Spherical coordinate system.

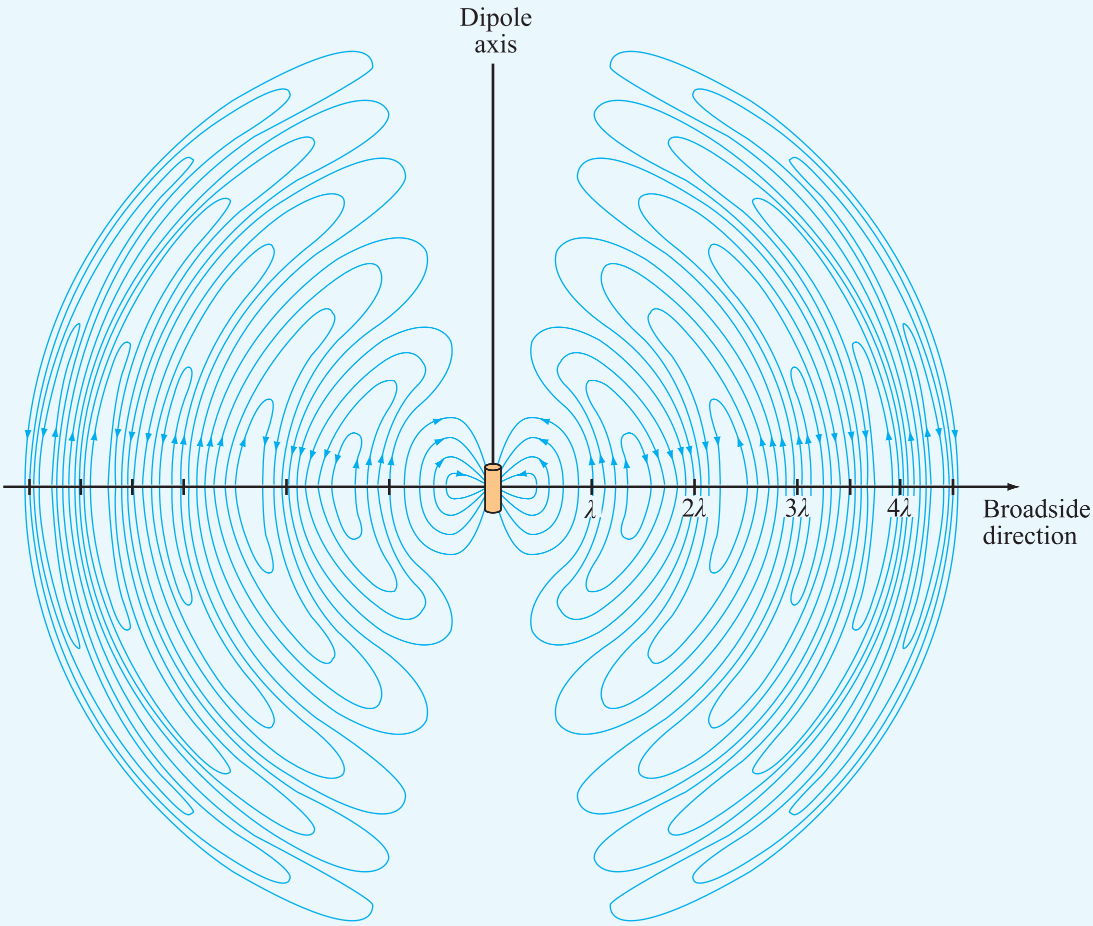

Figure 9-6 Electric field lines surrounding an oscillating dipole at a given instant.

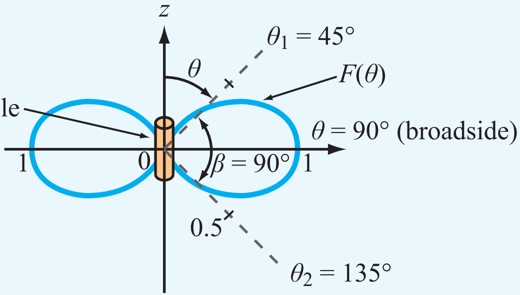

(a) Elevation pattern

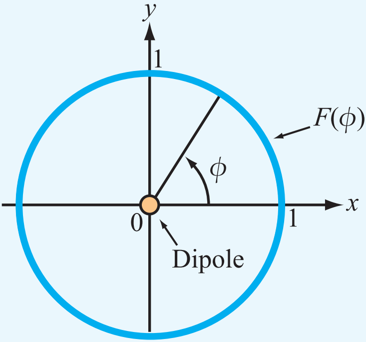

(b) Azimuth pattern

Figure 9-7 Radiation patterns of a short dipole.

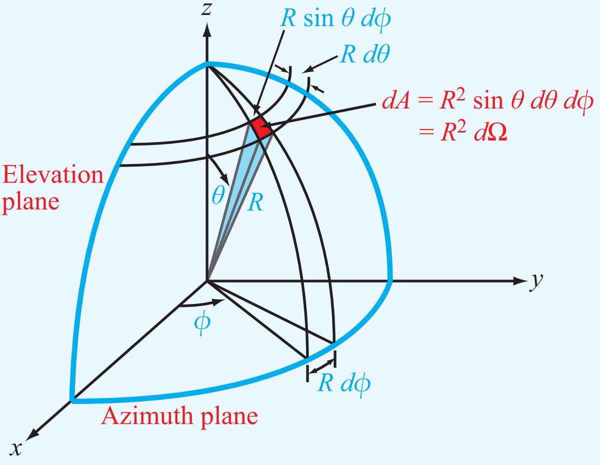

Figure 9-8 Definition of solid angle $d\Omega = \sin\theta \; d\theta \; d\phi$.

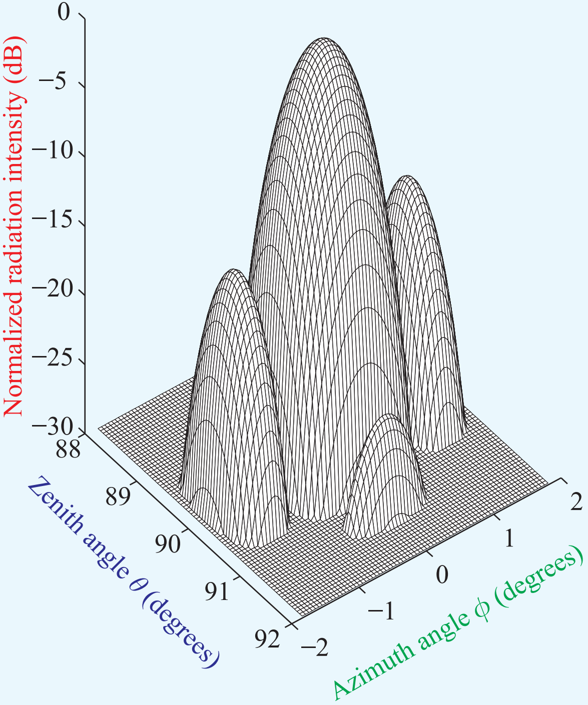

Figure 9-9 Three-dimensional pattern of a narrow-beam antenna.

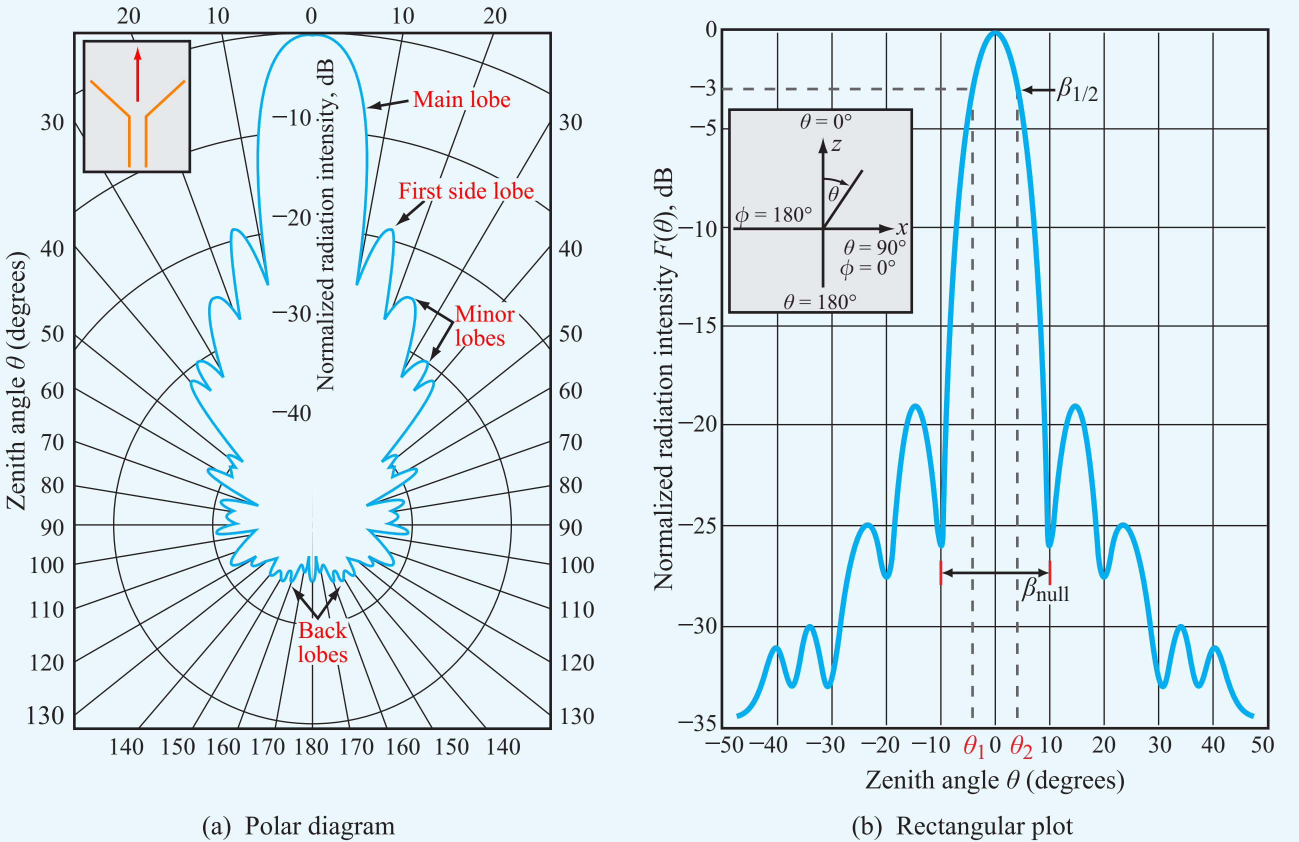

Figure 9-10 Representative plots of the normalized radiation pattern of a microwave antenna in (a) polar form and (b) rectangular form.

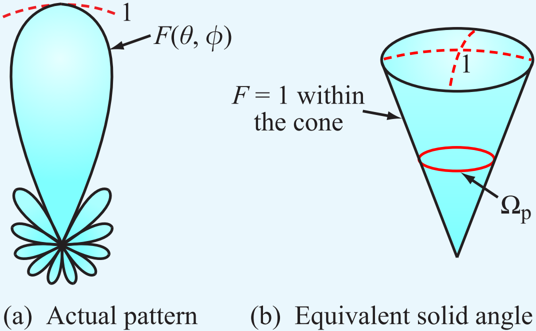

Figure 9-11 The pattern solid angle Ω_p defines an equivalent cone over which all the radiation of the actual antenna is concentrated with uniform intensity equal to the maximum of the actual pattern.

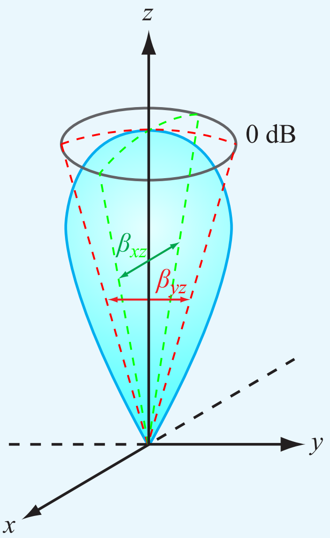

Figure 9-12 The solid angle of a unidirectional radiation pattern is approximately equal to the product of the half-power beamwidths in the two principal planes; that is, $\Omega_p \approx \beta_{xz}\beta_{yz}$.

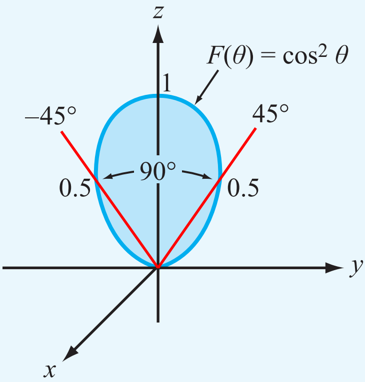

Figure 9-13 Polar plot of $F(\theta) = \cos^2 \theta$.

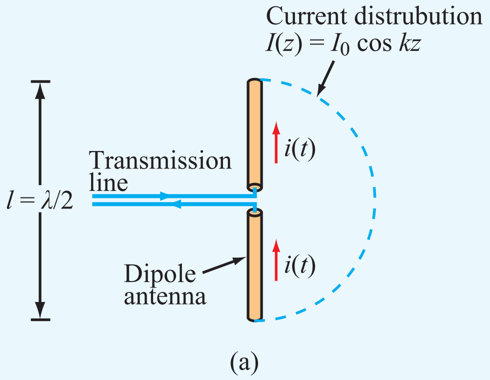

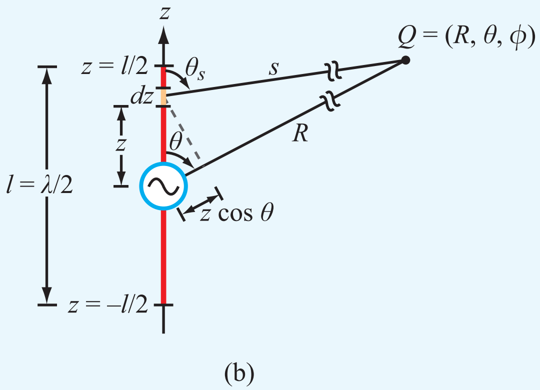

Figure 9-14 Center-fed half-wave dipole.

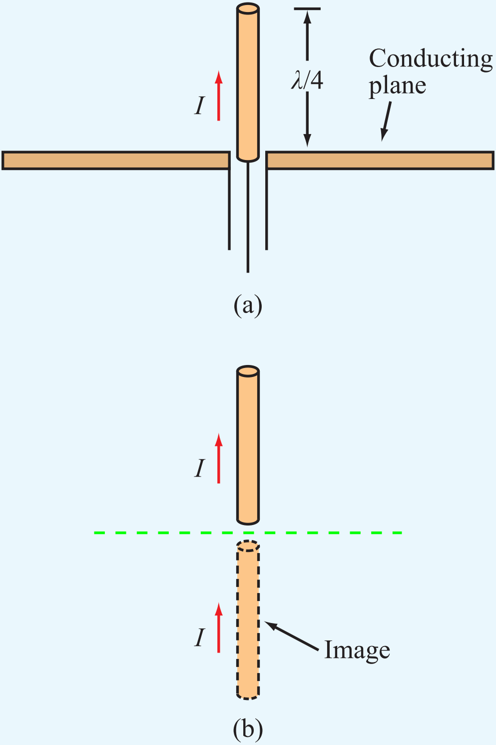

Figure 9-15 A quarter-wave monopole above a conducting plane is equivalent to a full half-wave dipole in free space.

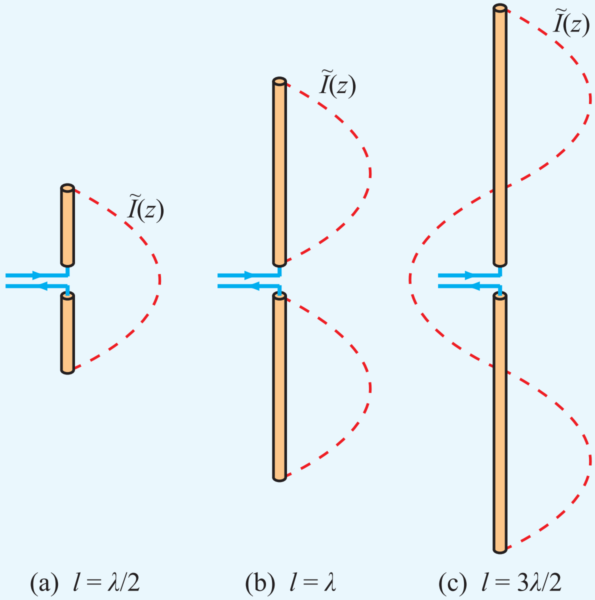

Figure 9-16 Current distribution for three center-fed dipoles.

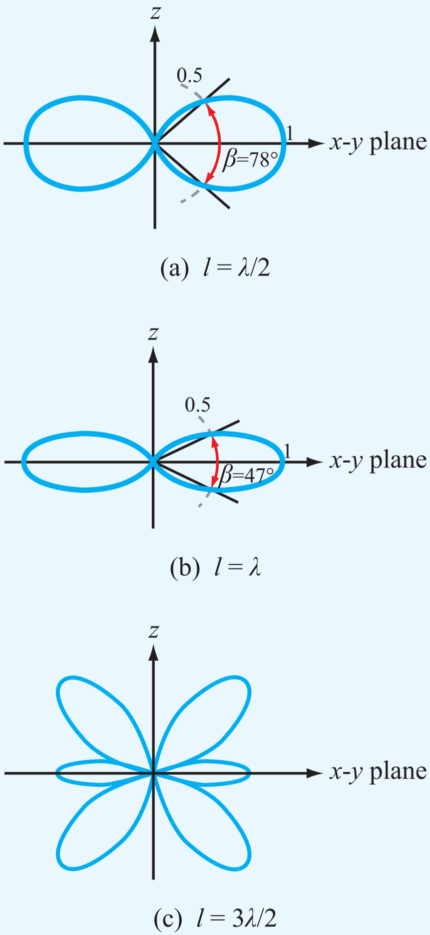

Figure 9-17 Radiation patterns of dipoles with lengths of $\lambda/2$, λ, and $3\lambda/2$.

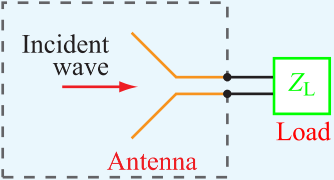

(a) Receiving antenna

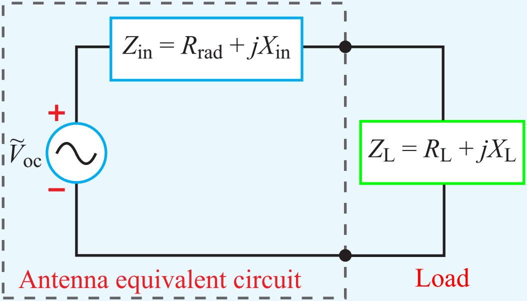

(b) Equivalent circuit

Figure 9-18 Receiving antenna represented by an equivalent circuit.

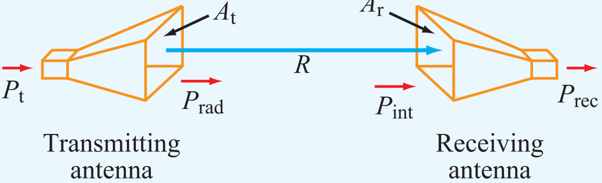

Figure 9-19 Transmitter–receiver configuration.

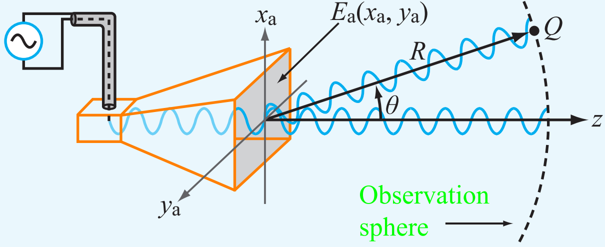

Figure 9-20 A horn antenna with aperture field distribution $E_a(x_a, y_a)$.

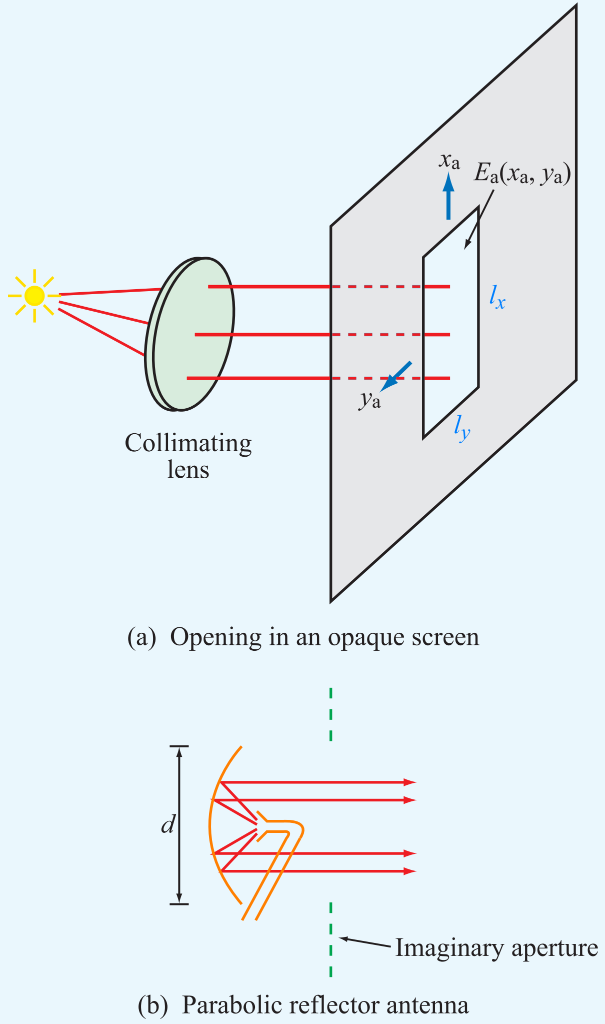

Figure 9-21 Radiation by apertures: (a) an opening in an opaque screen illuminated by a light source through a collimating lens and (b) a parabolic dish reflector illuminated by a small horn antenna.

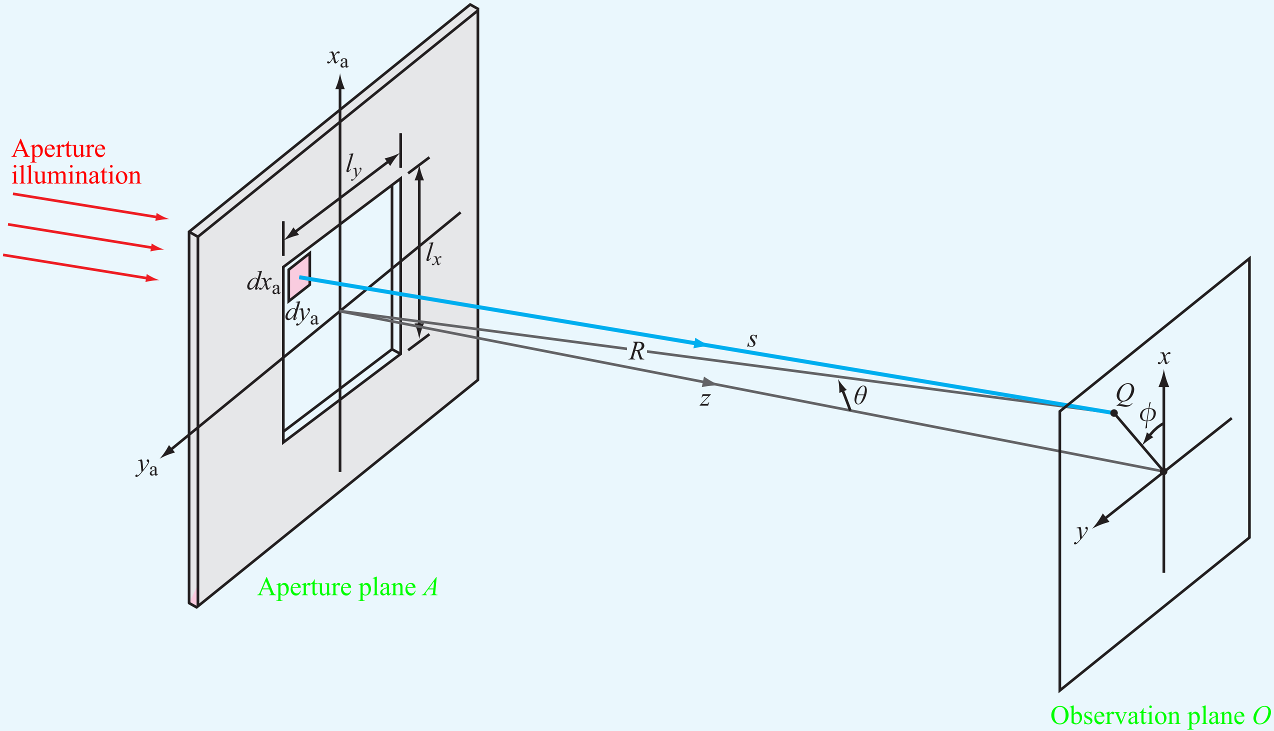

Figure 9-22 Radiation by an aperture in the x_a–y_a plane at $z = 0$.

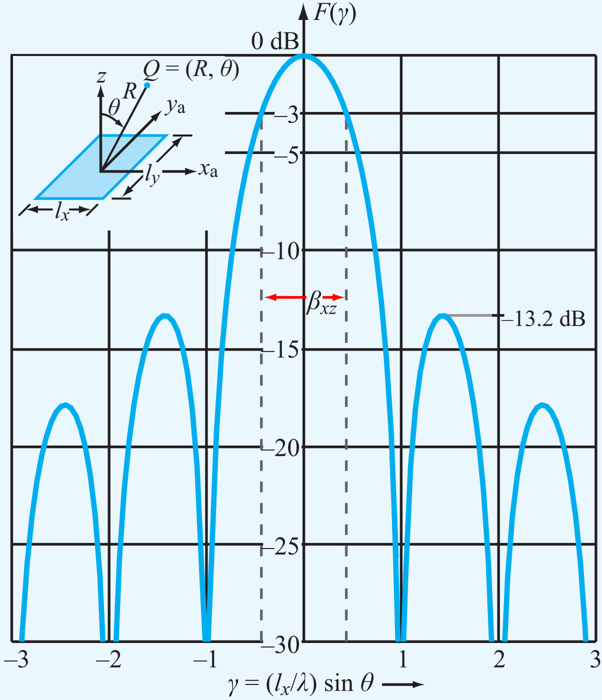

Figure 9-23 Normalized radiation pattern of a uniformly illuminated rectangular aperture in the x–z plane ($\phi = 0$).

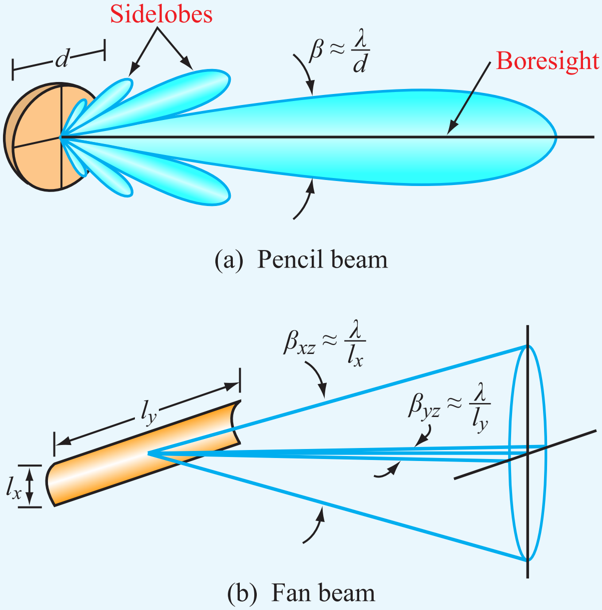

Figure 9-24 Radiation patterns of (a) a circular reflector and (b) a cylindrical reflector (side lobes not shown).

Figure 9-25 The AN/FPS-85 Phased Array Radar Facility in the Florida panhandle, near the city of Freeport. A several-mile no-fly zone surrounds the radar installation as a safety concern for electroexplosive devices, such as ejection seats and munitions, carried on military aircraft.

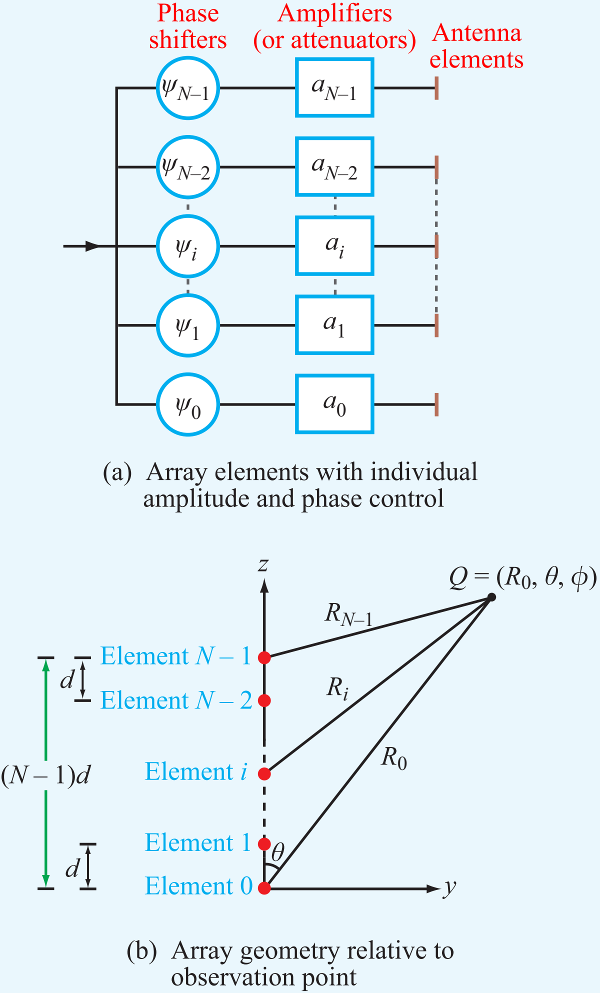

Figure 9-26 Linear-array configuration and geometry.

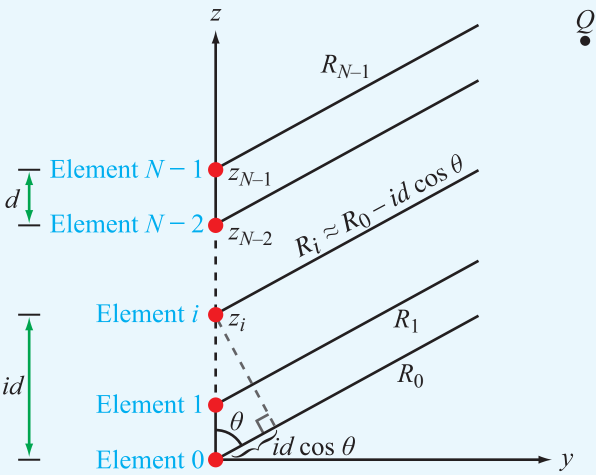

Figure 9-27 The rays between the elements and a far-away observation point are approximately parallel lines. Hence, the distance $R_i \approx R_0 - id\cos\theta$.

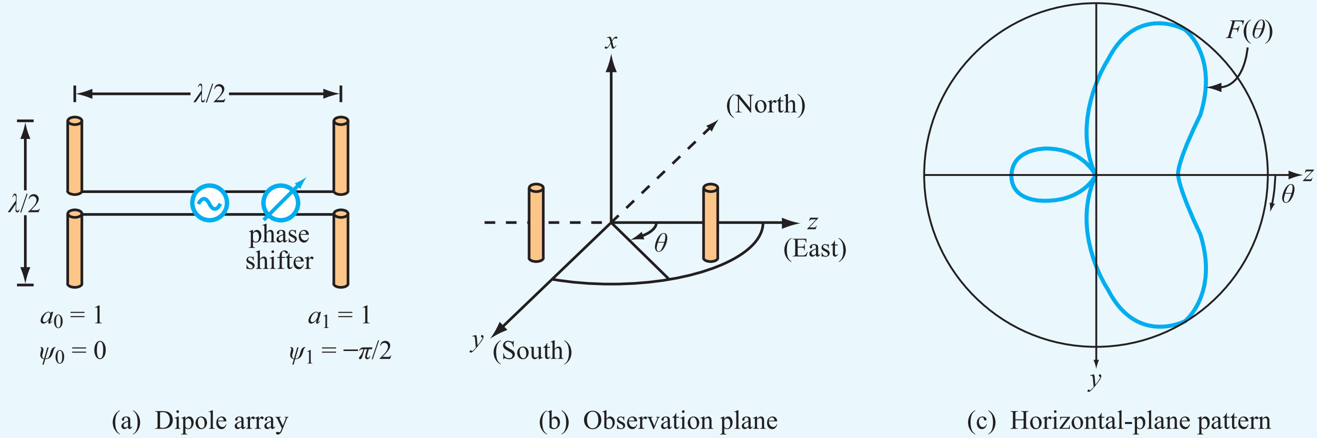

Figure 9-28 Two half-wave dipole array of Example 9.5.

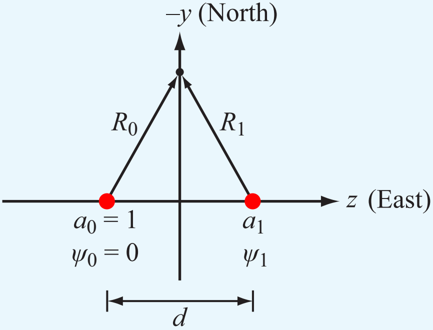

(a) Array arrangement

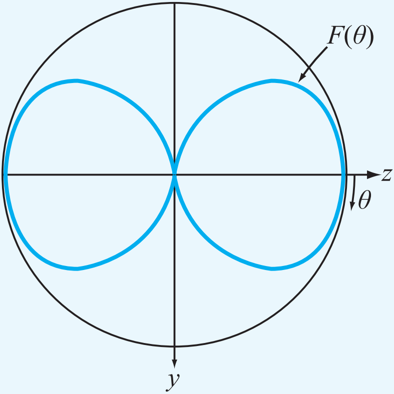

(b) Array pattern

Figure 9-29 (a) Two vertical dipoles separated by a distance d along the z axis; (b) normalized array pattern in the y–z plane for $a_0 = a_1 = 1$, $\psi_1 = \psi_0 = -\pi$, and $d = \lambda/2$.

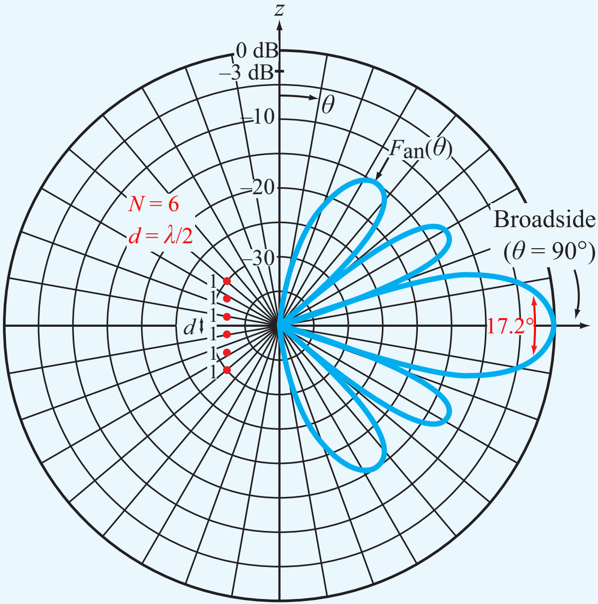

Figure 9-30 Normalized array pattern of a uniformly excited six-element array with interelement spacing $d = \lambda/2$.

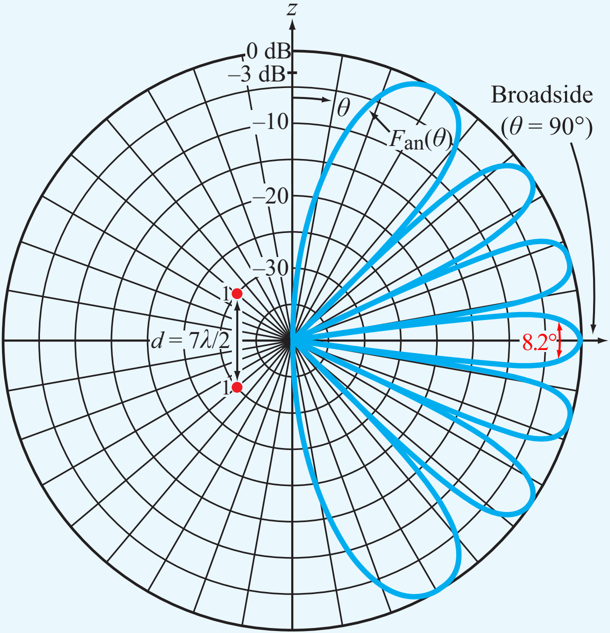

Figure 9-31 Normalized array pattern of a two-element array with spacing $d = 7\lambda/2$.

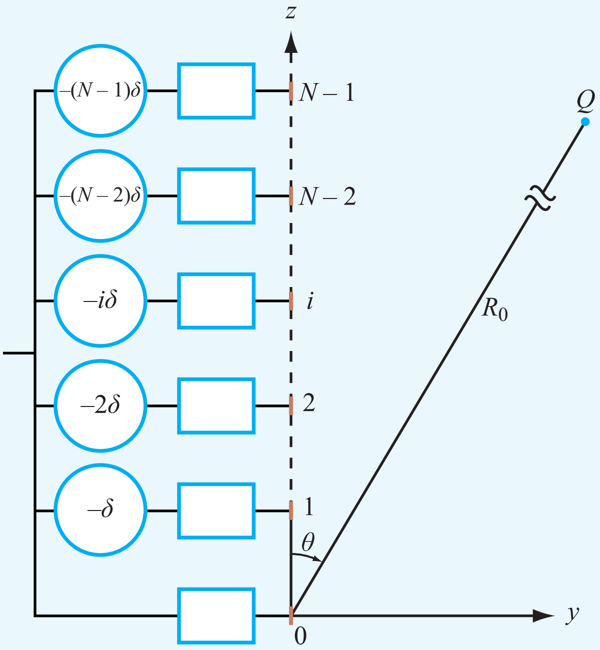

Figure 9-32 The application of linear phase.

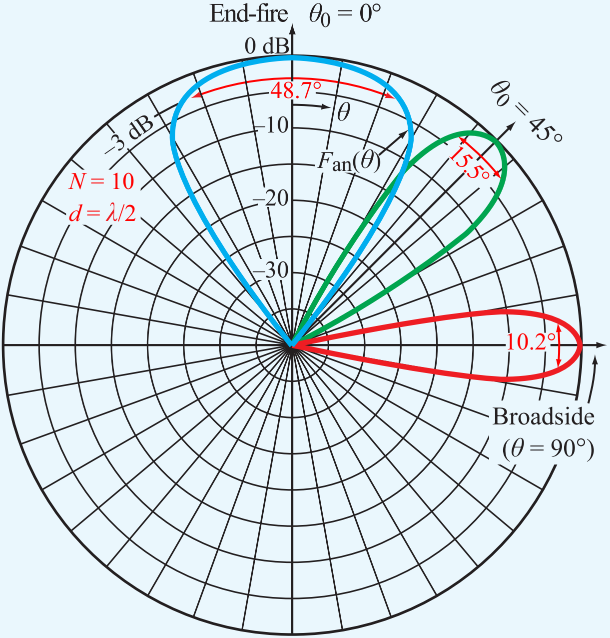

Figure 9-33 Normalized array pattern of a 10-element array with $\lambda/2$ spacing between adjacent elements. All elements are excited with equal amplitude. Through the application of linear phase across the array, the main beam can be steered from the broadside direction ($\theta_0 = 90°$) to any scan angle θ_0. Equiphase excitation corresponds to $\theta_0 = 90°$.

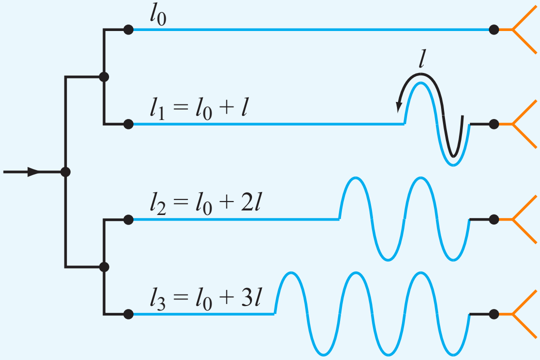

Figure 9-34 An example of a feeding arrangement for frequency-scanned arrays.

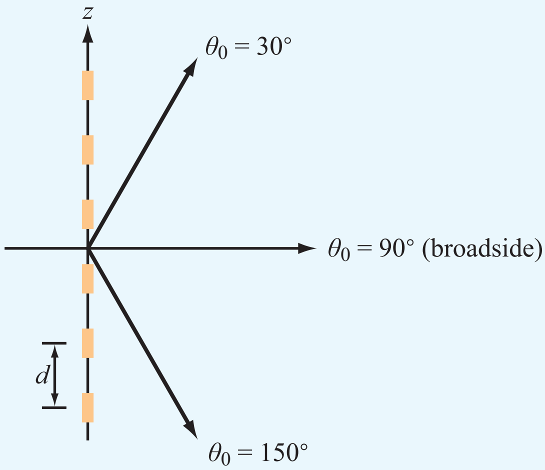

Figure 9-35 Steerable six-element array (Example 9.8).

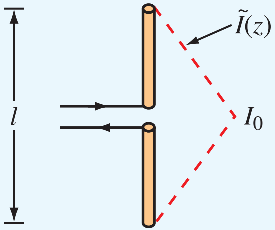

Figure P9.16 Triangular current distribution on a short dipole (Problem 9.16).

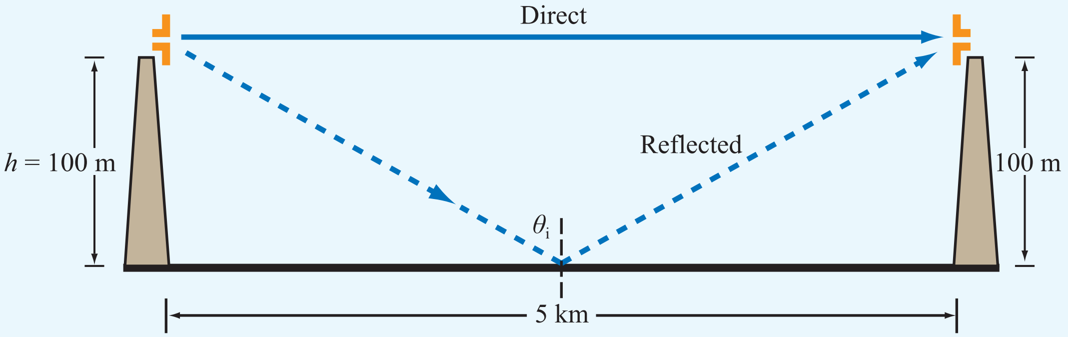

Figure P9.27 Problem 9.27.

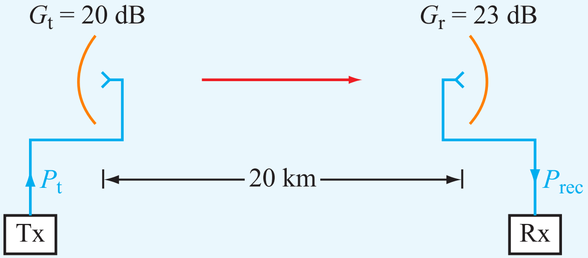

Figure P9.26 Communication system of Problem 9.26.

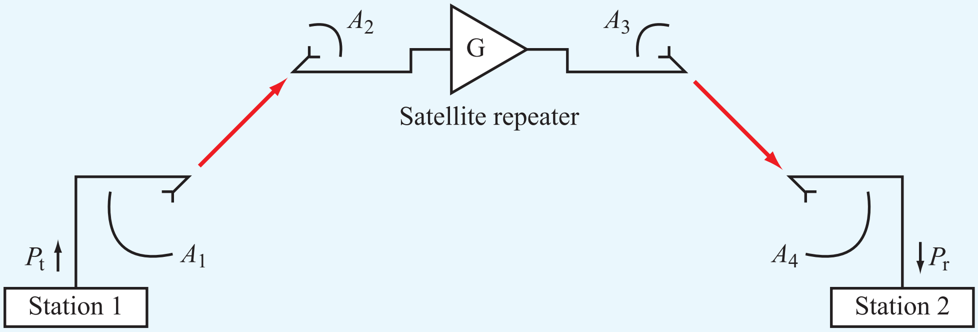

Figure P9.29 Satellite repeater system.

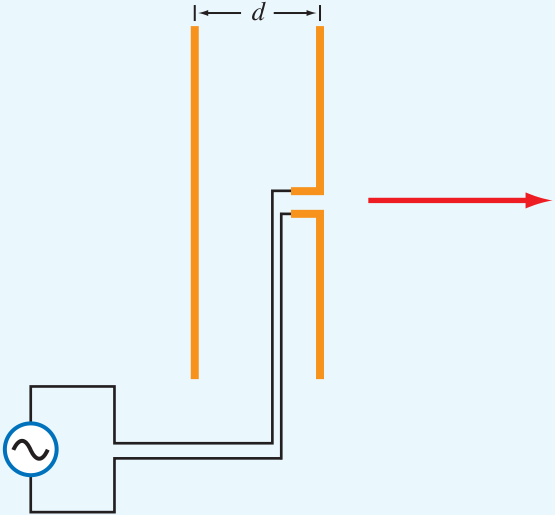

Figure P9.28 Problem 9.28.

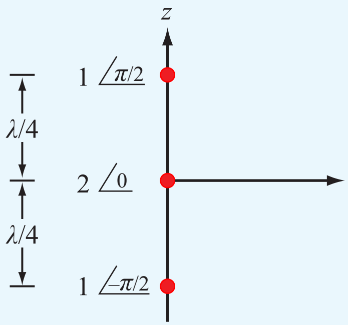

Figure P9.45 Three-element array of Problem 9.48.

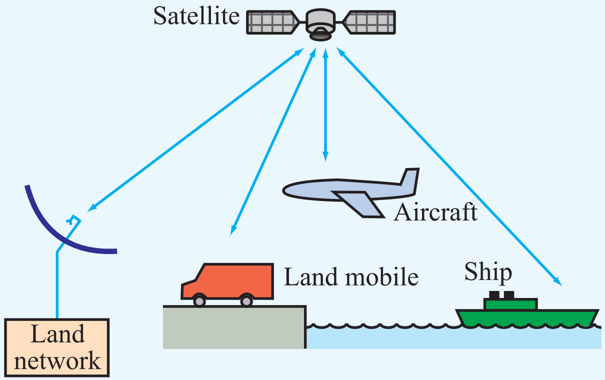

Figure 10-1 Elements of a satellite communication network.

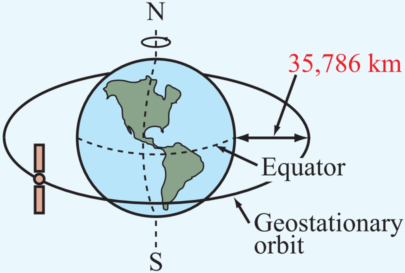

(a) Geostationary satellite orbit

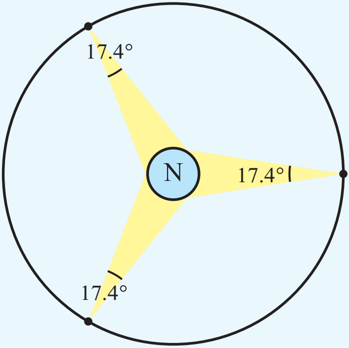

(b) Worldwide coverage by three satellites spaced 120° apart

Figure 10-2 Orbits of geostationary satellites.

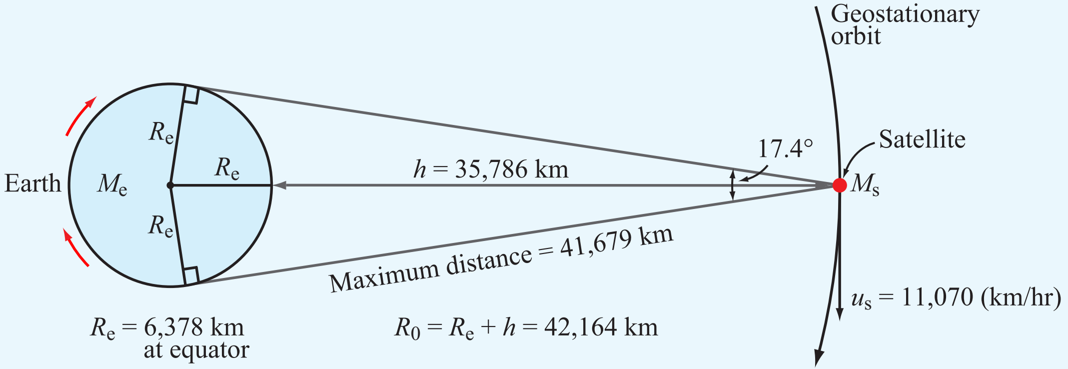

Figure 10-3 Satellite of mass m_s in orbit around Earth. For the orbit to be geostationary, the distance R_0 between the satellite and Earth's center should be 42,164 km. At the equator, this corresponds to an altitude of 35,786 km above Earth's surface.

Table 10-1 Communications satellite frequency allocations.

Use	Downlink Frequency (MHz)	Uplink Frequency (MHz)
Fixed Service		
Commercial (C-band)	3,700–4,200	5,925–6,425
Military (X-band)	7,250–7,750	7,900–8,400
Commercial (K-band)		
Domestic (USA)	11,700–12,200	14,000–14,500
International	10,950–11,200	27,500–31,000
Mobile Service		
Maritime	1,535–1,542.5	1,635–1,644
Aeronautical	1,543.5–1,558.8	1,645–1,660
Broadcast Service		
	2,500–2,535	2,655–2,690
	11,700–12,750	
Telemetry, Tracking, and Command		
137–138, 401–402, 1,525–1,540		

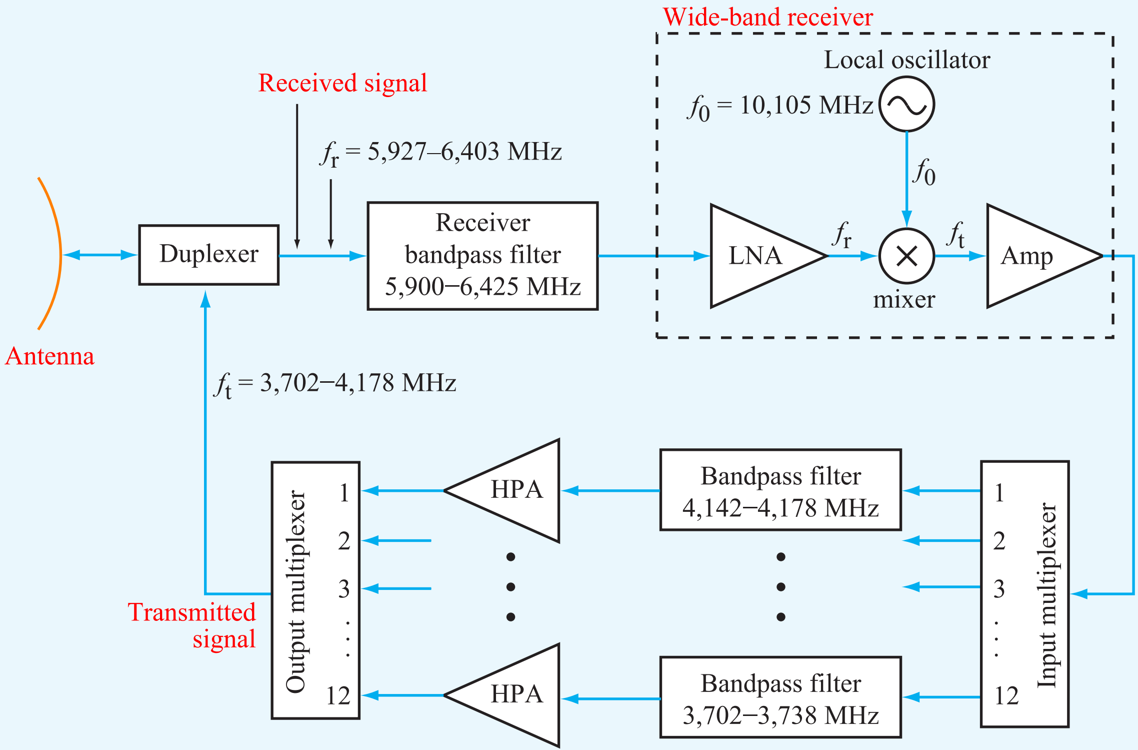

Figure 10-4 Elements of a 12-channel (transponder) communications system.

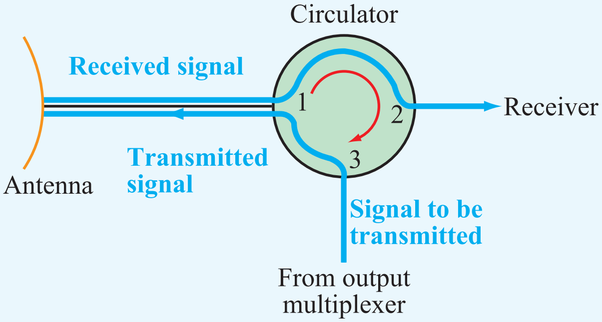

Figure 10-5 Basic operation of a ferrite circulator.

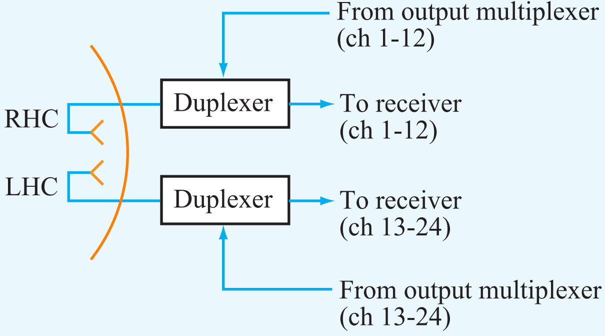

Figure 10-6 Polarization diversity is used to increase the number of channels from 12 to 24.

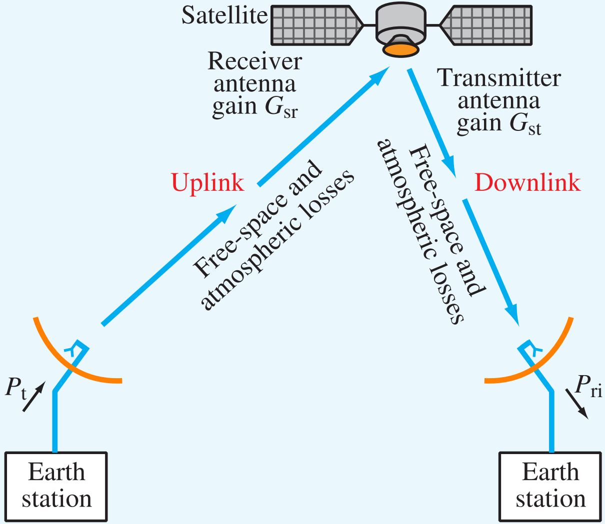

Figure 10-7 Satellite transponder.

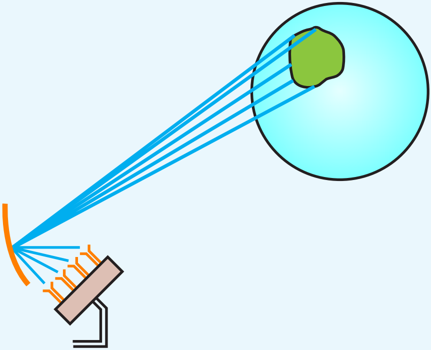

(a) Zone coverage

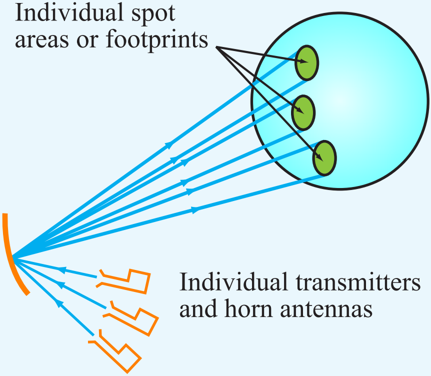

(b) Multi-spot beams

Figure 10-8 Spot and multibeam satellite antenna systems for coverage of defined areas on Earth's surface.

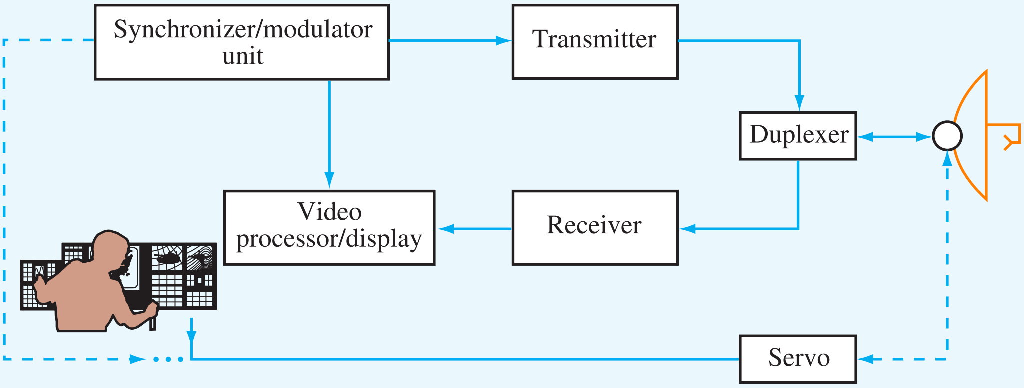

Figure 10-9 Basic block diagram of a radar system.

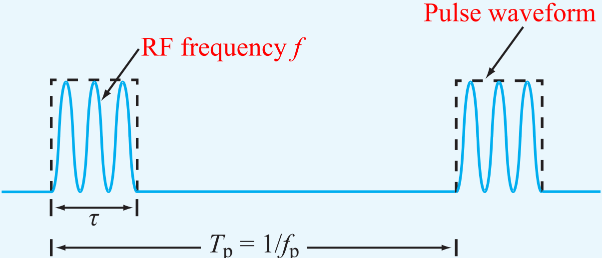

Figure 10-10 A pulse radar transmits a continuous train of RF pulses at a repetition frequency f_p.

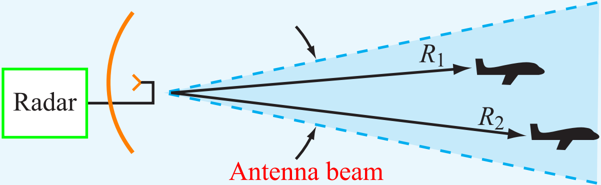

Figure 10-11 Radar beam viewing two targets at ranges R_1 and R_2.

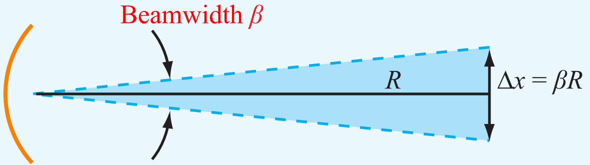

Figure 10-12 The azimuth resolution Δx at a range R is equal to βR.

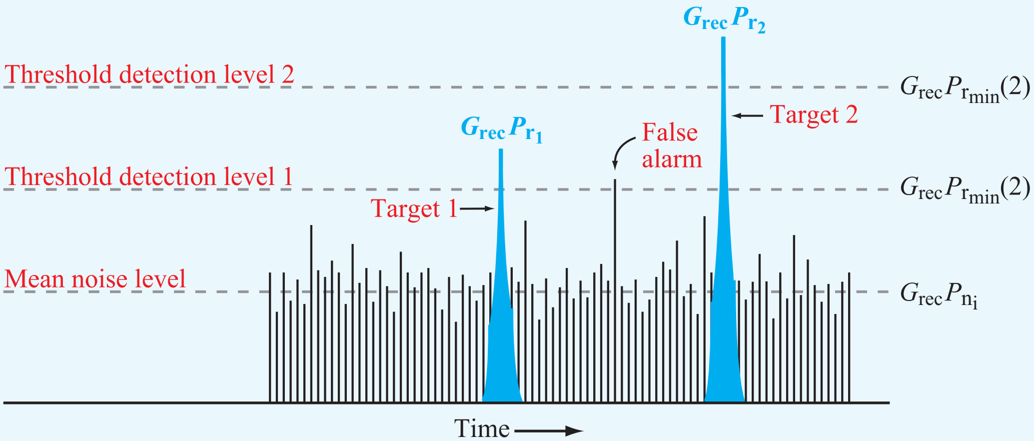

Figure 10-13 The output of a radar receiver as a function of time.

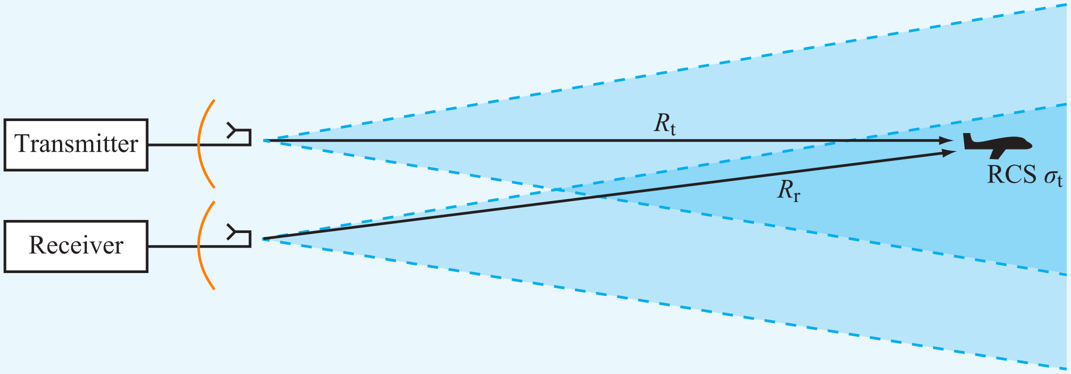

Figure 10-14 Bistatic radar system viewing a target with radar cross section (RCS) σ_t.

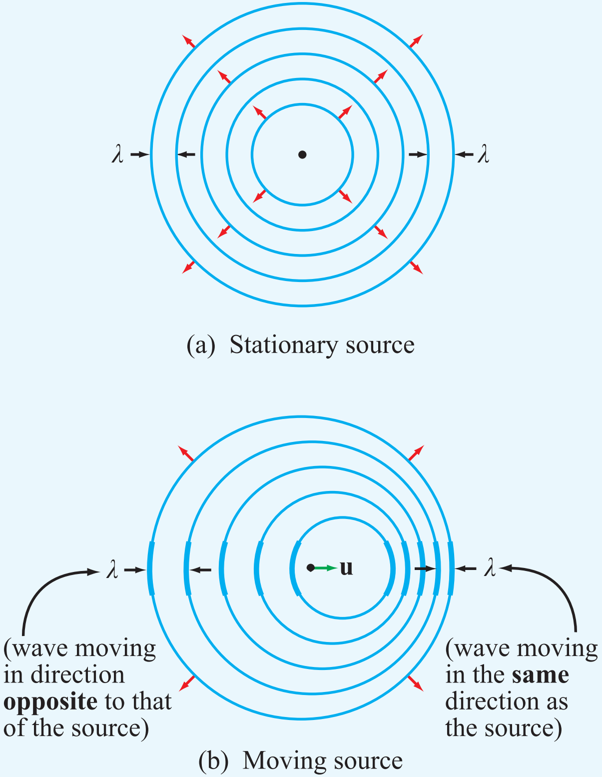

Figure 10-15 A wave radiated from a point source when (a) stationary and (b) moving. The wave is compressed in the direction of motion, spread out in the opposite direction, and unaffected in the direction normal to motion.

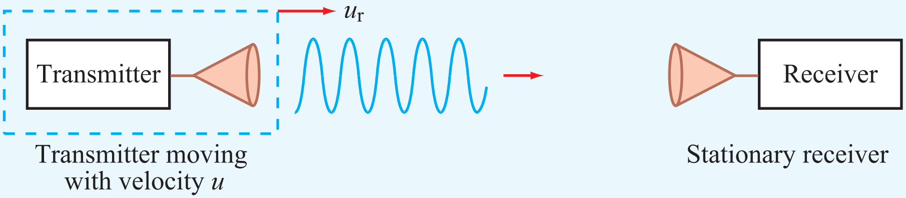

Figure 10-16 Transmitter with radial velocity u_r approaching a stationary receiver.

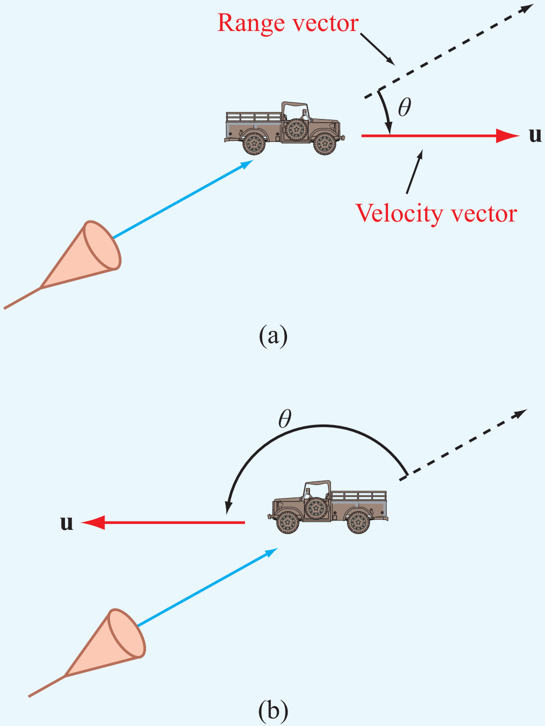

Figure 10-17 The Doppler frequency shift is negative for a receding target ($0 \leq \theta \leq 90°$), as in (a), and positive for an approaching target ($90° \leq \theta \leq 180°$), as in (b).

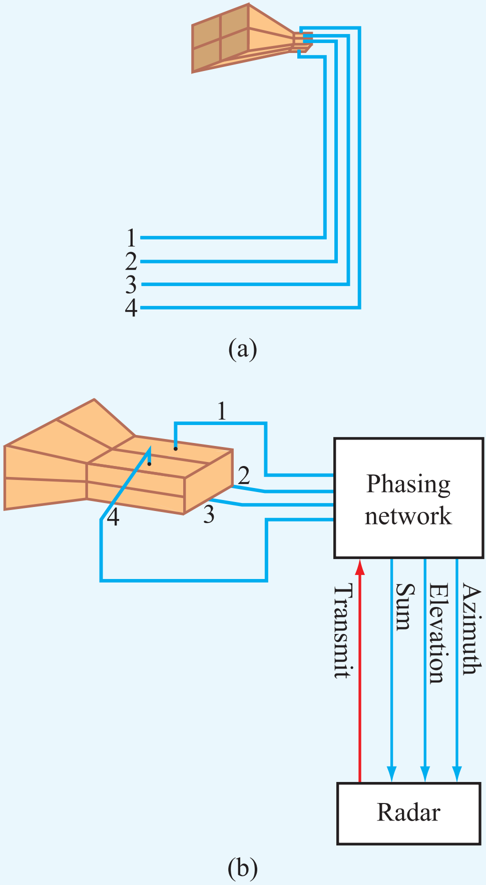

Figure 10-18 Antenna feeding arrangement for an amplitude-comparison monopulse radar: (a) feed horns and (b) connection to phasing network.

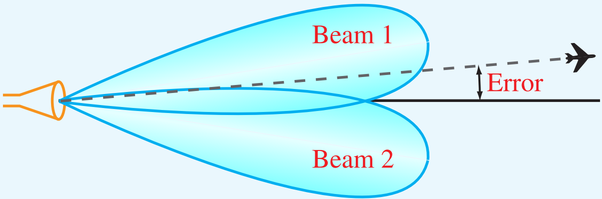

Figure 10-19 A target observed by two overlapping beams of a monopulse radar.

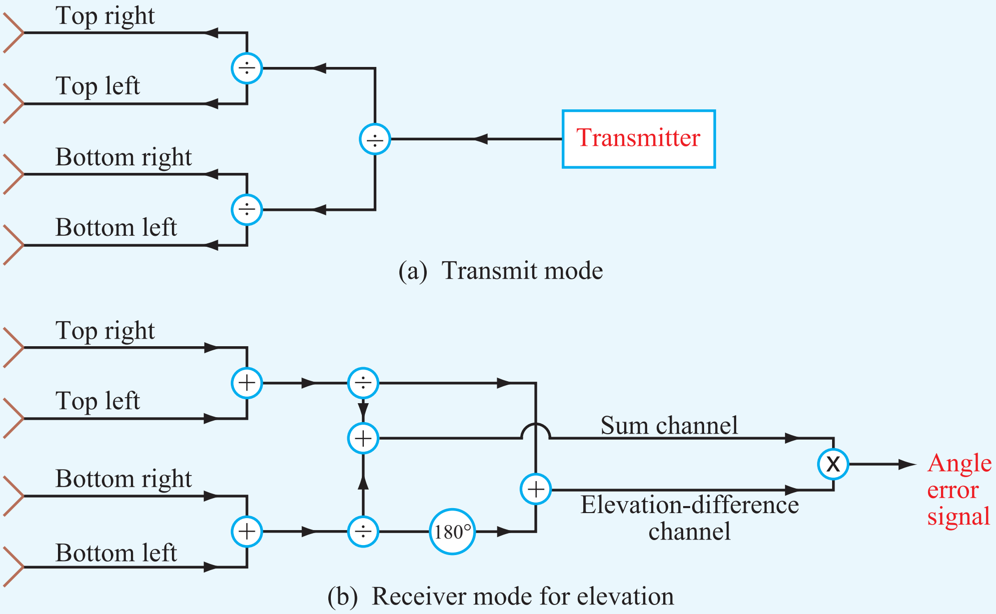

Figure 10-20 Functionality of the phasing network in (a) the transmit mode and (b) the receive mode for the elevation-difference channel.

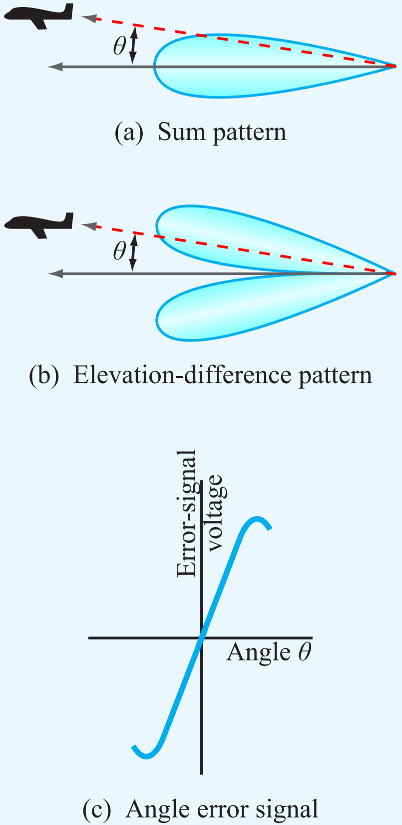

Figure 10-21 Monopulse antenna (a) sum pattern, (b) elevation-difference pattern, and (c) angle error signal.